PROCEEDINGS OF THE 24th ANNUAL INTERNATIONAL CONFERENCE ON SOIL, WATER, ENERGY & AIR

Volume 2

Proceedings of the 24th Annual International Conference on Soil, Water, Energy & Air

Volume 2

Bioremediation
Energy Engineering
Environmental Policy
Hazard Assessment
Site Investigation
Methods

Selected manuscripts from the 24th Annual International Conference on
Soil, Water, Energy & Air
San Diego, CA
March 17-20, 2014

Edited by:
Paul T. Kostecki
Edward J. Calabrese
David Ludwig
Christopher Teaf

ISBN: 978-0-9888932-2-1

AEHS Foundation, Inc.
150 Fearing Street
Amherst, MA 01002
www.AEHSFoundation.org

Table of Contents

Contributing Authors

Eferhire Aganbi, Department of Biological Sciences, University of Essex, Wivenhoe Park, Colchester, UK CO4 3SQ; Biochemistry & Molecular Biology Department, Delta State University, Abraka, Delta State Nigeria
Arturo Aburto-Medina, Department of Biological Sciences, University of Essex, Wivenhoe Park, Colchester, UK CO4 3SQ; Universidad Autonoma Metropolitana Lerma, Lerma de Villada, 52006, México
Andrew S. Ball, Department of Biological Sciences, University of Essex, Wivenhoe Park, Colchester, UK CO4 3SQ; School of Applied Sciences, RMIT University, Building 223, Bundoora West Campus, South Australia
Katherine Butler, McDaniel-Lambert Associates, 241 N Figueroa St, Los Angeles, California, USA, 90012
Rebecca Countway, McDaniel-Lambert Associates, 241 N Figueroa St, Los Angeles, California, USA, 90012
Nour Sh. El-Gendy, Egyptian Petroleum Research Institute, Nasr City, Cairo, Egypt
Anne Fahy, Department of Biological Sciences, University of Essex, Wivenhoe Park, Colchester, UK CO4 3SQ
A. Hamdy, Egyptian Petroleum Research Institute, Nasr City, Cairo, Egypt
Tetsuya Ishida, Department of Civil Engineering, the The University of Tokyo, Japan
Charles Lambert, University of California, Irvine, Environmental Health Sciences, 100 Theory Drive, Suite 100 , Irvine, California, 92617, USA
Yao Luan, Department of Civil and Environmental Engineering, Saitama University, Japan
Stephen Marsh, McKenna Long & Aldridge, LLP, San Diego, CA
Terry J. McGenity, Department of Biological Sciences, University of Essex, Wivenhoe Park, Colchester, UK CO4 3SQ
Paul McCaw, Santa Barbara County Public Health Department, Environmental Health Services Division, 2125 South Centerpointe Parkway, Room 333, Santa Maria, California 93455
Marleen F. Noomen, Department of Earth System Analysis, Faculty of Geo-Information Science and Earth Observation, University of Twente, Enschede, The Netherlands
David G. Rossiter, Department of Earth System Analysis, Faculty of Geo-Information Science and Earth Observation, University of Twente, Enschede, The Netherlands
John Sepich, Brownfield Subslab, San Antonio, TX
Shankar Subramanian, URS Corporation, 100 S. Wacker Drive, Suite 500, Chicago, IL 60606
Robert E. Sweeney, 707 Howell Avenue, Etna, CA, 9602
Sayed Salman Tabatabai, M.Sc. Alumnus, Department of Earth System Analysis, Faculty of Geo-Information Science and Earth Observation, University of Twente, Mashhad, 9184885115, Iran

Foreword

Each Spring for nearly a quarter century, the beautiful San Diego area has hosted a first class technical meeting which convenes life scientists, physical scientists, engineers, agency program managers, and the legal profession, among others, to present and discuss ongoing and emerging research in environmental fields. This volume includes a broad range of papers that are representative of those given at the March 2014 24th offering of the West Coast Conference on Soil, Water, Energy, and Air. The articles cover the figurative waterfront from risk assessment, to groundwater modeling, to environmental degradation, to highly sophisticated analytical procedures, to applied regulatory policy. Attended by as many as 700 participants and regularly 150 to 200 paper or poster presenters, the Conference has seen participants from over 40 countries in its history, with nearly all 50 states represented. It also includes a valuable series of hands-on workshops in areas such as hazardous materials management, site investigation, and various remedial strategies.

This Proceedings edition provides a valuable and practical view of the environmental analysis and response sciences as well as engineering and legal perspectives that are reflected in the participants at the 24th annual presentation of this Conference originated and coordinated by the AEHS Foundation headquartered in Amherst, Massachusetts. The Conference is extraordinarily well-done and, as in years past, it is our pleasure to preface this most recent edition in the long-running series. Presenters, exhibitors, sponsors, conference staff, Scientific Advisory Boards, editors, and especially the AEHS Foundation, all are to be commended for continuing to support this excellent annual event which shares the beautiful California spring season.

David F. Ludwig, Ph.D.
Arcadis U.S.

Christopher M. Teaf, Ph.D.
Florida State University

About the Editors

Dr. Paul T. Kostecki's professional career has focused on research, education and training in environmental contamination with an emphasis on human and ecological risk assessment and risk management of soils. His work includes soil ingestion estimates for children and adults; establishment of scientifically sound cleanup levels for soil; bioavailability of soil contaminants; fish as toxicological models for contamination assessment; and assessment and management of petroleum contaminated soils. Dr. Kostecki has developed and conducted over 55 conferences, workshops and courses both nationally and internationally, and has made presentations at over 100 national and international meetings. Since 1985, his conference at the University of Massachusetts Amherst on Contaminated Soils, Sediments and Water has attracted over 10,000 environmental professionals from over 50 countries. Dr. Kostecki has published over 100 articles and reports, co-edited/co-authored 35 Books and secured over $15M in research support.

Dr. Kostecki co-created the Association for Environmental Health and Sciences (AEHS) in 1989 and served as its Executive Director until 2009. In 2009, he established the AEHS Foundation. He helped found Amherst Scientific Publishers and co-created seven peer-reviewed journals: Journal of Soil and Sediment Contamination (1990); Human and Ecological Risk Assessment (1994); Journal of Phytoremediation (1998); Journal of Environmental Forensics (1999); Journal of Children's Health (2003); Non-Linearity Journal (2003); and Journal of Medical Risks (2004). In addition, Dr. Kostecki co-created the International Society for Environmental Forensics in 2002.

Dr. Kostecki served as Vice Provost for Research and Vice Chancellor for Research and Engagement at the University of Massachusetts Amherst from 2003 to 2009. He served as Special Advisor for the Clean Energy China Initiative, Office of the President, University of Massachusetts from 2009–2011. He briefly left the University of Massachusetts Amherst to establish the online education program for Simmons College, Boston, MA (2011 -2012). He is presently Professor of Environmental Health in the School of Public Health and Health Sciences, University of Massachusetts, Amherst.

Dr. Edward J. Calabrese is a Professor of Toxicology at the University of Massachusetts, School of Public Health and Health Sciences, Amherst. Dr. Calabrese has researched extensively in the area of host factors affecting susceptibility to pollutants, and is the author of over 750 papers in scholarly journals, as well as more than 10 books, including Principles of Animal Extrapolation; Nutrition and Environmental Health, Vols. I and II; Ecogenetics; Multiple Chemical Interaction; Air Toxics and Risk Assessment; and Biological Effects of Low Level Exposures to Chemical and Radiation. Along with Mark Mattson (NIH) he is a co-editor of the recently published book entitled Hormesis: A Revolution in Biology, Toxicology and Medicine.

He has been a member of the U.S. National Academy of Sciences and NATO Countries Safe Drinking Water committees, and on the Board of Scientific Counselors for the Agency for Toxic Substances and Disease Registry (ATSDR). Dr. Calabrese also serves as Chairman of the Biological Effects of Low Level Exposures (BELLE) and as Director of the Northeast Regional Environmental Public Health Center at the University of Massachusetts. Dr. Calabrese was awarded the 2009 Marie Curie Prize for his body of work on hormesis. He was the recipient of the International Society for Cell Communication and Signaling-Springer award for 2010. Dr. Calabrese received an honorary Doctor of Science from McMaster University, Hamilton, Ontario in 2013. Over the past 20 years Professor Calabrese has redirected his research to understanding the nature of the dose response in the low dose zone and underlying adaptive explanatory mechanisms. Of particular note is that this research has led to important discoveries which indicate that the most fundamental dose response in toxicology and pharmacology is the hormetic-biphasic dose response relationship. These observations are leading to a major transformation in improving drug discovery, development, and in the efficiency of the clinical trial, as well as the scientific foundations for risk assessment and environmental regulation for radiation and chemicals.

Dr. David F. Ludwig is a systems ecologist by training and a risk assessor by trade. He took an undergraduate Bachelor of Science degree from Rutgers University, a Master's in Marine Biology at the Virginia Institute of Marine Sciences, and a PhD in Systems Ecology at the University of Georgia Institute of Ecology. His career linked environmental consulting with university teaching. He worked in academia, the private sector, and for regulatory agencies, a breadth of background the gives him unique perspectives on environmental matters.

Dave's career spanned the globe. He worked in mainland Asia, Pacific Oceania, the Middle East, Europe, the Caribbean, and throughout North America. He is broadly published in the technical literature, and co-author of books on urban ecology and the ecology and toxinology of true viper snakes. He provides weekly insights regarding environmental sustainability in a column published on the AEHS Foundation web site, titled "PeopleSystems and Sustainability: This Week in the Global Environment".

Dr. Christopher M. Teaf is a Board-certified toxicologist with broad experience in evaluation of potential effects from chemical exposures related to industrial facilities, agriculture, waste management facilities, power generation, educational institutions, and products in general commerce. Dr. Teaf has served on the faculty of the Center for Biomedical & Toxicological Research at Florida State University since 1979, and as Director of Toxicology for Hazardous Substance & Waste Management Research since 1985.

Chris' areas of interest include risk assessments under environmental and occupational elements of federal, state or local regulations, risk communication, and development of risk-based targets to guide remedial actions. He has extensive experience in evaluation of environmental fate and potential health effects from petroleum, solvents, metals, pesticides, pharmaceuticals, biological agents (e.g., mold, microbes) and physical agents (e.g., particulates, asbestos. For over 30 years, he has directed or conducted research in environmental and occupational toxicology for the World Health Organization, NATO, U.S. EPA, U.S. Air Force, U.S. Department of Agriculture (USDA), Florida Department of Environmental Protection, Florida Department of Health, Florida Department of Community Affairs, and Agency for Toxic Substances & Disease Registry (ATSDR), among others. He served as Toxicologist for the Florida Landfill Technical

Advisory Group and the state Petroleum Technical Advisory Committee. He served on the Florida Governor's Financial and Technical Advisory Committee and was Chair of the Toxic Substances Advisory Council for the Florida Department of Labor. Chris has organized and taught many graduate and undergraduate courses and technical seminars for presentation to universities as well as international, federal, state and local agencies. He has served as Chair of the Dog Island Conservation District since 2004.

Dr. Teaf has served on editorial boards or as peer reviewer for a variety of journals and is Senior Editor for Human Health of the international journal *Human & Ecological Risk Assessment*. In addition to training, research and advisory services to many environmental agencies and private sector firms, he has provided environmental and toxicological services to the U.S. Attorney, Florida State Attorney, and Attorneys General of FL, OK, and WA. Chris has been qualified as an expert in federal and state courts, as well as administrative proceedings, in a number of states regarding toxicology, health risk assessment, and environmental chemistry.

THE EFFECT OF AN INDUCED BENZENE PLUME ON MICROBIAL COMMUNITIES IN A GROUNDWATER AQUIFER MESOCOSM

Eferhire Aganbi[1,3§], Arturo Aburto-Medina[1,2], Anne Fahy[1], Terry J. McGenity[1] and Andrew S. Ball[1, 4]

[1]Department of Biological Sciences, University of Essex, Wivenhoe Park, Colchester, UK CO4 3SQ; [2]Universidad Autonoma Metropolitana Lerma, Lerma de Villada, 52006, México; [3] Biochemistry & Molecular Biology Department, Delta State University, Abraka, Delta State Nigeria; [4] School of Applied Sciences, RMIT University, Building 223, Bundoora West Campus, South Australia.

ABSTRACT

This study investigated the degradation of a benzene plume by indigenous microbial communities in sediments and groundwater from the SIReN (Site for Innovative Research in Natural Attenuation). A sandbox mesocosm system and microcosms were inoculated with SIReN sediments/groundwater and spiked separately with plume (starting concentration of 1000 mg/l^{-1}) and various concentrations of benzene (5 – 500 mg/l^{-1}).

Benzene plume was degraded almost at the point of entry, while in aerobic microcosms benzene was degraded to varying degrees by day 6 compared to killed controls. DGGE analysis of 16S rRNA gene (rDNA) allowed the detection of species closely related to *Rhodoferax ferrireducens* (95% similarity) and *Dechloromonas aromatica* RCB (99% similarity). Other organisms detected were closely related to *Methylotenera mobilis* strain JLW8 (92 – 96% similarity); *Nitrosomonas halophila* strain Nm 1 (97% similarity); *Insolitispirillum peregrinum* subsp. integrum strain LMG 5407 (99% similarity); and *Lactococcus lactis* strain SWU15983 (97% similarity).

Our results demonstrated that benzene contamination had a profound impact on *in situ* microbial community structure and composition. Furthermore, the abundance of organisms closely related to methylotrophic bacteria may be indicative of a more 'active' role in bioremediation for this group than previously known. Results from this study add to available information on the identity of benzene-degrading taxa that may be useful for the bioremediation of hydrocarbon-contaminated aquifers under microaerophilic conditions.

Keywords: Natural Attenuation, Microaerophilic, Contaminant Plume, Biodegradation

[§]Corresponding author: Dr. Eferhire Aganbi; Biochemistry & Molecular Biology Department, Delta State University Abraka, P.M.B 1 Delta State Nigeria; Tel: +(234) 8102570906; efeaganbi@hotmail.com

1. INTRODUCTION

The BTEX compounds (benzene, toluene, ethylbenzene and xylene isomers), which may be found in association with PAHs in contaminated sites, have been widely recognized as toxins of concern in petroleum products such as gasoline. These volatile organic compounds are highly soluble and pose a drinking water hazard when they accumulate in groundwater. Several studies have described the BTEX compounds as the most prevalent contaminants found in aquifers, and this, coupled with their ease of mobility in such contaminated aquifers, have resulted in the production of contaminant plumes within groundwater environments (Coates and Anderson, 2000). A fundamental difference between marine and aquifer sediments is that contaminants such as the BTEX compounds cannot readily escape by volatilization. Instead, these contaminants are distributed in different phases (non-aqueous, aqueous or vapour phases) among the various media (water, soil/sediment and soil vapour) in subsurface aquifer environments (Wiedemeier et al., 1999).

Benzene has been described as the most common groundwater contaminant due to its higher water solubility and dissolution rate compared to other monoaromatics (Njobuenwu et al., 2005; Fahy et al., 2006). Furthermore, benzene contamination in groundwater has serious environmental implications due to its reported toxicity and identified carcinogenic properties. The continuous release of relatively soluble monoaromatics like benzene into groundwater has been described as leading to the formation of a contaminant plume within the aquifer (Dean, 1985; Bolliger et al., 1999). The mode of formation of groundwater plumes can be categorized under four different source scenarios including the release of aqueous-phase contaminants to vadose or unsaturated zones (Wiedemeier et al., 1999).

The SIReN aquifer (Site for Innovative Research in Natural Attenuation) located in the northwest of England is a sandstone aquifer situated beneath a chemical plant that has been operational for over sixty years. Investigations carried out so far on this site have focused on contaminant status and the geochemical characteristics of groundwater from 76 monitoring wells. The results confirmed the aquifer was subjected to long-term pollution with variations in the concentrations of contaminants and geochemical characteristics, including pH, and benzene was found to be the principal contaminant (Jones et al., 2001). Fahy et al. (2005) found that communities from benzene-contaminated groundwaters sampled from different wells differed greatly from each other and were less diverse compared with those from uncontaminated wells.

Based on correspondence analysis of community profiles against groundwater physiochemical parameters, Fahy et al. (2005) concluded that prevailing anoxic conditions driven by benzene oxidation was responsible for the differences observed in the composition of microbial communities rather than benzene stress/toxicity. In another study, aerobic benzene degradation was found occurring under more alkaline conditions (pH 8.9 and 9.4) than previously reported in three of the most contaminated wells despite prevailing low redox potentials (Fahy et al., 2006). In a follow-up study, Aburto et al. (2009) used 16S rRNA gene clone library analysis to investigate the *in situ* microbial communities in groundwaters from four of the heavily contaminated wells. We found phylotypes typical of both aerobic and anaerobic microbes, and concluded that while oxygen at low concentrations was important for initiating benzene biodegradation, anaerobic microbes may also be involved in the degradation using a range of terminal electron-accepting processes (TEAP).

To further investigate the microbial communities that played a significant role during natural attenuation processes in the SIReN site, we introduced an artificial benzene plume in a mesocosm system containing groundwater from well W6s (previously described as relatively clean; Jones et al., 2001; Aburto and Ball, 2009) and aquifer sediment from within the site. The aim was to investigate changes in indigenous microbial community structure in response to the induced benzene plume, and to observe the effects of a benzene concentration gradient on microbial communities.

2. MATERIALS AND PROCEDURE

2.1 Sampling sites and sandbox dimensions

Groundwater samples used in these sets of experiments were collected from a well within the SIReN site designated W6s with a relatively shallow depth and low BTEX concentrations (< 1 μg l^{-1}); meanwhile, aquifer sediment (brown, muddy sand) was collected from an area between two wells (W6s and W6d). The sandbox used as the mesocosm system was constructed from glass to avoid the sorption of benzene into the surrounding vessel. The length, height, width and volume of the entire box were: 80 cm, 10 cm, 10 cm and 8000 cm^3; it featured an antechamber that was separated from the rest of the box by a removable shutter. Antechamber length, height, width and volume were: 10 cm, 10 cm, 10 cm and 1000 cm^3 (Fig. 1).

2.2 Sample preparations, sandbox set-up and subsample collection

To obtain a homogenized sediment material, sediments were sifted twice using sieves with pore sizes of 0.8 cm and 0.4 cm, respectively. In order to make sediments less muddy, the SIReN sediments were mixed with sandstone from Burntstump quarry; this sandstone has the same formation as sandstone from the SIReN aquifer. Burntstump sandstone was also sifted using a finer sieve with a pore size of 0.2 cm before blending with the aquifer sediment (one part Burntstump sandstone to three parts of sieved SIReN sediment). The result was homogenized sandy sediment that was used for the experiments. Homogenized aquifer sediment was mixed with groundwater to the required slurry consistency, and was henceforth referred to as the aquifer material. Based on empirical calculations, 29 ml of groundwater was required for complete saturation of 100 ml homogenized sediment, implying that in a volume of 100 cm^3 of final aquifer material (groundwater + sediment), there was 29 ml of groundwater, which is the medium of transport for the benzene plume. Table 1 shows the main properties of final aquifer material used in the sandbox experiments.

Both antechamber and the rest of the sandbox were filled with either untreated (live experiment) or autoclaved (killed experiment) aquifer material until about 2 cm to the top of the box. For the live experiment, a 2000 ml glass bottle was also filled with non-sterile groundwater and connected to the sandbox antechamber to allow groundwater flow through the box. The glass bottle containing groundwater was placed on an elevated support to induce the flow of groundwater through the sandbox by gravity. Another glass bottle was put in place to collect the flow-through from the sandbox, and the amount of flow-through collected was measured daily. After an initial trial run using 100 mg/l^{-1} of benzene (24.51 μl), 1000 mg/l^{-1} of benzene (244.33 μl) was added to the antechamber (for live and killed experiments) and the sandbox was

incubated in the dark in a fumehood for 48 h at room temperature prior to subsampling. Room temperature varied for the duration of the experiments with an average of 17°C, maximum and minimum temperature readings were 22.9 and 9.6°C. Subsamples (1 ml) were collected in sterile 20 ml serum bottles from the sandbox weekly from six sampling points labeled SB0, SB1, SB2, SB3, SB4, and SB5 (Fig. 1). Collected subsamples were crimp sealed immediately with PTFE-lined septa and allowed an equilibration time of 6 h prior to benzene quantification by headspace analysis using gas chromatography (GC) with flame ionisation detection (FID). Following the same procedures above, a 2000 ml glass bottle filled with sterile groundwater was used in the killed experiment. To ensure consistency in the amounts of groundwater/sediment collected at each point, aquifer material was stirred slightly before subsamples were taken.

The proposed groundwater flow rate was 85 ml/day^{-1}, however, due to the clogging of tubes with sediment from the sandbox, the flow of groundwater was often interrupted and it was impossible to attain the proposed groundwater flow rate. Instead, an average flow rate of 22 ml/day^{-1} was attained during an incubation period of 68 days, with maximum and minimum rates of 81.7 and 2.7 ml/day^{-1}, respectively. For the killed experiment, an average flow rate of 72 ml/day^{-1} was achieved between day 0 and 54, with maximum and minimum rates of 239 and 8.2 ml/day^{-1}. Within these periods of incubation, the total amount of groundwater flow-through collected was 1287 ml for the live experiment and 2793 ml for the killed experiment.

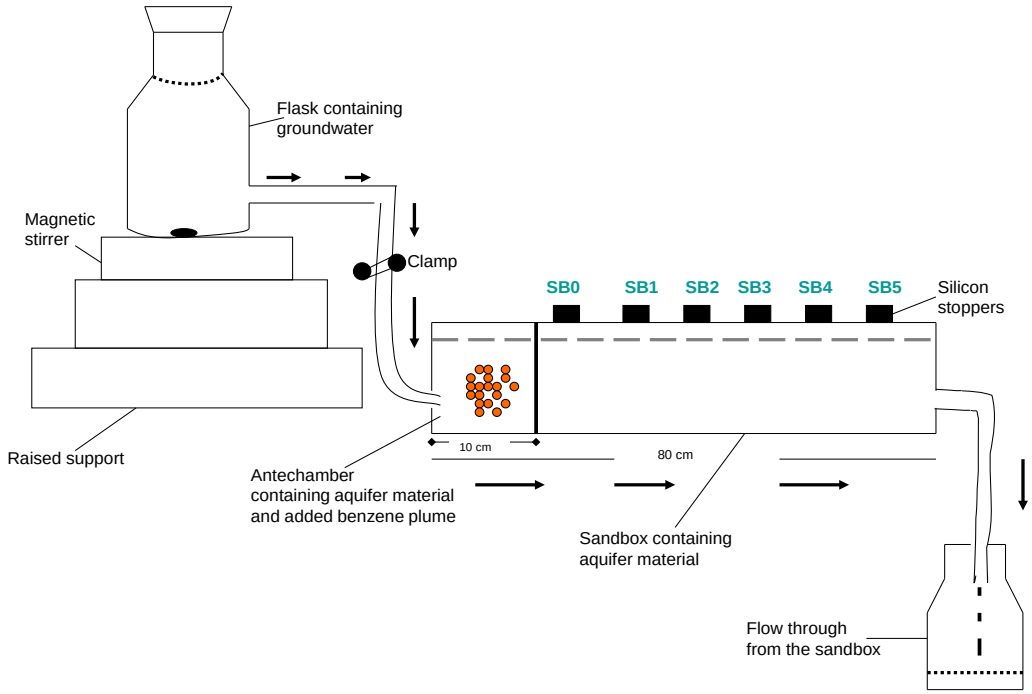

Fig. 1: A schematic representation of the sandbox experimental set-up, showing antechamber and sampling points SB0 to SB5; dark arrows indicate the direction of groundwater flow.

Table 1: Properties of final aquifer material used in the sandbox experiments.

Properties	Antechamber	Rest of Sandbox
Final volume of aquifer material (ml)	740	5950
Groundwater volume in aquifer (ml)	215	1726
Amount of benzene added (µl)	244.3	None added

2.3 Preparation of aerobic microcosms

Alongside the sandbox experiments, aerobic microcosms were established in sterile 110 ml serum bottles and inoculated with 10 ml of aquifer material exactly as used in the sandbox. Microcosms were prepared in triplicate with no benzene background and sterile killed controls prepared alongside. No nutrients were added to these microcosms. With the exception of the background controls, all microcosms were amended with the following concentrations of benzene: 5, 50, 100, 250, and 500 mg/l^{-1}. All samples were crimp sealed with PTFE-lined septa and incubated in the dark at room temperature without shaking, and the initial concentrations of benzene were measured from the headspace using a GC-FID after 6 h.

2.4 Benzene quantification in microcosms and sandbox subsamples

Benzene concentration in sample headspace was measured using a Philips PU4500 gas chromatograph with a glass packed column (10% apiezon on chrommowax, 60-80 mesh) and nitrogen as the carrier gas. To monitor benzene degradation in sandbox and microcosms over time, separate external standard solutions of benzene in the concentration range 0 – 500 mg/l^{-1} were prepared for the purpose of calibration. Benzene concentration in the sandbox was monitored over time by taking measurements in subsamples. Initially collected twice a week at points SB0 - SB5, this was later reduced to once a week for the duration of both live and killed experiments. Although both test and killed experiments were set up at different times, the same starting concentration of benzene (1000 mg/l^{-1}) was added to the antechamber and similar procedures were followed to ensure consistency. Benzene concentration was measured in subsamples and in microcosms after allowing an initial 6 h equilibration time at room temperature. GC conditions were: injector 250°C, column 100°C, and detector 250°C. In all cases, a 200 µl headspace volume was injected and measurements were taken at high instrument sensitivity.

2.5 Nucleic acid extraction and PCR

Nucleic acids were extracted from aerobic cultures once benzene degradation was established from sandbox subsamples collected between day 2 to day 68 using Lysis Matrix B columns (Bio 101 System, Q-Biogene®), and following the method described by Manefield et al. (2002). Briefly, 2 ml slurry (aerobic microcosms) or 1 ml sandbox subsample was transferred into sterile eppendorf tubes; these were centrifuged for 10 min at 2300 *g* (centrifuge model: Eppendorf 5415R) to compact sediment/microbes. In each case, pelleted cells were resuspended in 0.5 ml of 0.1 or 0.24 M sodium phosphate buffer (pH 8.0) and 0.5 ml of phenol-chloroform-isoamyl alcohol (25:24:1; pH 6.7 - 8). Following bead beating in lyzing matrix B tubes, cleaning and repeated centrifugation steps were carried out as detailed in the protocol. Nucleic acids were precipitated on ice for 30 min by adding 0.1 volume of 3 M sodium acetate (pH 5.2) and 2.5 volumes of ice-cold absolute ethanol. Pelleted nucleic acids were washed with 70% v/v ethanol and air-dried before resuspending in 100 µl of DEPC-treated water. DNA preparations were diluted as required (1:10 or 1:100) and used as template DNAs in the polymerase chain reaction (PCR).

Partial 16S rRNA gene fragments were obtained from PCR amplification using bacterial primers originally designed by Muyzer et al. (1993) and purchased from Invitrogen. Primer 1, forward primer with GC clamp (5'-CGC CCG CCG CGC GCG GCG GGC GGG GCG GGG GCA CGG GGG GCC TAC GGG AGG CAG CAG-3') and primer 2, reverse primer (5'-ATT ACC GCG GCT GCT GG-3'), specifically amplified the variable V3 region of the 16S rRNA gene (*Escherichia coli* positions 341-534) (Muyzer et al., 1993). PCR mixture contained 200 µM of each deoxyribonucleoside triphosphate (dNTP), 0.4 µM of each primer, 5 µl of PCR buffer supplied with the enzyme (Qiagen®), 5 µl of 1 mg l^{-1} α-casein, 2.5 U Taq DNA polymerase, and 5 µl of template DNA to a final reaction volume of 50 µl with sterile distilled water. Amplification was performed in a Gene Amp® PCR system 9700 Thermocycler (Applied Biosystems) as follows: an initial denaturation at 94°C for 2 min; 30 cycles of denaturation at 94°C for 1 min; annealing at 55°C for 1 min; extension at 72°C for 2 min; and a final elongation at 72°C for 10 min. Amplification of target PCR products was confirmed by electrophoresis on agarose gel (2% w/v). Loaded gels were run in 1× TAE buffer (40 mM Tris-acetate, 1 mM di-sodium-EDTA, pH 8.0) at 125 V for 40 min, ethidium bromide stained, and then viewed with a UV transilluminator (Gene Doc).

2.6 DGGE analysis of microbial communities

DGGE (denaturing gradient gel electrophoresis) analysis of PCR products with a GC clamp was performed without purification using the Bio-Rad DCODE system on gels consisting of 8% (w/v) polyacrylamide (acrylamide:bisacrylamide, 37:1), with a denaturing gradient from 40% to 60% [100% denaturant is 7 M electrophoresis grade urea (Sigma), and 40% v/v formamide (Fluka)] in 1× TAE buffer at a constant temperature of 60°C and 100 V initially for 30 min, then reduced to 60 V for 16 h.

Gels were stained by silver nitrate staining following previously described protocol (Radojkovic and Kušic, 2000; Mahmood et al., 2006) and later scanned. Dominant bands were excised within 1 h, resuspended in 30 µl sterile ultra high pure (UHP) water, and stored at 4°C overnight to allow the elution of DNA. The aqueous layer (5 – 10 µl) containing eluted DNA was reamplified as described previously, except a forward primer (5'-CCT ACG GGA GGC AGC AG-3') without the GC clamp was used. PCR products were run on agarose gel (2% w/v in 1× TAE

buffer at 125 V), ethidium bromide stained, and viewed with a UV transilluminator (Gene Doc) to confirm product of the right size. Only products with expected size were cleaned using QIAquick PCR Purification Kit (Qiagen) according to manufacturer's protocol. Cleaned PCR products were confirmed again by agarose gel electrophoresis as described previously prior to sequencing and identification.

2.7 Sequencing

Sequencing reaction contained 2-5 µl of cleaned PCR product, 4 µl of 5× sequencing buffer, 0.5 µl of the Big Dye Terminator v3.1 (PE Applied Biosystems), 1 µl of reverse or forward primer (0.2 µM), and sterile DEPC-treated water to a final volume of 20 µl. Cycle sequencing conditions were: 96°C for 15 s; 25 cycles of 96°C for 15 s; and 55° for 15 s, with a final extension of 60°C for 4 min.

The generated sequencing reaction products containing fluorescent DNA were purified by precipitation with 0.2 mM $MgSO_4$ in absolute ethanol before products were run on an ABI Prism 3100 Genetic analyzer (PE Applied Biosystems) following the manufacturer's protocol. Sequences were then processed with DNA Sequencing Analysis Software version 3.3, and sequence identities were compared with the GenBank nucleotide database library by FastA analysis. Prior to manuscript submission, BLAST searches were conducted to update sequence identities.

3. DATA AND ANALYSIS

3.1 Benzene degradation by microbial communities in sandbox and microcosms

Sandbox experiments were established to mimic a benzene-contaminated sandstone aquifer in the laboratory and aimed to monitor the flow of an induced benzene plume, as well as investigate changes in indigenous microbial communities in response to a benzene plume based on PCR-DGGE analysis of 16S rRNA genes. Fig. 2 shows the degradation curves for benzene at points SB0, SB1, SB2, SB3, SB4 and SB5 for both test and killed experiments. In the live experiment (Fig. 2A), benzene concentration in the sandbox increased gradually at SB0 only while concentrations were consistently low at points SB1 to SB5. The highest mean benzene concentration of 32.43 mg/l^{-1} was obtained at SB0 on day 8. Concentrations, however, began to decrease at SB0, and by day 68 when final measurements were taken, benzene concentration was 3.55 mg/l^{-1}.

In the same manner, benzene concentrations increased gradually only at SB0 during the killed experiment (Fig. 2B), however, the increase was at least ten times the amount detected within the same period in the live experiment. This indicated that benzene was involved in some processes (e.g. microbial degradation) that reduced the amounts transported to SB0 in the live experiment, hence the low concentrations detected.

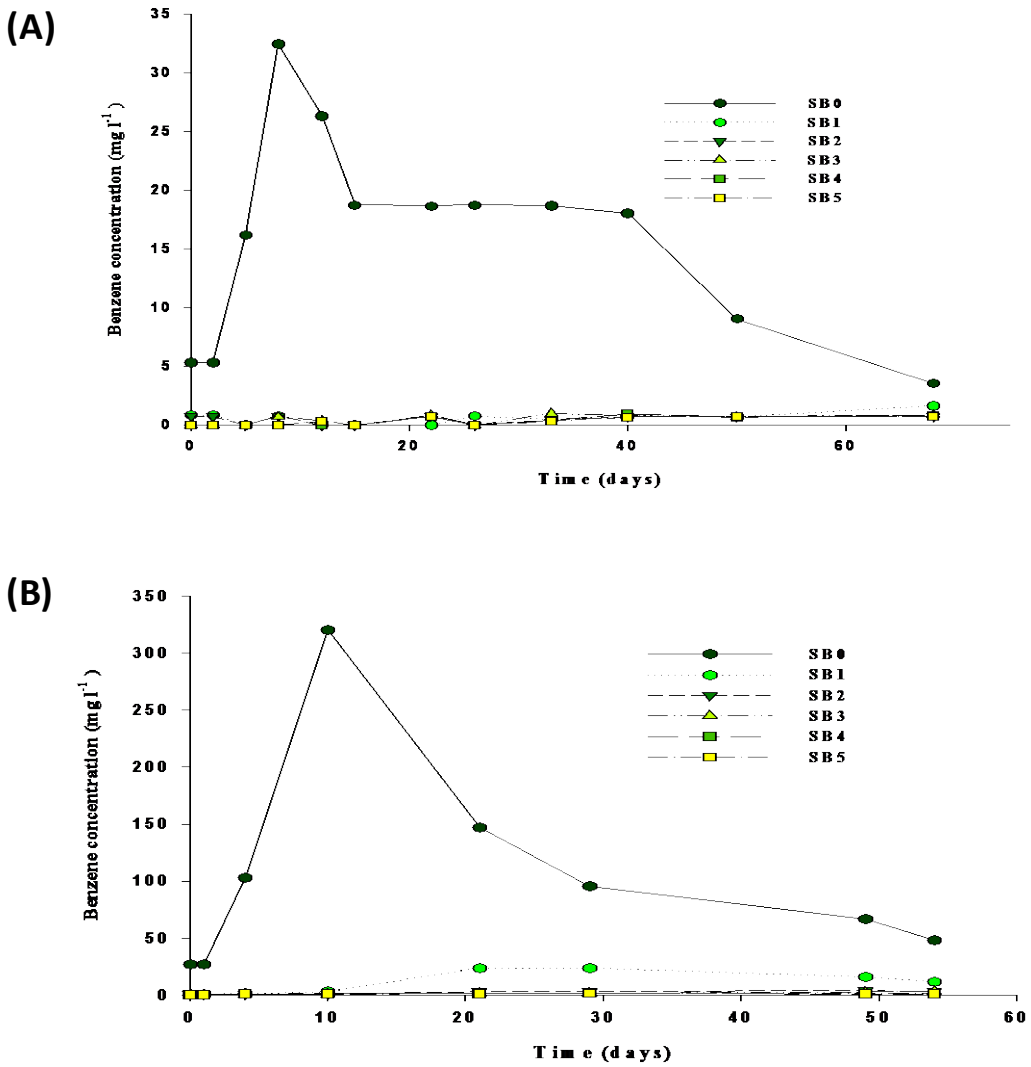

Fig. 2: Curves for benzene degradation(s) in the sandbox over the period of incubation at points SB0 to SB5 [A] test (live) experiment; [B] killed experiment; mean concentrations used, n = 2.

To further analyse the possibility that abiotic processes alone were not responsible for the consistently lower benzene levels observed at SB0, and indeed the rest of the sandbox during the live experiment, we estimated the distance moved by the plume head in the sandbox using the sandbox dimensions and the amount of flow-through collected for each period. Based on the assumption that the head of the benzene plume moved in small distances of 1 cm, we obtained a mean flow rate of approximately 22 ml/day^{-1} and 72 ml/day^{-1} for live and killed experiments, respectively. Therefore, assuming neither degradation nor abiotic processes were affecting benzene movement in the live experiment, the plume head was already at SB0 on day 2 when first benzene measurements were taken, and should be detected at SB1 by day 12. Then, by day 68, the benzene plume should be mid-way between SB4 and SB5, hence high benzene concentrations relative to the amounts added should be detected at SB4 by day 68. However, the observed movement pattern for the plume head in the live experiment was contrary to that

estimated since the benzene plume never moved far from SB0, and was probably being utilized straight away by benzene-degrading microorganisms in the sandbox (Fig. 2A).

In contrast, the average flow rate of 72 ml/day^{-1} obtained for the killed experiment suggested that the plume head moved faster than initially assumed (1 cm). This notwithstanding, benzene concentration increased rapidly at SB0 (up to ten times the amount detected in the live experiment) within the first 10 days, while aquifer material in the sandbox remained sterile. There were also noticeable increases in benzene concentration at SB1 during the killed experiment compared with SB1 in the live experiment. The sandbox quickly became contaminated during the killed experiment, resulting in a significant decrease in benzene concentrations by day 21 (Fig. 2B). This could be attributed to microbial degradation brought on by the regrowth of unkilled microorganisms in aquifer sediment. As was the case in the live experiment, observed degradation at SB0 also prevented the formation of a concentration gradient across points SB0 to SB5 in the sandbox. For the aerobic microcosms, benzene concentrations in nearly all test samples (exceptions for 500 mg/l^{-1}-amended cultures) decreased significantly by day 6 compared with killed controls ($P< 0.05$) [data not shown].

3.2 Effects of benzene plume and concentration gradient on indigenous microbial communities

DGGE analysis of PCR-amplified 16S rRNA genes was carried out to examine the effect of the introduced benzene plume on the aquifer microbial communities. DNA was extracted from subsamples taken from points SB0 to SB5 at different time points throughout the incubation period, and the bacterial community structure was examined by PCR amplification of 16S rRNA genes, followed by DGGE analysis (Fig. 3 and 4). Similar banding patterns were observed in the profiles for initial aquifer material and samples collected from point SB0 only between day 2 and day 15 (Fig. 3). The presence of new bands are also shown, indicating the occurrence of a new species at point SB0 that were absent from the original aquifer community. Fig. 3 shows the DGGE profiles for samples collected across the sandbox (SB0 to SB5) at day 15 of the live experiment. Again, new bands that were absent from initial aquifer sediment were observed and are clearer at sampling points SB0, SB1 and SB2. Numbered bands were sequenced, and details of their closest or most similar relatives are given in Table 2. Prominent among these were bands 10 and 11 obtained in samples from SB0, SB1 and SB2; sequences derived from these two bands were most similar to *Rhodoferax ferrireducens* (94% similarity) and *Albidiferax ferrireducen* (91% similarity).

The fact that bands 10 and 11 were not detected in the rest of the sandbox strongly suggests that they were specifically stimulated by the presence of benzene at these points in the sandbox.

The DGGE profiles for samples collected at days 2 and 33 across the sandbox is shown in Fig. 4, and like the DGGE profiles in Fig. 3, the samples analyzed shared common bands, but also showed either the appearance of new bands or the disappearance of prominent bands. For example, band SK7 was prominent in all samples on day 2, but was no longer prominent on day 33 in SB0. Given that SB0 was the point where high benzene concentration was detected in the sandbox, it is possible that the species represented by this band are either benzene intolerant, or may have been out-competed by benzene-degrading microorganisms. As a confirmation, organisms represented by this band were closely related to *Lactococcus lactis* strain IL1403 (97% similarity), an organism with no known benzene degradative ability or intolerance.

Interestingly, there was the emergence of two new bands (SK11 and SK13) in the profiles obtained from SB0 on day 33. Although there are faint traces of similar bands to SK11 in the rest of the 33rd day samples, band SK13 was only present at point SB0 where most of the benzene plume was detected. Neither band SK11 or SK13 was detected for any of the samples on day 2 (i.e. before benzene had reached SB0), or indeed in the original aquifer material. Cluster analysis based on the unweighted-pair group method averages (UPGMA) confirmed that while time was an important factor in the clustering of the communities, the most different component was SB0 day 33 (data not shown), which was the only sampling time that benzene degradation was observed. The closest relatives for sequenced bands labeled in Fig. 4 are presented in Table 3.

With the exception of bands SK11, SK12 and SK13, all the other bands sequenced matched closely with Betaproteobacteria isolates (HTCC349 or BP-5), strains of an uncharacterised aquatic bacterium, and/or strains of known methylotrophs (96 – 97% similarity). Band SK11 (SB0 day 33) was closely related to a Betaproteobacterium isolate PB7 (95% similarity) and *Rhodoferax ferrireducens* (95% similarity). In the same way, sequences for bands 10 and 11 (SB1 and SB2, day 15) (Fig. 3B) were also most similar to isolate PB7 and *Rhodoferax ferrireducens* (91 – 96% similarity). The sequence for band SK13, on the other hand, matched closely with *Dechloromonas aromatica* RCB (99% similarity) and strain BH203 (100% similarity). Apart from its involvement in perchlorate reduction, *Dechloromonas aromatica* RCB is one of the two *Dechloromonas* strains in pure culture now known to degrade benzene anaerobically using nitrate as an electron acceptor (Coates et al., 2001). The results obtained from the PCR-DGGE analysis of the sandbox samples revealed the existence of a diverse microbial community in the sandbox aquifer that included hydrocarbon-tolerant *Methylophilus* spp. In addition, the introduction of a benzene plume led to the stimulation of benzene-degrading communities represented by bands SK11 and SK13 for SB0 on day 33 (Fig. 4), the point and time at which benzene degradation was observed.

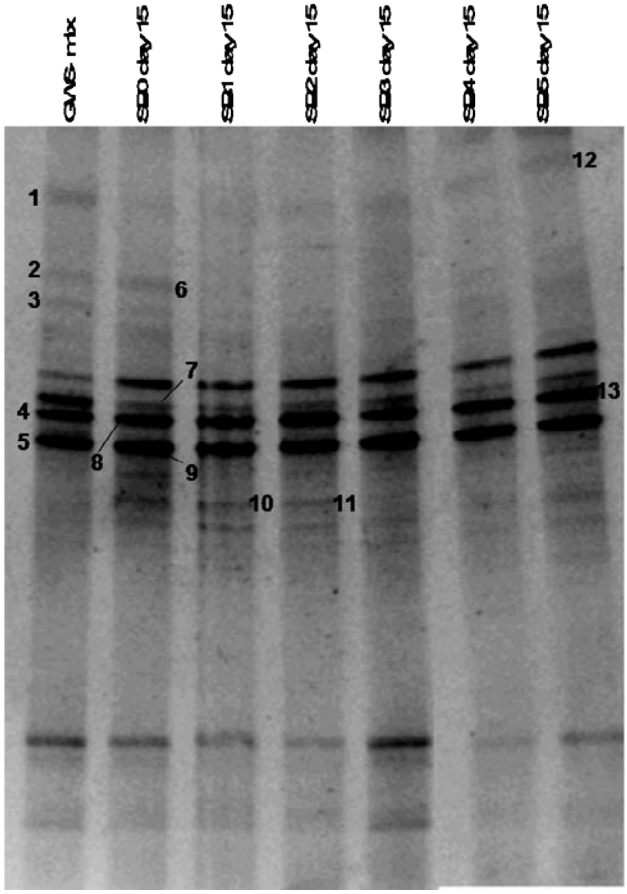

Fig. 3: DGGE profiles of PCR-amplified 16S rRNA genes from sandbox mesocosm (live experiment), samples collected across sandbox from points SB0 to SB5 on day 15; GWS-mix = initial aquifer material with no benzene added, sequences were obtained for numbered bands, see Table 2.

Table 2: Sequenced bands (Fig.3) and their 16S rRNA gene sequence similarities to closest relatives. GWS-mix to bands 1 – 5, SB0 day 15 to bands 6 - 9, SB1 day 15 to band 10, SB2 day 15 to band 11, and SB5 day 15 to bands 12 – 13.

Band number	Closest relative (s)	Accession number	% Similarity
1	*Methylotenera versatilis* strain 301	NR_074693	93
2 / 6	*Methylotenera mobilis* JLW8 strain JLW8	NR_102842.1	93
3	Beta proteobacterium HTCC349	AY429717	96
4	*Methylotenera mobilis* JLW8 strain JLW8	NR_102842.1	92
5	*Nitrosomonas halophila* strain Nm 1	NR_104817	97
7	*Lactococcus lactis* strain SWU15983	KF673548.1	97
8	*Insolitispirillum peregrinum* subsp. integrum strain LMG 5407	NR_044315.1	99
9	*Hydrogenophaga bisannensis* strain K102	NR_044268.1	93
10	*Rhodoferax ferrireducens*	AM265401	94
11	*Albidiferax ferrireducens*	NR_074760.1	91
12	*Corynebacterium resistens* DSM 45100	NR_074826.1	98

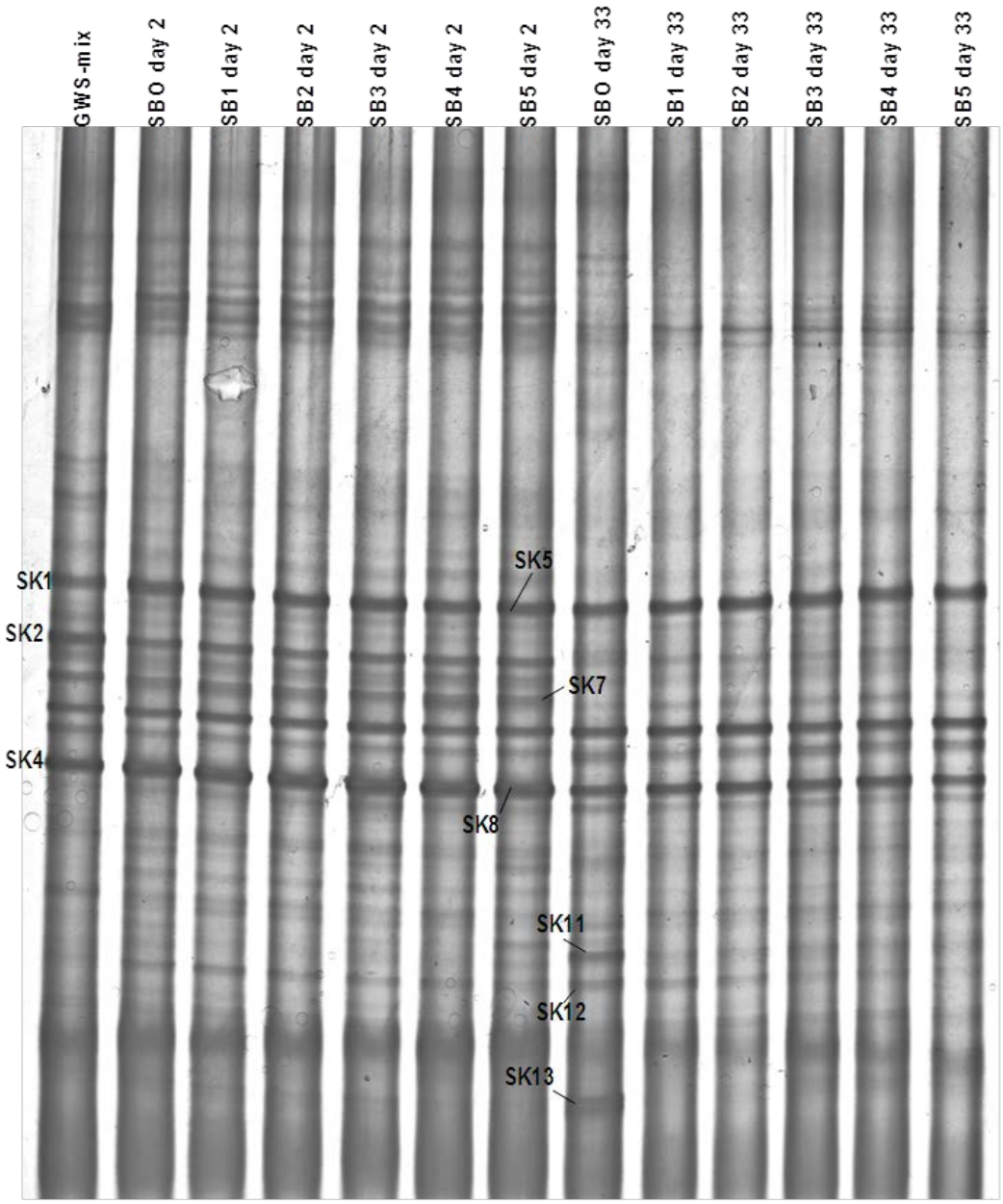

Fig. 4: DGGE profiles of PCR-amplified 16S rRNA genes from sandbox mesocosm (live experiment), samples were collected from points SB0 to SB5 at day 2 and day 33; GWS-mix = initial aquifer material with no benzene added, see Table 3 for identity of sequenced bands.

Table 3: Sequenced bands (Fig.4) and their 16S rRNA gene sequence similarities to closest relatives. GWS-mix to bands SK1, SK2 & SK4; SB5 day 2 to bands SK5, SK7 & SK8; and SB0 day 33 to bands SK11- SK13.

Band number	Closest relative (s)	Accession number	% Similarity
SK1 /SK 5	*Methylotenera mobilis* strain JLW8	NR_102842.1	96
SK2	*Nitrosomonas halophila* strain Nm1	NR_104817.1	97
SK4 / SK 8	*Methylotenera mobilis* strain JLW8	NR_102842.1	96
SK7	*Methylophilus methylotrophus*	AB193724	93
SK11	*Rhodoferax ferrireducens*	AM265401	95
SK12	*Dechloromonas aromatica* RCB	CP000089	89
SK13	*Dechloromonas aromatica* RCB	CP000089	99

4. CONCLUSION

The sandbox experiment was designed to mimic a benzene-contaminated sandstone aquifer in the laboratory, and aimed to investigate changes in indigenous microbial communities in response to an induced benzene plume based on PCR-DGGE analysis of 16S rRNA genes. Additionally, it also aimed to monitor microbial responses to a benzene concentration gradient introduced as the benzene plume moved across the sandbox. Benzene degradation curves for the sandbox live experiment (Fig. 2A) revealed there was no benzene concentration gradient across the sandbox, instead, most of the benzene plume never reached SB1 and was eventually degraded by benzene-degrading microbes stimulated mainly before and at point SB0. However, there is an indication that some benzene did eventually reach points SB1 and SB2, since organisms with sequences most similar to *Rhodoferax ferrireducens* were detected at these points by day 15 (bands 10 and 11, Fig. 3). Recently, Kaden et al. (2014) proposed based on their study, the reclassification of *Albidiferax ferrireducens* to the genus *Rhodoferax*. The original flow rate of 85 ml/day^{-1} was not obtained, and instead an average flow rate of 22 ml/day^{-1} meant that the plume was moving approximately four times slower than intended. Nevertheless, the detection of *Rhodoferax ferrireducens* (91 - 95% similarity) and *Dechloromanas aromatica* RCB (99% similarity) (bands 10 and 11, Fig.3; SK11 and SK13, Fig. 4) as the closest identified species at SB0 strongly suggests that they were responsible for the degradation of benzene observed at this point.

Rhodoferax ferrireducens has been described as a potentially important organism in the subsurface; its many roles include the unique ability to convert sugars into electricity (Chaudhuri and Lovley, 2003), and the capability to grow on a range of aromatic substrates coupled with Fe (III) reduction. For example, clones from an iron-reducing enrichment originating from a diesel-contaminated groundwater were shown to be dominated by a bacterium closely related to *Rhodoferax ferrireducens* (Eriksson et al., 2005). Another study involving the genome-scale metabolic modeling of *R. ferrireducens* revealed the presence of novel genes for benzoate degradation in addition to previously identified genes (Risso et al., 2009). The pathways leading to the degradation of benzoate appears to be the route for aromatic hydrocarbon metabolism in *R. ferrireducens*, and furthermore, it has been suggested that the genes involved are likely to be active under aerobic and anaerobic conditions (Risso et al., 2009).

Although we could not observe aerobic benzene degradation in microcosms dominated by *Rhodoferax* spp. (Fahy et al., 2006), we have detected *Rhodoferax antarcticus* in adapted benzene-degrading microcosms from sample 308i from the SIReN site (Aburto and Peimbert, 2011), and most importantly, we have found clones that are closely related to *Rhodoferax ferrireducens* (96% similarity) in groundwater samples also from the SIReN site (wells DW3d and W18i) [Aburto et al., 2009]. The clones in question were also highly similar to other clones recovered from a benzene-contaminated aquifer in Germany (Alfreider and Vogt 2007), and to a couple of clones from a petroleum-contaminated site in Michigan, USA (Allen et al., 2007). Recent studies have also detected the predominance of *Rhodoferax* spp. (*antarcticus* and *ferrireducens*) in landfills (Han and Kim, 2010) and BTEX-contaminated groundwater (Táncsics et al., 2012), providing more evidence that these species are associated to oxygen-limited aromatic hydrocarbon-contaminated subsurface environments. Consistent with these reports, this study clearly demonstrated the stimulation of species closely affiliated to *Rhodoferax ferrireducens* (95% similarity) in response to the induced benzene plume, confirming that

Rhodoferax ferrireducens played an important role in the degradation of benzene and its derivatives in the sandbox mesocosm.

An important question that arises is the type of terminal electron-accepting process (TEAP) being used to carry out the benzene degradation in the SIReN aquifer since members of the genus *Rhodoferax* are known facultative anaerobes and have been reported as capable of using a range of electron acceptors, including Fe(III), nitrate, and oxygen (Finneran et al., 2003). A second band (SK13) detected at point SB0 where benzene degradation was observed matched closely with two unidentified bacteria, bacterium BH203 and a perchlorate-reducing bacterium (100% similarity), as well as *Dechloromonas aromatica* RCB (99% similarity). Perchlorate-reducing microorganisms have previously been isolated from contaminated sites and some of these isolates have been described as closely related to different species of the genus *Dechloromonas* (Bruce et al., 1999; Coates et al., 1999a; Coates et al., 1999b; Waller et al., 2004). This indicates that members of the genus *Dechloromonas* are also capable of chlorate reduction. *Dechloromonas aromatica* has also been detected in landfills (Han and Kim, 2010) and BTEX-contaminated groundwater (Táncsics et al., 2012).

More importantly, the strain *Dechloromonas aromatica* RCB is a known benzene-degrading bacterium that carries out benzene degradation coupled with nitrate reduction (Coates et al., 2001) despite not containing known genes for anaerobic catabolism, but genes for aerobic degradation (Salinero et al., 2009). There are strong indications that this strain had the leading role in the degradation of benzene in the sandbox mesocosm due to its unique band (SK13, Fig. 4) being only visible at the benzene plume location (SB0), and at the time when most of the benzene had been used (day 33).

Other microbial species that matched closely with sequenced bands in particular were species of methylotrophic bacteria that may have played a role in aerobic benzene degradation. *Methylotrophs* have not been known to utilize hydrocarbon substrates directly. However, it has been suggested that they played the role of pollution-resistant microorganisms and can improve bioremediation substantially by increasing the capabilities of indigenous hydrocarbon-degrading microorganisms (Roane et al., 2001; De Marco et al., 2004). For example, novel methylotrophic strains with traits of resistance to pollutants such as benzene and xylenes have been isolated (De Marco et al., 2004). It was shown that these strains were able to grow using a number of C1 compounds (including methane, methylamines, methanol and formate) in a pollutant-saturated atmosphere.

Furthermore, the methylotroph *Methylibium petroleiphilum* has been reported to degrade methyl tert-butyl ether (Nakatsu et al., 2006). Additionally, hydrocarbon plumes detected in the *Deepwater Horizon* oil spill were dominated by methylothrophs after the well was capped (Redmond and Valentine, 2012). The application of *Methylotrophs* in the bioremediation of aromatic hydrocarbons remains speculative since no evidence has been provided to substantiate this claim. Nevertheless, the detection of organisms closely related to *Methylotenera mobilis* strain JLW8 and four strains of *Methylophilus* spp. in samples from our sandbox aquifer material and microcosms (DGGE data not shown) suggest that these species may be playing a more active role in the SIReN aquifer community than previously known.

We conclude that the detection of species related to known anaerobic hydrocarbon degraders like *Rhodoferax ferrireducens* and *Dechloromonas aromatica* RCB in the sandbox strongly indicated that these organisms played a key role in the degradation of benzene under microaerophilic

conditions. Further studies on their diversity and specific function in terms of hydrocarbon degradation in subsurface sediments with trace amounts of oxygen is required to increase present understanding about their potential use as model hydrocarbon-degraders during monitored natural attenuation processes in the SIReN site in particular, and contaminated aquifer environments in general. There is also the need to explore the specific role(s) of members of the family *Methylophilaceae* in the treatment of contaminated groundwater and/or as microbial indicators of hydrocarbon contamination.

5. ACKNOWLEDGEMENTS

This work was carried out as part of the Bioremediation LINK Programme: project ISMoNACh (Integrated Strategy for Monitoring Natural Attenuation using Chemical Fingerprinting and Molecular Analysis). We thank Anne Fahy for collecting groundwater/sediment samples from the SIReN and providing helpful suggestions.

6. REFERENCES

Aburto, A.; Fahy, A.; Coulon, F.; Lethbridge, G.; Timmis, K.N.; Ball, A.S. and McGenity, T.J. (2009) Mixed aerobic and anaerobic microbial communities in benzene-contaminated groundwater. *J. Appl. Microbiol*. **106**: 317 – 328.

Aburto, A. and Ball, A.S. (2009) Bacterial population dynamics and separation of active degraders by stable isotope probing during benzene degradation in a BTEX-impacted aquifer. *Rev. Int. Contam. Ambient.* **25** (3): 147 – 156.

Aburto, A. and M. Peimbert (2011) Degradation of a benzene–toluene mixture by hydrocarbon-adapted bacterial communities. *Ann. Microbiol* **61**(3): 553-562.

Alfreider, A. and C. Vogt (2007) Bacterial diversity and aerobic biodegradation potential in a BTEX-contaminated aquifer. *Water Air & Soil Pollution.* **183**(1): 415.

Allen, J. P., E. A. Atekwana, et al. (2007) The Microbial Community Structure in Petroleum-Contaminated Sediments Corresponds to Geophysical Signatures. *Appl. Environ. Microbiol.* **73**(9): 2860-2870.

Bolliger, C., Höhener, P., Hunkeler, D., and Häberli, K.a.Z.J. (1999) Intrinsic bioremediation of a petroleum hydrocarbon-contaminated aquifer and assessment of mineralization based on stable carbon isotopes. *Biodegradation* **10:** 201-217.

Bruce, R.A.; Achenbach, L.A. and Coates, J.D. (1999) Reduction of (per) chlorate by a novel organism isolated from paper mill waste. *Environ. Microbiol.* **1:** 319-329.

Chaudhuri, S.K. and Lovley, D.R. (2003) Electricity generation by direct oxidation of glucose in mediatorless microbial fuel cells. *Nat. Biotechnol*. **21** (10): 1229 – 1232.

Coates, J.D. and Anderson, R.T. (2000) Emerging techniques for anaerobic bioremediation of contaminated environments. *Trends in Biotechnology.* **18:** 408-412.

Coates, J.D., Chakraborty, R., Lack, J.G., O'Connor, S.M., Cole, K.A., Bender, K.S. and Achenbach, L.A. (2001) Anaerobic benzene oxidation coupled to nitrate reduction in pure culture by two strains of *Dechloromonas*. *Nature* **411:** 1039-1043.

Coates, J.D., Bruce, R.A., Patrick, J .and Achenbach, L.A. (1999a) Hydrocarbon bioremediative potential of (Per) chlorate-reducing bacteria. *Bioremediation Journal* **3:** 334.

Coates, J.D., Michaelidou, U., Bruce, R.A., O'Connor, S.M., Crespi, J.N. and Achenbach, L.A.

(1999b) Ubiquity and diversity of dissimilatory (Per) chlorate-reducing bacteria. *Appl. Environ. Microbiol.* **65:** 5234-5241.

Connon, S.A., Tovanabootr, A., Dolan, M., Vergin, K., Giovannoni, S.J. and Semprini, L. (2005) Bacterial community composition determined by culture-independent and -dependent methods during propane-stimulated bioremediation in trichloroethene-contaminated groundwater. *Environ. Microbiol.* **7:** 165-178.

De Marco, P., Pacheco, C.C., Figueiredo, A.R. and Moradas-Ferreira, P. (2004) Novel pollutant-resistant methylotrophic bacteria for use in bioremediation. *FEMS Microbiol. Lett.* **234:** 75-80.

Dean, B.J. (1985) Recent findings on the genetic toxicology of benzene, toluene, xylenes and phenols. *Mutation Research* **154:** 153-181.

Eriksson, S., Ankner, T., and Abrahamsson, K. and Hallbeck, .L. (2005) Propylphenols are metabolites in the anaerobic biodegradation of propylbenzene under iron-reducing conditions. *Biodegradation* **16:** 253-263.

Fahy, A., Lethbridge, G., Earle, R., Ball, A.S., Timmis, K.N. and McGenity, T.J. (2005) Effects of long-term benzene pollution on bacterial diversity and community structure in groundwater. *Environ Microbiol* **7:** 1192-1199.

Fahy, A., McGenity, T.J., Timmis, K.N. and Ball, A.S. (2006) Heterogeneous aerobic benzene-degrading communities in oxygen-depleted groundwaters. *FEMS Microbiol. Ecol.* **58:** 260-270.

Finneran, K.T., Johnsen, C.V. and Lovley, D.R. (2003) *Rhodoferax ferrireducens* sp. nov., a psychrotolerant, facultatively anaerobic bacterium that oxidizes acetate with the reduction of Fe (III). *Int. J. Syst. Evol. Microbiol* **53:** 669-673.

Han, J.S. and C.G. Kim (2010) Characterization of molecular biological indicators to define stabilization of landfills. *Korean J. Chem. En.* **27**(3): 868-873.

Jones, D., Lethbridge, G., and McCarthy, P. and Thomson, S. (2001) Project SIReN: Phase 2a. Conceptual site model and groundwater model. R & D Technical Report P2-208/TR/2. Environment Agency UK.

Kaden, R., Spröer, C.; Beyer, D. and Krolla-Sidenstein, P. (2014) *Rhodoferax saidenbachensis* sp. nov., a new psychrotolerant adapted, very slowly growing bacterium within the family *Comamonadaceae* , reassignment of *Albidiferax ferrireducens* to the genus *Rhodoferax* and amended description of the genus *Rhodoferax. Int. J. Syst. Evol. Microbiol.* **64** (4): 1186 – 1193.

Mahmood, S., Freitag, T.E. and Prosser, J.I. (2006) Comparison of PCR primer-based strategies for characterization of ammonia oxidizer communities in environmental samples. *FEMS Microbiol. Ecol.* **56**: 482 – 493.

Manefield, M., A. S. Whiteley, et al. (2002) RNA stable isotope probing, a novel means of linking microbial community function to phylogeny. *Appl. Environ._Microbiol.* **68**(11): 5367-5373.

Muyzer, G., De Waal, E.C. and Uitterlinden, A.G. (1993) Profiling of complex microbial populations by denaturing gradient gel electrophoresis analysis of polymerase chain reaction-amplified genes coding for 16S rRNA. *Appl. Environ. Microbiol.* **59:** 695-700.

Nakatsu, C. H., Hristova, K., Hanada, S. et al. (2006) Methylibium petroleiphilum gen. nov., sp. nov., a novel methyl tert-butyl ether-degrading methylotroph of the Betaproteobacteria. *Int. J. Syst. Evol. Microbiol.* **56**(5): 983-989.

Njobuenwu, D.O., Amadi, S.A. and Ukpaka, P.C. (2005) Dissolution rate of BTEX

contaminants in water. *Ca. J. Chem. En.* **83:** 985-989.

Radojkovic, D. and Kušic, J. (2000) Silver staining of denaturing gradient gel electrophoresis gels. *Clin. Chem.* **46** (6): 883 – 884.

Redmond, M. C. and Valentine, D.L. (2012) Natural gas and temperature structured a microbial community response to the Deepwater Horizon oil spill. Proceedings of the National Academy of Sciences, **109** (50): 20292 – 20297.

Risso, C., Sun, J., Zhuang, K., Mahadevan, R., DeBoy, R. et al. (2009) Genome-scale comparison and constraint-based metabolic reconstruction of the facultative anaerobic Fe (III)-reducer *Rhodoferax ferrireducens*. *BMC Genomics* **10**: 447.

Roane, T.M., Josephson, K.L. and Pepper, I.L. (2001) Dual-bioaugmentation strategy to enhance remediation of cocontaminated soil. *Appl. Environ. Microbiol.* **67:** 3208-3215.

Salinero, K., K. Keller, et al. (2009) Metabolic analysis of the soil microbe *Dechloromonas aromatica* str. RCB: indications of a surprisingly complex life-style and cryptic anaerobic pathways for aromatic degradation. *BMC Genomics* **10**(1): 351.

Táncsics, A., S. Szoboszlay, et al. (2012) Quantification of Subfamily I.2.C Catechol 2,3-Dioxygenase mRNA Transcripts in Groundwater Samples of an Oxygen-Limited BTEX-Contaminated Site. *Environ. Sci. Technol.* **46** (1): 232 – 240.

Waller, A.S., Cox, E.E. and Edwards, E.A. (2004) Perchlorate-reducing microorganisms isolated from contaminated sites. *Environ. Microbiol.* **6:** 517-527.

Wiedemeier, T.H., Rifai, H.S., Newell, C.J. and Wilson, J.T. (1999) *Natural attenuation of fuels and chlorinated solvents in the subsurface.* Pages 27 – 29, John Wiley & Sons, Inc.

APPLICATION OF DIFFERENT BIO-CATALYSTS FOR BIO-DIESEL PRODUCTION FROM WASTE COOKING OIL AS A SUSTAINABLE AND GREEN ENERGY PROCESS

Nour Sh. El-Gendy[§] and A. Hamdy
Egyptian Petroleum Research Institute, Nasr City, Cairo, Egypt

ABSTRACT

In Egypt, solid municipal waste density averages 300 kg/m^3. Organic materials constitute up to 60% of these wastes. The annual consumption of vegetable oil in Egypt exceeds two million MT/year. Consequently, millions of liters of waste cooking oil (WCO) are annually discarded. All of these add to the cost of waste management and cause several environmental and economic problems. The depletion of conventional petro-diesel, with its accelerating and frequently fluctuating price, together with growing environmental concerns, has steadily gained attention for bio-diesel production.

In this study, some domestic waste such as animal bones, eggshells and mollusk shells were used to produce heterogeneous bio-catalysts through a simple calcination process. The physicochemical characteristics of the prepared bio-catalysts were done by thermogravimetric analysis (TGA/DSC), X-ray diffraction (XRD), laser Raman spectroscopy, scanning electron microscopy (SEM) and Fourier transform infrared (FTIR) spectroscopy. A comparative study for bio-diesel production from WCO using the produced bio-catalysts, standard Novozyme 435, and laboratory chemical calcium oxide (CaO) was carried out. All of the prepared bio-catalysts show high bio-diesel production activity (> 90% fatty acid methyl esters [FAME] in 1 h). The produced bio-diesel shows a high quality product with good and acceptable fuel properties compared with those of Egyptian petro-diesel standards, and ASTM D6751 and EN 14214 standards of bio-diesel.

The production of bio-diesel from WCO using heterogeneous bio-catalysts produced from domestic waste offers a triple positive impact solution to economic, environmental, and energy problems.

Keywords: Bio-diesel, heterogeneous bio-catalyst, animal bones, eggshells, mollusks shells, Novozyme 435

[§]Corresponding Author: Nour Sh. El-Gendy, Ass. Prof. Environmental Biotechnology, Head Manager Petroleum Biotechnology Lab., Egyptian Petroleum Research Institute, Nasr City, Cairo, Egypt, 11727; Fax: (+202) 2 274 7433; Cellular: (+20) 100 1443208; nourepri@yahoo.com

1. INTRODUCTION

Because of the energy and global warming crisis, development of renewable energy sources has been a potential concern worldwide. Bio-diesel has attracted attention in recent years as a renewable fuel with less pollutant emissions when compared to mineral diesel and its combustion, since a significant decrease in carbon monoxide, hydrocarbons, and particulate matter is observed (El-Gendy *et al*., 2014). Bio-diesel is produced by transesterification of vegetable oils, animal fats, and microbial oil (algae, yeast, bacteria, and fungi) with short chain alcohols (methanol is the most recommendable, producing fatty acid methyl esters [FAME]) in the presence of a catalyst (homogenous or heterogeneous). In order to decrease the overall cost of bio-diesel production, many researchers are interested in waste cooking oil (WCO), which would reduce bio-diesel production costs up to 60–90% (Talebian-Kiakalaieh *et al*., 2013).

Homogeneous acid catalysts, such as sulphuric and hydrochloric acids, and homogeneous alkaline catalysts, such as sodium hydroxide, potassium hydroxide, and sodium methoxide, are used in bio-diesel synthesis; however, there are problems associated with both types of catalysts. Acid catalysts take more time for bio-diesel synthesis and are also corrosive in nature. Although alkaline catalysts take less time, they increase the pH of the bio-diesel, which thus requires rinsing with water to remove the leftover catalyst resulting in wastewater generation and loss of FAME, and consequently, resulting in the loss of yield. To overcome these constraints, research has focused on finding a suitable heterogeneous catalyst that can be easily separated and gives a high yield and conversion. Heterogeneous solid acid and solid base catalysts presently used include: zeolites, metal catalysts, Mg/Al hydrotalcite, KF/Ca-Mg-Al hydrotalcite, KF/Al_2O_3, alummina-loaded compounds, ion-exchange resins, vanadyl phosphate, dolomites, double-layered hydroxide, sodium aluminate, $SnCl_2$, calcium oxide, calcium methoxide, and calcium ethoxide. However, all of these catalysts, with the exception of calcium oxide, need a complex and lengthy process for synthesis, which will increase the overall cost of bio-diesel synthesis. Although Al_2O_3-supported alkali metal oxide catalysts are highly basic and very active, their active phases are highly sensitive to moisture and easily leached by methanol in comparison to CaO (Helwani *et al*., 2009, Leung *et al*., 2010, and Ngamcharussrivichai *et al*., 2010). In order to make the bio-diesel production more sustainable, the utilization of natural and/or waste heterogeneous catalysts has been of recent interest (Helwani *et al*., 2009, Boro *et al*., 2012, and Sanjay, 2013). Bio-diesel can be prepared using heterogeneous catalysts obtained from natural hydroxyapatite (Ngamcharussrivichai *et al*., 2010, Chakraborty *et al*., 2011, and Obadiah *et al*., 2012), CaO prepared from natural calcium (dolomite and calcite) (Ngamcharussrivichai *et al*., 2010), and natural waste shells (Engin *et al*., 2006, Viriya-empikul *et al*., 2010 and 2012, Boey *et al*., 2011, and Boro *et al*., 2011).

In Egypt, millions of liters of oil that are used for frying foods are discarded each year into sewage systems, thus polluting waterways, causing waste management problems, and consequently, adding to the cost of treating effluent. Solid waste density in Egypt averages about 300 kg/m^3, with 60% consisting of organic waste (El-Gendy and Madian, 2013). Production of bio-diesel from WCO using heterogeneous catalysts prepared from organic waste would offer a triple-impact solution to economic, environmental, and waste management problems.

In this work, the synthesis of bio-diesel from WCO was investigated using different heterogeneous bio-catalysts prepared from different organic waste products. The efficiency of the prepared green catalyst was compared to that of the chemical CaO and the well-known

immobilized enzyme, Novozyme 435. The qualification of the produced bio-diesel relevant to international standards was also investigated.

2. MATERIALS AND METHODS

2.1 Materials

Pure calcium oxide (CaO) as a heterogeneous catalyst and methanol (AR Grade) were purchased from Fluka Chemicals Ltd. (Gillingham, UK). Novozyme 435 (*Candida antarctica* lipase B) was a gift from Novozyme A/S, Bagsvaerd Denmark and was supplied as an immobilized enzyme on macro-porous acrylic resin.

2.2 Collection and preparation of waste cooking oil

Waste cooking oil (WCO) was collected from a local restaurant. The collected WCO was centrifuged and filtered to remove any suspended matter and burned food bits, etc. It was then heated to 105^{o}C for 2 h to remove any unwanted water present by evaporation. The fatty acid composition of the WCO was made up of palmitic acid (24.4%), stearic acid (46.4%), oleic acid (24.6%), and linoleic acid (4.6%). The WCO was characterized by a high total acid number, density, and viscosity, recording: 2.15 mg KOH/g oil, 0.9327 g/cm^3, and 64 cSt, respectively.

2.3 Catalyst preparation

The waste animal bones (AB), eggshells (ES), and mollusk shells (MS) were collected from local butcheries, bakeries, and seafood shops, respectively. They were washed with tap water, dried at 100^{o}C for 2 h in an oven, and then grinded using a grinding mill (pulverisette6, FRITSCH, Germany) with a rotational speed of 340 rpm and a time of 8 min. They were then sieved to constant sizes (< 0.07 mm). Calcination was performed in a muffle furnace at different temperatures (400-1100^{o}C) for 2 h. The laboratory chemical CaO catalyst was activated by calcination at 800^{o}C for 2 h under a N_2 atmosphere before use, since CaO is poisoned very fast by atmospheric water vapor and CO_2. The calcined catalysts were then stored in dark screw-capped vessels to avoid a reaction with humidity and CO_2 in the air before usage.

2.4 Catalyst characterization

In order to determine the thermal transition of the grinded animal bones, eggshells, and mollusk shells, differential scanning calorimetric-thermal gravimetric analysis (DSC-TGA) was performed by Q600 SDT Simultaneous DSC-TGA (New Castle, DE, USA). Nitrogen was purged at the rate of 100 mL/min. Temperature was programmed from ambient temperature to 1100^{o}C at the ramp rate of 10^{o}C/min.

To determine the crystalline phases of each catalyst at different calcination temperatures, X-ray diffraction patterns were determined on a high-resolution X-ray diffractometer (XRD; PANalytical XPERT PRO MPD, The Netherlands), coupled with a Cu kα radiation source (λ= 1.5418 A^{o}) operated at 40 kV and 40 mA. The diffraction patterns were recorded at room temperature in the angular range of 4^{o}-70^{o} (2θ), with step size 0.02^{o} (2θ) and scan step time 0.5 (s). The crystalline phases were identified using the ICDD-PDF database. The crystalline size of

the catalyst was calculated from the XRD data using Scherrer's formula, as reported by Qin *et al*. (2009).

Laser Raman spectroscopic measurements were performed with a dispersive Raman spectrometer (BRUKER-SENTERRA, Germany) equipped with an integral microscope (Olympos). The excitation source was a neodymium-doped yttrium aluminum garnet (Nd:YAG) laser (532 nm), focused with a 100x long focal length objective microscope, providing a power of 20 mW on the sample.

The chemical composition of wastes before and after calcination was determined by energy dispersive X-ray analysis (EDX, Oxford X-Max, England) conjugated with transmission electron microscope TEM (JEM 2100, Jeol, Japan). The energy of the acceleration beam employed was 200 KeV.

The surface morphology of the catalyst was studied using JEOL-model JSM-53000 scanning electron microscope (SEM). The working sample was analyzed at three different locations to ensure reproducibility.

Particle-sizer model Beckman Coulter Multisizer-3 (Nyon, Switzerland) was used for determination of particle size distribution. The specific surface areas of the prepared bio-catalysts were measured with the BET method.

For the Fourier transforms Infrared (FTIR) studies, an analytical FTIR (Perkin Elmer Spectrum One, USA) instrument was used. The samples were measured as KBr discs by mixing the sample with KBr (spectroscopic grade) and the solid samples were transferred into the cell after melting using an infrared lamp. The spectra of all studied samples were measured in the range of 400-4000 cm^{-1}, with a suitable scan resolution of 4 cm^{-1} and a scan rate of 16 cm/min.

2.5 Transesterification

The batch transesterification reactions were conducted in a laboratory-scale setup using a two-necked 250 mL flask equipped with a reflux condenser and a thermometer on a magnetic heat stirrer, with parameters set to 60^{o}C, 300 rpm, and 60 min. The methanol to oil molar ratio (M:O) was 9:1 and a catalyst of 9 wt% (catalyst/oil weight ratio) was used. After the prescribed time of the reaction, the mixture was allowed to separate overnight. The lower layer made up of glycerol and solid bio-catalyst was centrifuged to obtain pure glycerol and catalyst, which can be re-used again. The upper layer made up of bio-diesel and un-reacted methanol was drained out and transferred into the sample flask of a rotary evaporator to recycle methanol at 65^{o}C and 20 kPa. The obtained purified bio-diesel was then bottled and kept for characterization studies. The yield of bio-diesel was calculated according to Boro *et al.* (2011).

The activity of the prepared bio-catalysts was compared with that of the commercially available and most effective CaO and lipase (Novozyme 435).

2.6 Gel permeation chromatographic (GPC) analysis

Analytical GPC (Waters 600 E, USA) was used for the determination of bio-diesel purity. GPC was equipped with a set of styragel columns: HR4, HR5E, 7.8 X 300 mm^2, and a refractive index detector (model Waters 4110). The mobile phase was tetrahydrofurane (THF) of HPLC grade,

the flow rate was 1 mL/min, the sample size was 20 µL, the column operating temperature was 40^{o}C, and the run time was 50 min.

2.7 Physicochemical characterization of the produced bio-diesel

The purified product obtained from oil transesterification was tested to estimate and evaluate its fuel properties using the standard methods of analysis for petroleum products (American Society for Testing and Materials [ASTM] Standards Methods, 1991). The results were compared with the Egyptian standards for petro-diesel and European and American standards of bio-diesel (EN14214 and D-6751, respectively).

All of the properties were analyzed in two replicates and the final results given below were obtained as average values.

3. RESULTS AND DISCUSSION

3.1 Characterization of the prepared bio-catalysts

In order to explain the effect of calcination temperature, the calcination process of each collected waste was investigated with TGA/DSC. Figure 1 shows the thermal analysis results along with the weight loss when the temperature was raised from room temperature to 1100^{o}C.

Upon calcination of AB, the TGA analysis revealed a total weight loss of ≈ 34%. A dominant weight loss of ≈ 28% was observed at temperatures below 700^{o}C. The heat flow chart does not declare the production of a new product.

The thermogravimetric analysis of ES and MS showed that no significant decomposition occurred upon heating to 650 and 600^{o}C, respectively, recording a weight loss of ≈ 5%. While the dominant decomposition was ≈ 47 and 46%, weight loss occurred within the 700 – 800^{o}C range (peaking at 787 and 768^{o}C, respectively), and remained sustained thereafter up to 1100^{o}C. The DSC curves support the TGA curves, with the heat flow chart illustrating an endothermic peak at 787 and 768^{o}C for ES and MS, respectively. This reveals the production of new compound. According to Singh and Singh (2005), the weight loss might be attributed to the decomposition of $CaCO_3$ through the loss of carbon dioxide (CO_2) and production of calcium oxide (CaO), and also due to the possible removal of absorbed water molecules, which occurs according to the following dissociation equation:

$$CaCO_3(s) \leftrightarrow CaO(s) + CO_2(g)$$

During the calcination process there was no observed change in bone color, while the XRD patterns of AB (Figure 2a) showed a change from an amorphous to crystalline structure of fluorapatite ($Ca_5(PO_4)_3F$; JCPDS card number: 060-0667). Raman spectra (Figure 3a) are consistent with the XRD patterns. The vibration bands at 436 and 959 cm^{-1}of natural and calcined AB at 700^{o}C match those of fluorapatite.

It was observed during calcination that the ES and MS turned white and grey, respectively. According to Engin *et al.* (2006), this indicates that calcium carbonate ($CaCO_3$) is converted to CaO with the elevation of calcination temperatures. The XRD patterns (Figure 2b) revealed that the ES are mainly calcite ($CaCO_3$; JCPDS card number: 024-0027) and remained unchanged up

to calcination at 600^{o}C. Calcination at 700^{o}C showed a mixture of $CaCO_3$ and lime (CaO). The XRD patterns showed a pure crystalline (CaO; JCPDS card number: 043-1001) for calcination temperatures 800 – 1100^{o}C. The XRD patterns of natural MS are mainly aragonite ($CaCO_3$; JCPDS card number: 024-0025), and upon calcination at 400^{o}C, it was changed to calcite ($CaCO_3$; JCPDS card number: 005-0586) and remained unchanged up to calcination at 600^{o}C. Meanwhile, calcination at 700^{o}C showed a mixture of calcite ($CaCO_3$; JCPDS card number: 005-0586) and lime (CaO; JCPDS card number: 043-1001). The XRD patterns showed a pure crystalline (CaO; JCPDS card number: 043-1001) for calcination temperatures ranging from 800 – 1100^{o}C.

The $Ca(OH)_2$ phase, which can be formed by hydration of CaO, appeared in the XRD patterns of calcined AB at $\geq$ 700^{o}C (Figure 2a). The presence of $Ca(OH)_2$ lowered the transesterification activity of calcined AB in comparison to that of calcined ES and MS, which is mainly composed of pure CaO (Ngamcharussrivichai *et al*., 2010).

Raman spectra (Figure 3) are consistent with the XRD patterns. The vibration bands at 150, 282, 714, and 1087 cm^{-1} of natural ES (Figure 3b) correspond to calcite ($CaCO_3$). For natural MS, the vibration bands at 155, 197, 650, 703, and 1086 cm^{-1} (Figure 3c) correspond to those of aragonite ($CaCO_3$). The vibration bands at 360, 1075, 1334, and 1463 cm^{-1} of calcined ES and MS at 800^{o}C (Figure 3 b and c) correspond to pure lime (CaO).

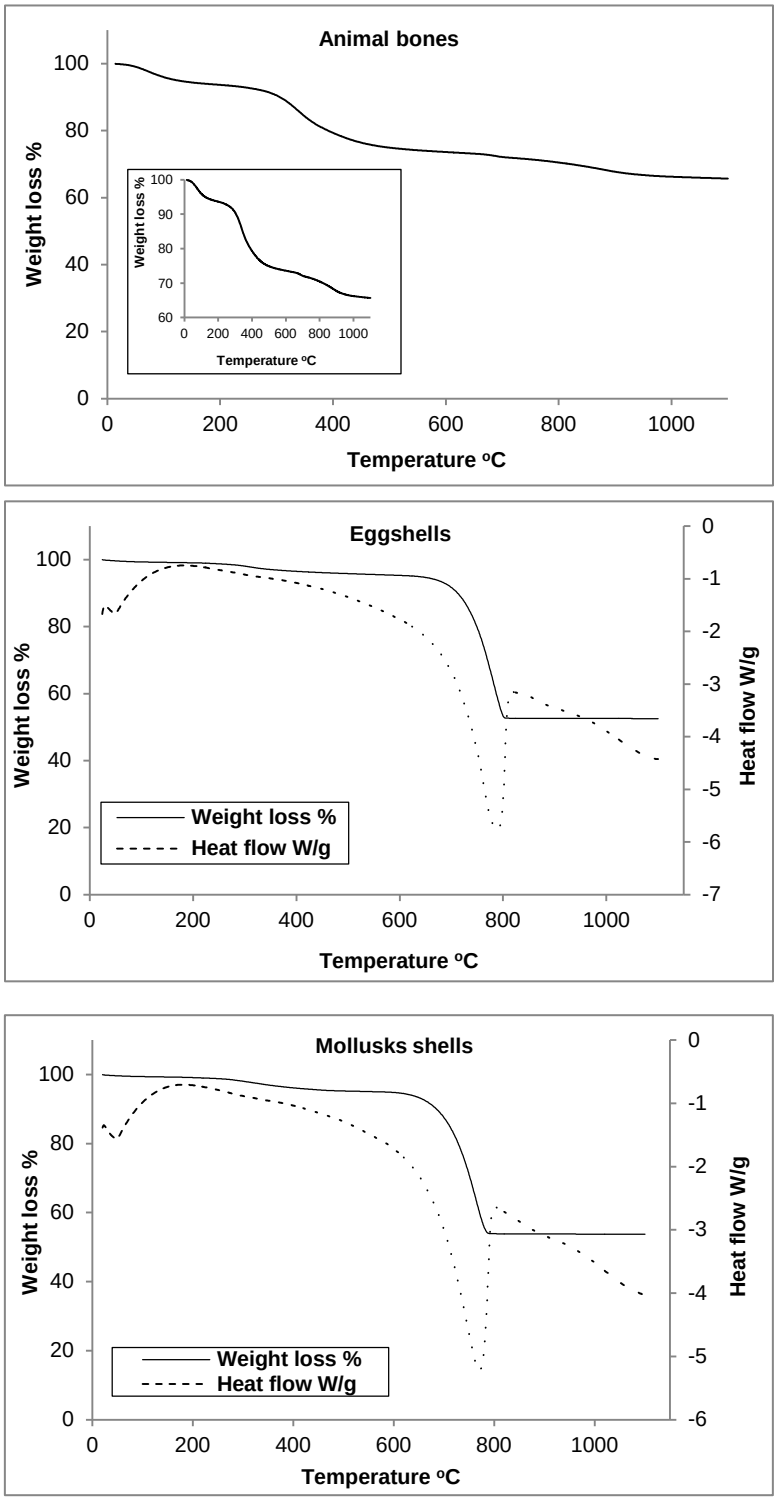

Figure 1. TGA/DSC curves

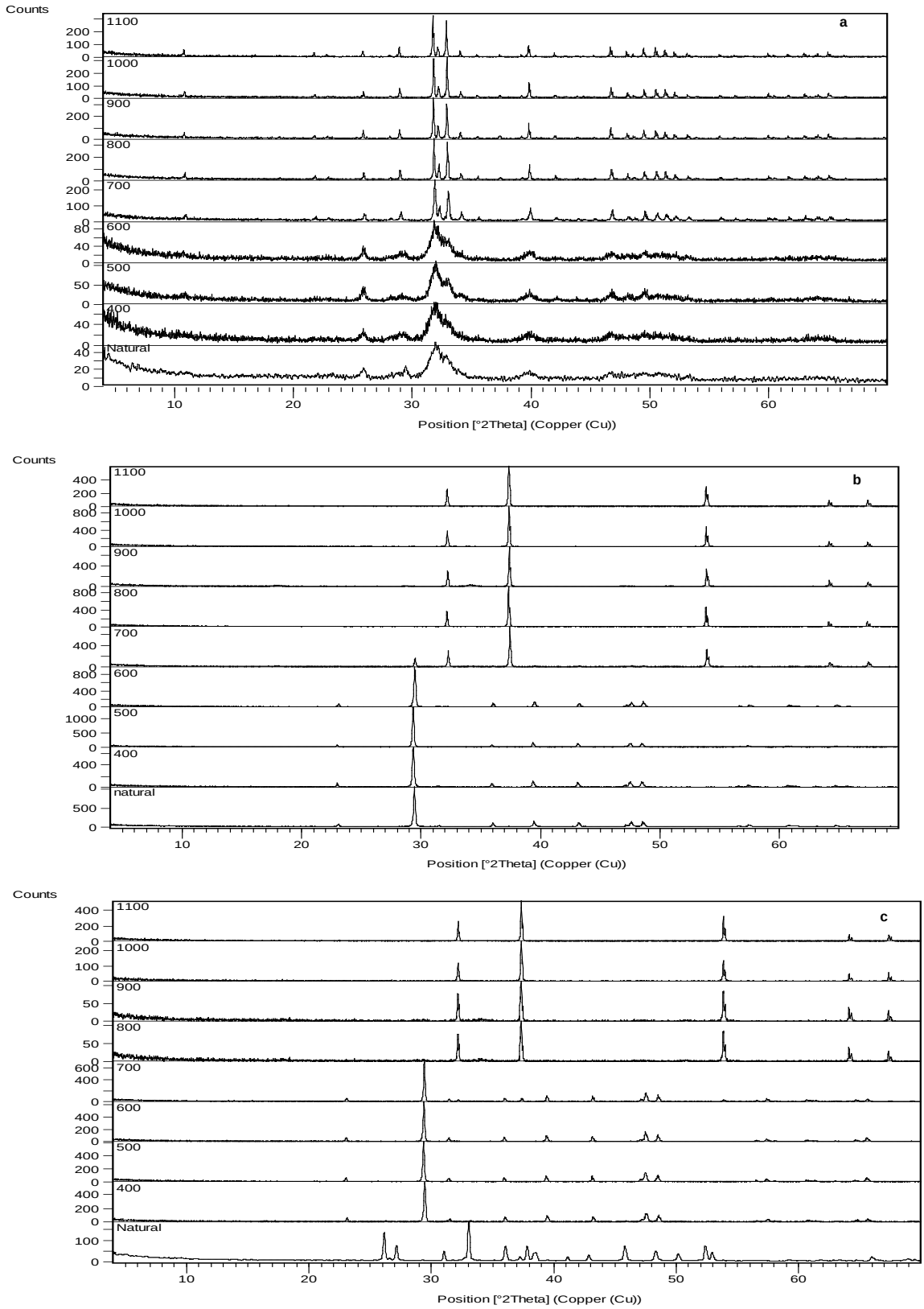

Figure 2. XRD patterns of animal bones (a), eggshells (b) and mollusk shells (c) during calcination at different temperatures

The crystalline size was calculated from the XRD data, increasing by calcination from ≈ 13.26 nm in natural AB to 46.6 nm in calcinated AB at 700^{o}C. This shows that the crystallinity of AB increased upon calcination. Similar observations were reported by Monshi *et al.* (2012). The uncalcinated ES was recorded as ≈ 41.79 nm and it also increased by calcination at 800^{o}C, recording ≈ 47.39 nm. Borgwardt (1989) and Liu *et al.* (2010) reported that calcination of $CaCO_3$ leads to the formation and growth of CaO. When $CaCO_3$ decomposes at high temperatures, small CaO grains form and then the contact grains form necks and begin to grow, resulting in an increase in the average grain size. The natural MS was recorded as ≈ 42.15 nm, which was decreased upon calcination at 800^{o}C, recording ≈ 38.77 nm. A similar observation was reported by Yoosuk *et al.* (2010) and was attributed to the presence of water molecules during calcination of $CaCO_3$ to CaO.

Narrow and high intense peaks of the calcinated wastes (AB, at temperature ≥ 700^{o}C; and ES and MS, at temperature ≥ 800^{o}C) could define the well-crystallized nature of the prepared bio-catalysts. A similar observation was reported by Boey *et al.* (2011) on the preparation of a bio-catalyst from waste cockle shells (*Anadara granosa*) for bio-diesel production from palm olein.

In order to investigate the effects of the calcination process on the chemical composition of biomass (catalyst), EDX was carried out. EDX analysis (Table 1) confirmed the XRD of AB, as it showed that chemical composition of AB was not highly affected by calcination, and it also revealed that the chemical composition of ES and MS was highly affected by calcination. The uncalcinated shells exhibit oxygen as the main component (52.64 and 56.62, wt%), while in calcinated shells at 800^{o}C, calcium represents the major component (63.15 and 62.32, wt%), respectively. Similar observations were reported by Viriya-empikul *et al.* (2010), where the main component in calcinated shells at 800^{o}C was calcium. Stoichiometrically, this is true, as Ca is the main constituent (≈ 71%) in CaO, while oxygen is the major constituent in $CaCO_3$ (≈ 48%). The basic properties of the catalysts, which should be expected from the CaO species, is considered to be a key factor in yielding bio-diesel. The majority of the catalysts for shells is Ca, and its content in the prepared bio-catalysts can be ranked in the following decreasing order: ES (63.15%) ≥ MS (62.32%) > AB (29.26%).

Table1. Chemical composition of biomass-derived catalysts

Biomass	**Chemical composition (wt%)**
Natural animal bones	C (16.68%) F (0.96%) O (56.84%) Na (0.68%) Mg (0.11%) P (5.17%) Ca (19.56%)
Calcinated animal bones at 700^{o}C	C (5.8%) F (1.61%) O (49.84%) Na (0.48%) Mg (0.31%) P (12.7%) Ca (29.26%)
Natural eggshells	C (14.85%) Na (0.17%) Mg (0.38%) Ca (31.96%) O (52.64%)
Calcinated eggshells at 800^{o}C	C (3.08%) Mg (0.22%) Ca (63.15%) O (33.55%)
Natural mollusk shells	C (17.35%) Mg (0.01%) Ca (26.01%) O (56.62%)
Calcinated mollusk shells at 800^{o}C	C (3.47%) Mg (0.05%) Ca (62.32%) O (34.16%)

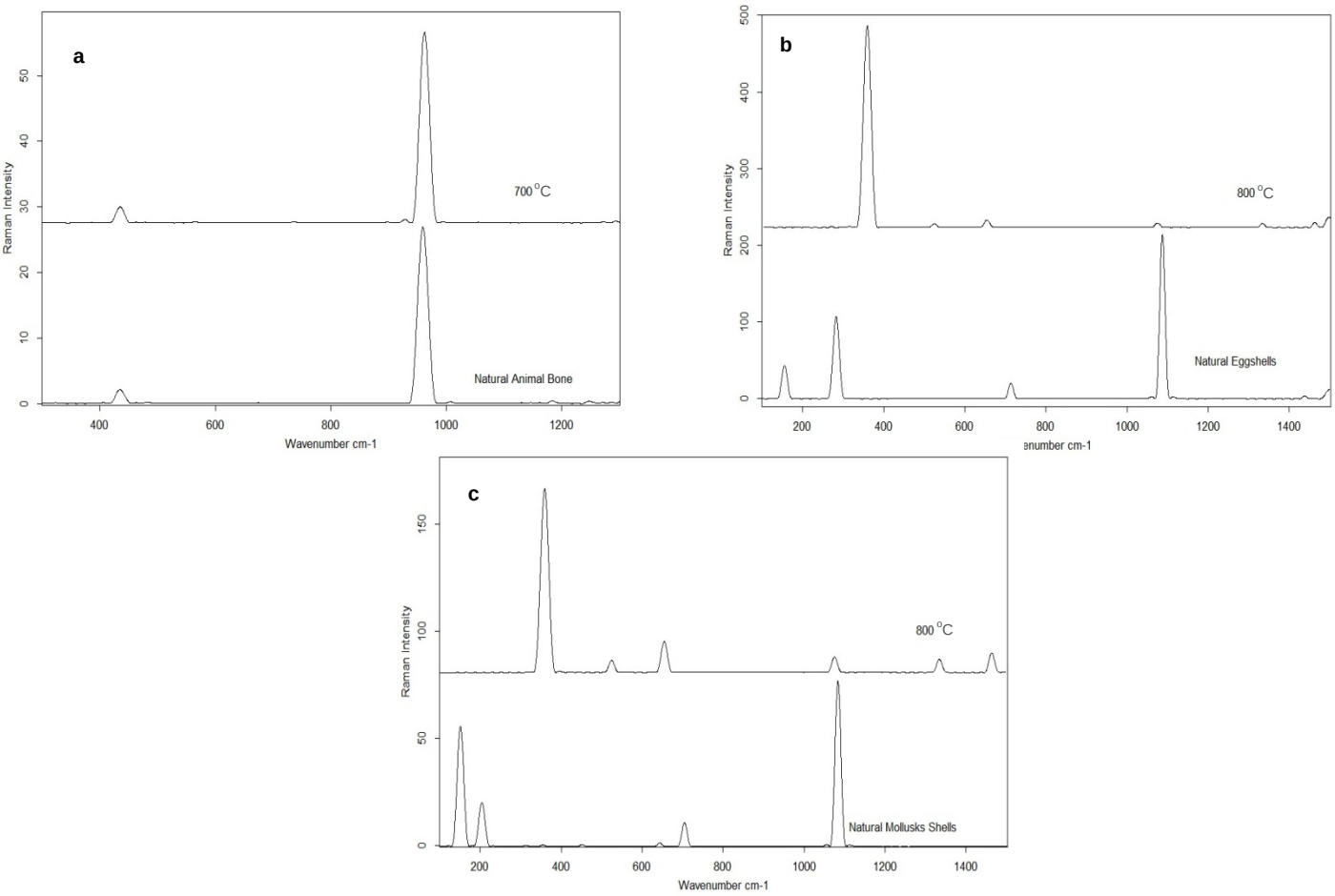

Figure 3. Raman spectra of animal bones (a), eggshells (b), and mollusk shells (c) at different calcination temperatures

The FTIR patterns of AB (Figure 4a) show no significant changes after the calcination process. According to Shafiei *et al.* (2012), the peaks around 1049-1096 and 962 cm^{-1} correspond to asymmetric and symmetric stretching vibrations of PO_4^{3-}, respectively. Meanwhile, the peaks around 572-631 and 474 cm^{-1} correspond to bending asymmetric and symmetric vibrations of PO_4^{3-}, respectively. The spectra indicates that the AB is free of carbonates, however, the band around 1400-1455 cm^{-1} assigned to γ_3 (C-O) vibration in carbonate is not found, but this band can be seen in the spectra of natural ES and MS.

The FTIR patterns of ES and MS with respect to the calcination process (Figure 4b and c), show major peaks around 1423-1471, 860-875, and 709-712 cm^{-1}, patterning natural shells, which disappeared in that of the calcinated ES and MS at 800^{o}C. According to Engin *et al*. (2006), these peaks are attributed to asymmetric stretch, the out-of-plane bend and in-plane bend vibration modes for CO_3^{-2} molecules. Also, upon calcination at 800^{o}C, weak bands around 2509-2522 and 1786-1793 cm^{-1} disappeared and new weak peaks appeared at 1093 and 1047 cm^{-1} in calcined ES, and at 1111 cm^{-1} in calcined MS. The observed changes in FTIR patterns might indicate the complete transformation of $CaCO_3$ to CaO. Similar observations were reported by Roschat *et al.* (2012).

The morphology of natural and calcined AB at 700^{o}C was investigated by SEM (500x magnification). The natural AB appeared like an amorphous mass aggregation with a small surface area (Figure 5a) that changed to crystalline porous particles with a high surface area upon calcination (Figure 5b). The developed catalyst has a flat structure with the presence of strips at regular intervals. The SEM images also revealed an increase in the roughness of bone surface with calcination and showed the existence of voids or pores distributed over the catalyst surface. This may indicate calcination increasing the porosity of bone. The morphology of natural and calcined shells at 800^{o}C was also investigated by SEM (500x magnification). Natural ES displayed a typical layered architecture (Figure 5c) that changed to a "honeycomb" porous surface (Figure 5d) upon calcination. SEM micrographs of the catalysts derived from MS (Figure 5f) show that upon calcination the morphology of MS changed from layered bulky substances without any clear pores on its surface (Figure 5e) to porous particles of various size and shapes.

For the prepared catalysts, the BET surface area (S_{BET}) was recorded as: 45.13, 6.45, and 12.63 m^2/g; with a total pore volume of: 0.044, 0.013, and 0.006 cm^3/g; and an average pore diameter of: 1.9, 4.12, and 0.97 nm for AB, ES, and MS, respectively. The shell-derived catalysts were considered to be less porous than that of the AB catalyst due to their recorded lower pore volume relative to that of AB.

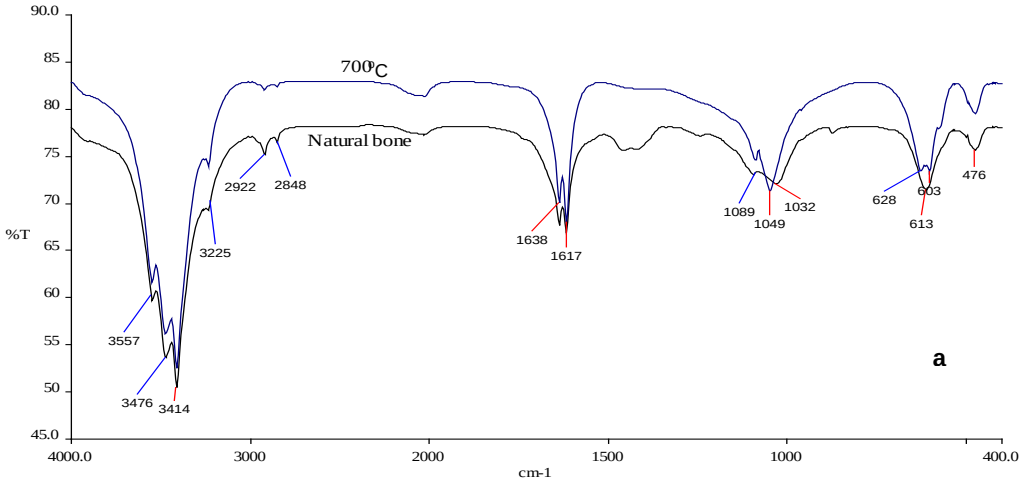
700°C
Natural bone
%T
cm-1
3557
3476
3414
3225
2922
2848
1638
1617
1089
1049
1032
628
603
613
476
a

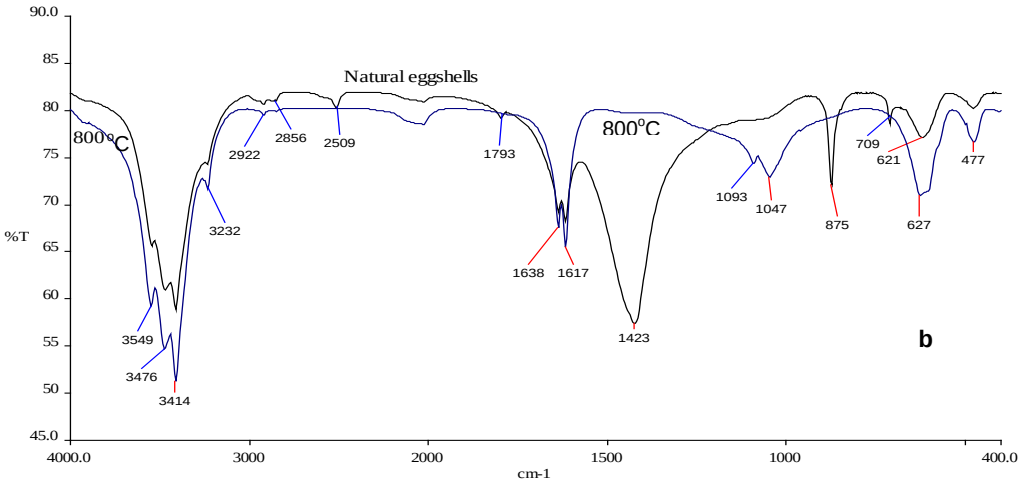
Natural eggshells
800°C
800°C
%T
cm-1
3549
3476
3414
3232
2922
2856
2509
1793
1638
1617
1423
1093
1047
875
709
621
627
477
b

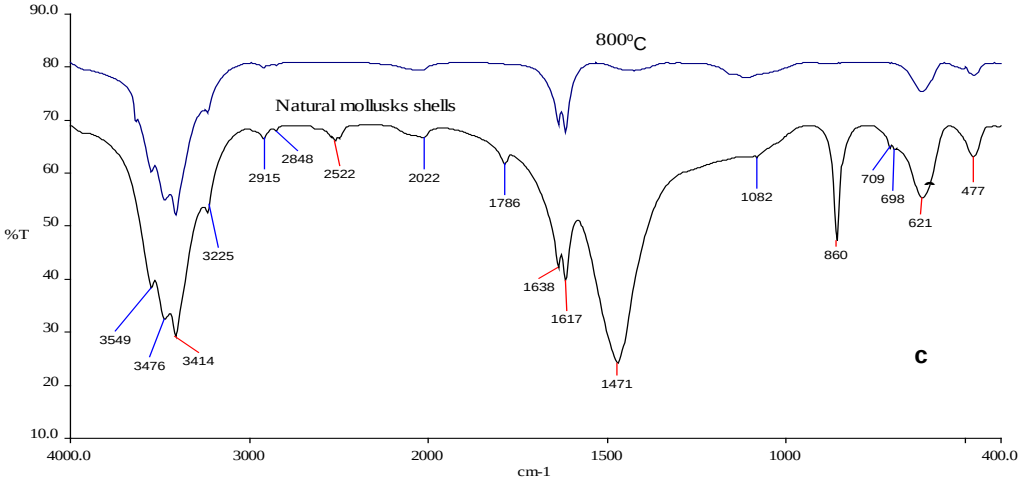
800°C
Natural mollusks shells
%T
cm-1
3549
3476
3414
3225
2915
2848
2522
2022
1786
1638
1617
1471
1082
860
709
698
621
477
c

Figure 4. FTIR spectra of animal bones (a), eggshells (b), and mollusk shells (c) at different calcination temperatures

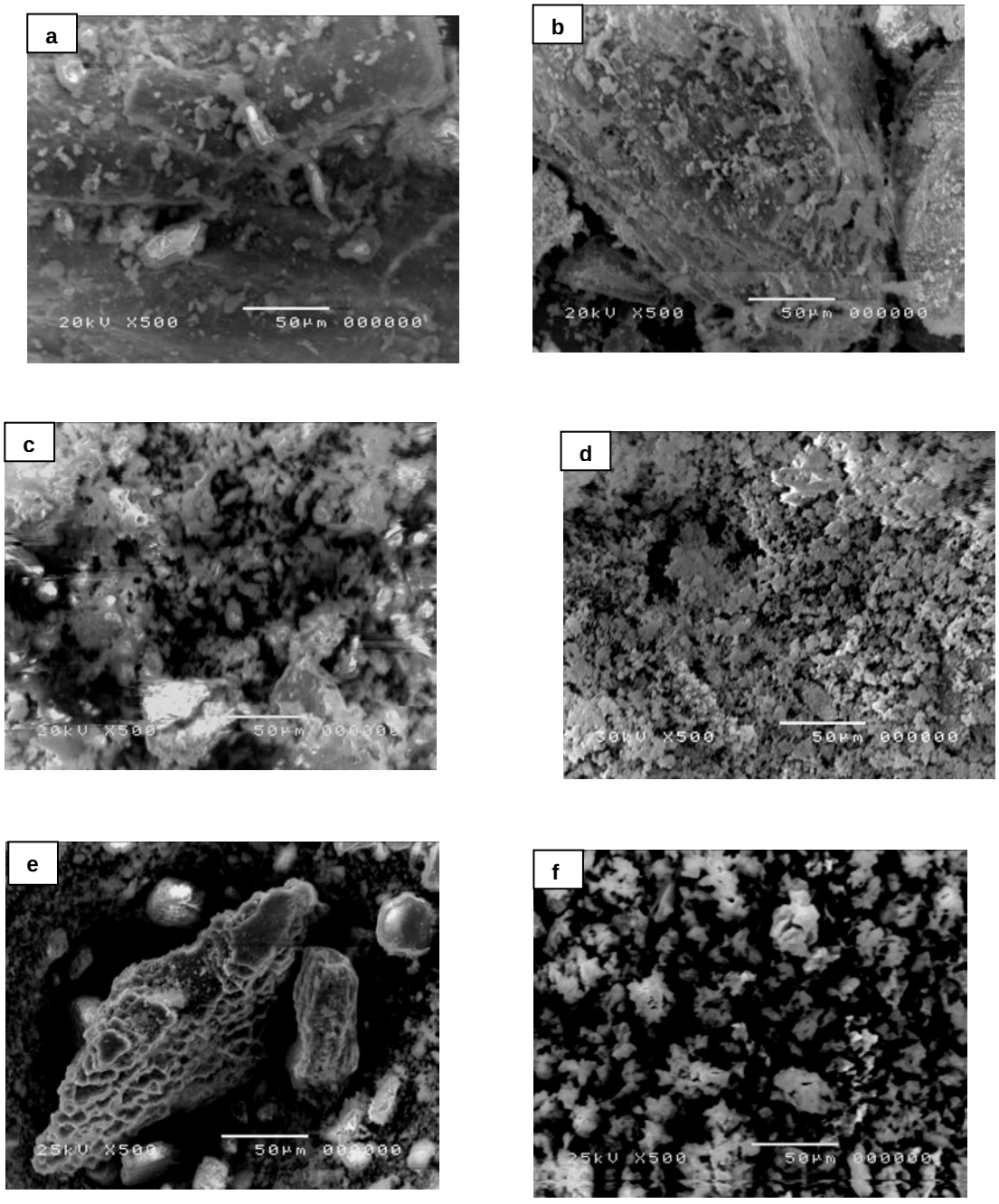

Figure 5. SEM images of natural animal bones (a) and calcined animal bones at 700^{o}C (b), natural eggshells (c) and calcined eggshells at 800^{o}C (d), and natural mollusk shells (e) and calcined mollusk shells (f) at 800^{o}C

Viriya-empikul *et al.* (2010) reported that all shell-derived catalysts are considered to be less porous due to their trace pore volume. Usually, smaller size grains provide a higher specific surface area, but in this study, there is a recorded discrepancy where the average particle diameter recorded: 9.32, 7.82, and 10.27 µm for AB, ES, and MS, respectively. This discrepancy might be due to the agglomerations of the calcined particles that are observed as clusters with different sizes (SEM micrographs, Figure 5), and/or due to the recorded differences in porosity of the prepared bio-catalysts. The average particle size distribution can markedly affect settling and filtering characteristics in a slurry reactor. A large part of the particle size distribution for the prepared bio-catalysts is within the size range of 6.5-10.5, 6.3-8.2, and 6.4-11 µm, and the rest was within the range of 10.5-13.5, 8.2-10, and 11-17.2 µm for AB, ES, and MS, respectively. Due to the relatively large particle sizes, it is easy to separate the catalyst from the products after the reaction through filtration or centrifugation. According to Roschat *et al.* (2012), a high porosity catalyst is a key requirement in achieving high conversion efficiency for the heterogeneous process, thereby, a high surface area or high catalytic sites are necessary. Thus, the bio-catalyst prepared from AB for application in bio-diesel production is recommended. Sharma *et al.* (2011) also reported a high pore size to be desirable for better diffusion of reactants and product molecules. Thus, the bio-catalyst prepared from ES for application in bio-diesel production is recommended.

From the viewpoints of preparation time, energy consumption, and cost of catalyst preparation, the temperatures of 700 and 800^{o}C were selected as perfect calcination temperatures to prepare bio-catalysts from animal bones (AB) and mollusk shells (ES and MS), respectively.

3.2 Physicochemical characteristics of the produced bio-diesel from different catalysts

The activity of the prepared bio-catalysts for production of bio-diesel was compared with that of the commercially available and most effective heterogeneous basic catalyst, CaO and Novozyme 435. Data listed in Table 2 revealed that the chemical CaO, and CaO prepared from waste ES and MS, gave higher bio-diesel yields with better qualification than those obtained using $Ca_5(PO_4)_3F$ prepared from waste AB, or that obtained using Novozyme 435. The bio-diesel yields recorded: 95, 94, 93, 90, and 87%, respectively. The density of the produced bio-diesel was recorded as: 0.8717, 0.8922, 0.8952, 0.9095, and 0.9155 g/cm^3, with a % decrease from that of the used WCO: ≈ 6.54, 4.34, 4.02, 2.49, and 1.84%, respectively. The kinematic viscosity of the produced bio-diesel was recorded as: 5.05, 5.32, 5.5, 9.3, and 10.84 cSt, with a % decrease from that of the used WCO: ≈ 92.11, 91.69, 91.41, 85.47, and 83.06%, respectively. While the total acid number (TAN) of the produced bio-diesel was recorded as: 0.24, 0.28, 0.3, 0.7, and 0.81 mg KOH/g oil, with a % decrease from that of the used WCO: ≈ 88.84, 86.98, 86.05, 67.44, and 62.33%, respectively.

The flow properties (density and viscosity) of the produced bio-diesel are within the recommendable range of the standards. However, those prepared by AB and Novozyme bio-catalysts have a higher viscosity than the standards, thus, they would have inferior injection and atomization performance, but offer lubrication and protection for moving parts of an engine.

The TAN of the produced bio-diesel meets the standard limits indicating that the free fatty acid content will not cause operational problems such as corrosion and pump plugging caused by deposit formation.

Density is one of the most important characteristics of bio-diesel. In a combustion system, pumps and injectors require a precise amount of fuel to provide proper combustion. Fuel density is the main characteristic that determines the amount or mass of fuel injected into the combustion chamber (Dzida and Prusakiewicz, 2008). The kinematic viscosity plays an important role in the performance of injector and fuel atomization. If the viscosity is too low, the fuel may not provide sufficient lubrication for the fuel injection pump. However, if the viscosity of fuel is too high or too viscous, the problem is in the injection and would produce larger droplets, resulting in poor combustion (Soetaredjo *et al*., 2011). This parameter is also useful for evaluating the methyl ester content of bio-diesel samples since there is a correlation between the content of esters and the viscosity; the higher the viscosity, the lower the ester content (Ma and Hanna, 1999).

The produced bio-diesel has a lower calorific value (CV) than Egyptian petro-diesel standards, but is within the recommendable range of international bio-diesel standards.

Dubé *et al.* (2004) and Jiang *et al.* (2011) reported that GPC could help to simultaneously detect the content of diglycerides, triglycerides, glycerol, and FAME in the process of transesterification with a refractive index detector. In this study, GPC analysis revealed that the main component of WCO is fatty acid glycerin ester, with an average molecular weight (MW) distribution of 1851 and a retention time (RT) of 29.452 min. After transesterification, the peak of fatty acid ester (MW 1851) disappeared and a new peak appeared at a RT of around 33 min, with an average molecular weight of 508, 515, and 507 in the case of chemical CaO, and CaO prepared from waste ES and MS, respectively. This may indicate that fatty acid glycerides have been transformed into FAME (bio-diesel).

Table 2. **Bio-diesel yield and its physicochemical characteristics**

Parameters	Bio-diesel chemical CaO	Bio-diesel AB-catalyst	Bio-diesel ES-catalyst	Bio-diesel MS-catalyst	Bio-diesel Novozyme 435	Egyptian petro-diesel standards	Bio-diesel (EN14214)	Bio-diesel (D-6751)
Yield, wt%	95%	90%	94%	93%	87%	---	---	---
Density@ 15.56^{o}C, g/cm	0.8717	0.9095	0.8922	0.8952	0.9155	---	0.86-0.90	---
Viscosity @40^{o}C, cSt	5.05	9.3	5.32	5.5	10.84	1.6-7	3.5-5	1.9-6
Total acid number, mg KOH/g	0.24	0.7	0.28	0.3	0.81	Nil	< 0.5	< 0.8
Sulfur, wt%	Nil	Nil	Nil	Nil	Nil	< 1.2	< 0.01	< 0.05
Flash point, ^{o}C	136	150	137	140	160	> 55	> 101	> 130
Calorific value, MJ/kg	38.49	37.20	39.80	38.15	37.00	> 44.3	32.9	----

In the case of transesterification of WCO with Novozyme 435 or $Ca_5(PO_4)_3F$ prepared from waste AB, the presence of the two peaks indicates incomplete transesterification.

The produced bio-diesel has two major advantages: 1) they are all free of sulfur, thus, their combustion will not produce acidic sulfur oxides, which would lead to the corrosion of engine parts and environmental pollution; and 2) they have a high flash point ranging between 136-160^{o}C, which can prevent auto ignition and fire hazards, making them quite safe for handling, transportation, and storage. The properties of the produced bio-diesel are completely acceptable and meet most of the specifications, therefore, it can be ranked as a realistic fuel and as an alternative to petro-diesel.

The better bio-diesel yield and characteristics of that produced using the chemical CaO, and CaO prepared from waste shells, might be attributed to the reported high basic strength ($H_- = 26.5$) of CaO, which consequently would possess high activity and a long service lifetime (Liu *et al*., 2008).

3.3 Reusability of different catalysts

When the transesterification reaction is finished, the catalyst is separated from the mixture and reused again without any subsequent treatment in a new reaction under the same conditions as before. All of the prepared bio-catalysts and chemical CaO can be repeatedly used up to 5 times with no apparent loss of activity, however, Novozyme 435 lost its activity and was only used once, but this might be attributed to lipase denaturation by high methanol concentration.

4. CONCLUSIONS

The prepared bio-catalysts have the major advantages of easy separation, reusability and high yield production of good quality bio-diesel. Moreover, these bio-catalysts present good catalytic activity in a bulk solid form, which would open the possibility to perform a continuous catalytic process for bio-diesel production in both slurry and fixed bed configuration reactors.

The use of organic waste for the production of useful and efficient bio-catalysts, and waste cooking oil as inexpensive feedstock for bio-diesel production, would solve energy, environmental, economic, and waste management problems.

Further work is currently being undertaken in the Egyptian Petroleum Research Institute EPRI Biotechnology Laboratory for optimization of the transesterification reaction using the prepared bio-catalysts and Novozyme 435.

5. REFERENCES

ASTM. 2008. D6751. Standard specification for bio-diesel fuel (B100) blend stock for distillate fuels. American Society for Testing Materials, West Conshohocken, PA.

ASTM. 1991. Annual Book of ASTM Standards: sections. Petroleum Products, Lubricants, and Fossil Fuels. Volumes 0.5.01 – 05.03. American Society for Testing Materials, West Conshohocken, PA.

Boey PL, Maniam GP, Abd Hamid S, and Ali DMH. 2011. Utilization of waste cockle shell (*Anadara granosa*) in biodiesel production from palm olein: Optimization using response surface methodology. Fuel. 90: 2353-2358.

Borgwardt RH. 1989. Sintering of nascent calcium oxide. Chem. Eng. Sci. 44: 53–60.

Boro J, Deka D, and Thakur AJ. 2012. A review on solid oxide derived from waste shells as catalyst for biodiesel production. Renew Sustain. Energy Rev. 16: 904-910.

Boro J, Thakur AJ, and Deka D. 2011. Solid oxide derived from waste shells of *Turnonilla striatula* as a renewable catalyst for biodiesel production. Fuel Process. Technol. 92: 2061-2067.

Chakraborty R, Bepari S, and Banerjee A. 2011. Application of calcined waste fish (*Labeo rohita*) scale as low-cost heterogenous catalyst for biodiesel synthesis. Bioresour. Technol. 102: 3610–3618.

Dubé MA, Zheng S, Mc Lean DD, and Kates M. 2004. A comparison of attenuated total reflectance-FTIR spectroscopy and GPC for monitoring biodiesel production. J. Am. Oil Chem. Soc. 81(6): 599-603.

Dzida M and Prusakiewicz P. 2008. The effect of temperature and pressure on the physicochemical properties of petroleum diesel oil and biodiesel fuel. Fuel. 87: 1941-1947.

El-Gendy NSh, Deriase SF, and Hamdy A. 2014. The optimization of biodiesel production from waste frying corn oil using snails shells as a catalyst. Energy Sources, Part A. 36(6):1-15.

El-Gendy NSh and Madian HR. 2013. Ligno-cellulosic biomass for production of bio-energy in Egypt. Lambert Academic Publishing LAP, GmbH & Co. KG. Germany.

Engin B, Demitras H, and Eken M. 2006. Temperature effects on eggshells investigated by XRD, IR and ESR techniques. Radiat. Phys. Chem. 75: 268-277.

Helwani Z, Othman MR, Aziz A, Fernando WJN, and Kim J. 2009. Technologies for production of biodiesel focusing on green catalytic techniques: A review. Fuel Process. Technol. 90: 1502-1514.

Jiang DY, Bai Y, and Guo H. 2011. Exhaust emissions and combustion performances of ethylene glycol monomethyl ether palm oil monoester as a novel biodiesel. Afr. J. Biotechnol. 10(72): 16300-16313.

JUS EN. 2004. JUS EN 14214. "Automotive fuels. Fatty acid methyl esters (FAME) for diesel engines-requirements and test methods". Standardization, Institute, Belgrade, Serbia.

Leung DYC, Wu X, and Leung MKH. 2010. A reiew on biodiesl production using catalyzed transesterification. Apll. Energy. 87: 1083-1095.

Liu X, He H, Wang Y, Zhu S, and Piao X. 2008. Transesterification of soybean oil to biodiesel using CaO as a solid base catalyst. Fuel. 87: 1076–1082.

Liu WQ, Low NW, Feng B, Wang GX, and da Costa JC. 2010. Calcium precursors for the production of CaO sorbents for multicycle CO capture. Environ. Sci. Technol. 44: 841–847.

Ma F and Hanna MA. 1999. Biodiesel production: A review. Bioresour. Technol. 70: 1–15.

Monshi A, Foroughi MR, and Monshi MR. 2012. Modified scherrer equation to estimate more accurately nano-crystallite size using XRD. World J. Nano Sci. Eng. 2: 154-160.

Ngamcharussrivichai C, Nunthasanti P, Tanachai S, and Bunyakiat K. 2010. Bio-diesel production through transesterification over natural calciums. Fuel Process. Technol. 91: 1409-1415.

Obadiah A, Swaroopa GA, Kumar SV, Jeganathan KR, and Ramasubbu A. 2012. Biodiesel production from palm oil using calcined waste animal bone as catalyst. Bioresour. Technol. 116: 512–516.

Qin C, Li C, Hu Y, Shen J, and Ye M. 2009. Facile synthesis of magnetite iron oxide nanoparticles using 1-methyl-2-pyrrolidone as a functional solvent. Colloids Surf. A. 336: 130-134.

Roschat W, Kacha M, Yoosuk B, Sudyoadsuk T, and Promarak V. 2012. Bio-diesel production based on heterogeneous process catalyzed by solid waste coral fragment. Fuel. 98: 194-202.

Sanjay B. 2013. Heterogenous catalyst derived from natural resources for biodiesel production: A review. Res. J. Chem. Sci. 3(6): 95-101.

Shafiei F, Behroozibakhsh M, Moztarzadeh F, Haghbin-Nazarpak M, and Tahriri M. 2012. Nanocrystalline fluorine-substituted hydroxyapatite [$Ca_5(PO4)3(OH)_{1-x}F_x(0 \leq x \leq 1)$] for biomedical applications: preparation and characterization. Micro Nano Lett. 7(2): 109–114.

Sharma B, Rasid U, Anwar F, Erhan S, 2011. Lubricant properties of Moringa oil using thermal and tribological techniques. J. Therm. Anal. Calorim. 96: 999-1008.

Singh NB and Singh NP. 2005. Formation of CaO from thermal decomposition of calcium carbonate in the presence of carboxylic acids. J. Thermal Anal. Calorim. 89: 159-162.

Soetaredjo FE, Ayucitra A, Ismadji S, and Maukar AL. 2011. KOH/Bentonite catalysts for transesterification of palm oil to biodiesel. Appl. Clay Sci. 53: 341-346.

Talebian-Kiakalaieh A, Amin NAS, and Mazaheri H. 2013. A review on novel processes of bio-diesel production from waste cooking oil. Appl. Energy. 104: 683-5710.

Viriya-Empikul N, Krasae P, Nualpaeng W, Yoosuk B, and Faungnawakij K. 2012. Biodiesel production over Ca-based solid catalysts derived from industrial wastes. Fuel. 92: 239-244.

Viriya-Empikul N, Krasae P, Puttasawat B, Yoosuk B, Faungnawakij K, Chollacoop N, and Faungnawakij K. 2010. Waste shells of mollusk and egg as bio-diesel production catalysts. Bioresour. Technol. 101: 3765–3767.

Yoosuk B, Udomsap P, Puttasawat B, and Krasae P. 2010. Improving transesterification activity of CaO with hydration technique. Bioresour. Technol. 101: 3784-3786.

NUMERICAL SIMULATION ON THE OIL BIOREMDIATION PROCESS OF REAL-SCALE SOIL USING A MICROBIOLOGICAL MODEL

Yao Luan[1§] and Tetsuya Ishida[2]

[1]Department of Civil and Environmental Engineering, Saitama University, Japan; [2] Department of Civil Engineering, The University of Tokyo, Japan

ABSTRACT

Degradation of oil using microbials, known as bioremediation, is a promising method used to remedy oil-contaminated soil. In this study, numerical analysis of the bioremediation of in-situ soil in the groundwater zone is carried out. Finite element modeling in the groundwater direction is established. The boundary nodes are set to a constant value of dissolved oxygen concentration to coincide with oxygen supply from the injection well. Microbial biomass growth and the corresponding kinetics of oil degradation is simulated using a microbial model. For the principal environmental factor, dissolved oxygen and its transport in saturated soil is also simulated. The microbial activity and the amount of dissolved oxygen is numerically coupled in the analysis. The results are compared with measured data from the in-situ experiment, which show that within three years, most of oil in the downstream groundwater direction can be effectively degraded, and the overall process can be reasonably reproduced in the analysis.

Keywords: Oil contamination, Biodegradation, Modeling, In-situ soil

[§]Corresponding Author: Yao Luan, Department of Civil and Environmental Engineering, Saitama University, Shimo-Okubo 255, Sakura-ku, Saitama-shi, 338-8570, Japan; Tel: +81-48-858-3565; luanyao@mail.saitama-u.ac.jp

1. INTRODUCTION

Contamination of soil from oil spills has become an important environmental issue around the world. Decontamination technologies include combustion, distillation, washing and biodegradation. Biodegradation, also known as bioremediation, is to decompose oil using microbials. The cost is relatively low and easy to conduct. However, bioremediation is a complicated bio-chemical process and is greatly influenced by environmental factors such as temperature, water, and oxygen. To reasonably evaluate or predict the effect of bioremediation, it is necessary to couple microbial activity with those environmental factors.

In the author's research group, an analytical system was established to simulate aerobic bioremediation of oil-contaminated soil (Luan and Ishida. 2013). In this system, the oil degradation rate is modeled based on microbial growth rate, which is the function of environmental factors such as temperature, water, and oxygen, as well as oil concentration. Those factors are simulated based on their transport properties in soil. Using this system, numerical analysis was conducted and the results were verified using laboratory experiments. In this paper, the focus is on in-situ soil under natural environmental conditions. The objective is to simulate the bioremediation process reasonably. Before that is discussed, the analytical system will be briefly introduced.

2. THE ANALYTICAL SYSTEM OF BIOREMEDIATION

Biodegradation and environmental factors are coupled physically. Microbial activity depends on the environment and also changes the local environment. As Figure 1 shows, the analytical system consists of the environmental sub-system and the microbial model. The environmental sub-system deals with the environment in soil. Four transport models are optional, depending on the specific environmental condition. They are the heat transport model, water transport model, oxygen transport model and oil transport model, respectively. In each model, soil is assumed to be a porous continuum, and the transport of mass or heat is described using continuous flow. The solutions are temperature, water content, dissolved oxygen concentration, and oil concentration, respectively. The microbial model kinetically simulates microbial growth and oil degradation. Microbial growth rate is a function of those solutions delivered from the environmental sub-system. In each time interval, the amounts of reactants and products, as well as generated heat, are calculated in the microbial model. They are delivered back to the environmental sub-system for the subsequent calculations of heat or mass transport. Herein the details of the environmental sub-system are omitted.

The principal chemical composition of oil is hydrocarbons. For heavy oil, a large portion is octadecane ($C_{18}H_{38}$). If neglecting intermediate reactions, a chemical reaction equation is stoichiometrically written as,

$$C_{18}H_{38} + 22.5O_2 + NH_4^+ \rightarrow C_5H_7O_2N + 13CO_2 + 17H_2O + H^+ \quad (1)$$

where, $C_5H_7O_2N$ is the molecular formula of microbial biomass (Edwards and Nirmalakhandan, 1999; Lamy *et al*, 2013; Komilis *et al*, 2010).

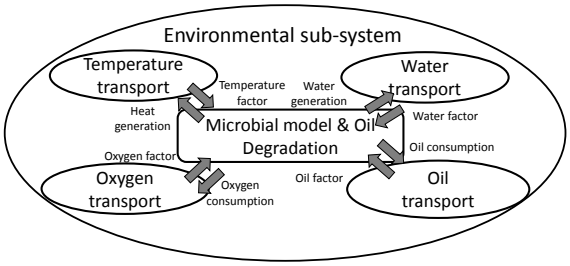

Figure 1 Framework of the analytical system

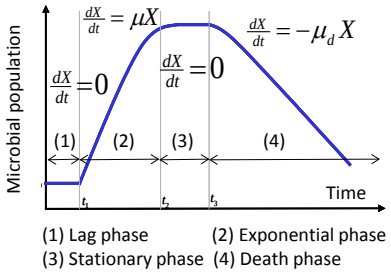

Figure 2 Curve of microbial population

Microbial growth can be generally divided into four phases (Figure 2): 1) lag phase; 2) exponential phase; 3) stationary phase; 4) death phase. In the exponential phase, each microbial cell divides to form two cells, resulting in an exponential increase of population. At this time, microbials are in their healthiest state and oil is degraded efficiently, hence, the model assumes that biodegradation occurs only in the exponential phase. The growth, stagnation and death of microbials can be expressed as,

$$\frac{dX}{dt} = \alpha\mu X - \beta\mu_d X \quad (2)$$

where, X: microbial weight density (kg/m^3), which represents their population in unit soil volume; μ: environmental-dependent growth rate (/day); μ_d: death rate (/day); and α and β: the parameters indicating the growth phase and the death phase, respectively. The values of α and β can be 1.0 or 0.0 according to the life of microbials.

The environmental-dependent microbial rate μ is expressed as,

$$\mu = \mu_T(T) \cdot f_{O2}(\rho_{O2d}) \cdot f_{H2O}(\theta_{H2O}) \cdot f_{CH}(\rho_{CH}) \quad (3)$$

where, μ_T: temperature factor; f_{O2}: oxygen factor; f_{H2O}: water factor; f_{CH}: oil factor; T: temperature (°C); θ_{H2O}: volumetric water content (m^3/m^3); ρ_{O2d}: dissolved oxygen concentration (kg/m^3); and ρ_{CH}: oil concentration (kg/m^3).

Using the microbial growth rate in the exponential phase, based on Eq. 1, the oil degradation rate, oxygen consumption rate, and water generation rate can be stoichiometrically obtained as,

$$\frac{dQ_i}{dt} = k_i \cdot \frac{M_i}{M_{CHON}} \cdot \frac{dX}{dt} \tag{4}$$

where, i represents the reactant or product; M_{CHON}: molecular mass of microbial; M_i: molecular mass of the reactants or product; and k_i: coefficient of reactants or product in Eq. 1. For example, when i indicates oxygen, M_i becomes the molecular mass of oxygen, and k_i is the coefficient with the value of 22.5.

3. IN-SITU EXPERIMENT OF BIOREMEDIATION

Numerical analysis was applied to an in-situ bioremediation, which is briefly introduced in this section (Figure 3). It was conducted by Konoike Construction Co., Ltd. between 2003 and 2006 (Tanaka et al., 2006). The soil contamination was caused by a heavy oil spill, and soil of high oil concentration near the contamination source was excavated and decontaminated. In deeper layers, residual oil remained and was spread with the aid of groundwater. Two vertical injection wells (I1 and I2) were drilled and oxygen release compounds (ORC) and nutrients were injected periodically, which could diffuse downstream. Moreover, two vertical monitoring wells (M1 and M2) were drilled in the downstream area, 1 meter and 5 meters from I2, respectively. Groundwater was sampled from the injection well I2 and the monitoring wells. Total Petroleum Hydrocarbon (TPH) was quantitatively analyzed to obtain residual oil concentration (Ministry of the Environment, Government of Japan, 2006).

Meanwhile, a slurry experiment and column experiment were carried out in the laboratory (Figure 4). Soil samples of similar composition and permeability, along with the in-situ soil were prepared. In the slurry experiment, 10 g of soil was suspended in water in which oil and sufficient nutrients were preliminarily added. The suspension was often shaken to ensure sufficient oxygen. For the column experiment, soil was filled into acrylic pipes with an inner diameter of 3 cm and length of 10 cm. Four such pipes were connected to assemble a soil column. Water of 7-8 mg/L dissolved oxygen (DO), as well as sufficient nutrients, were flowed through the inlet. The applied flow velocity was 0.003 cm/min, similar with that of the groundwater. TPH analysis was then conducted.

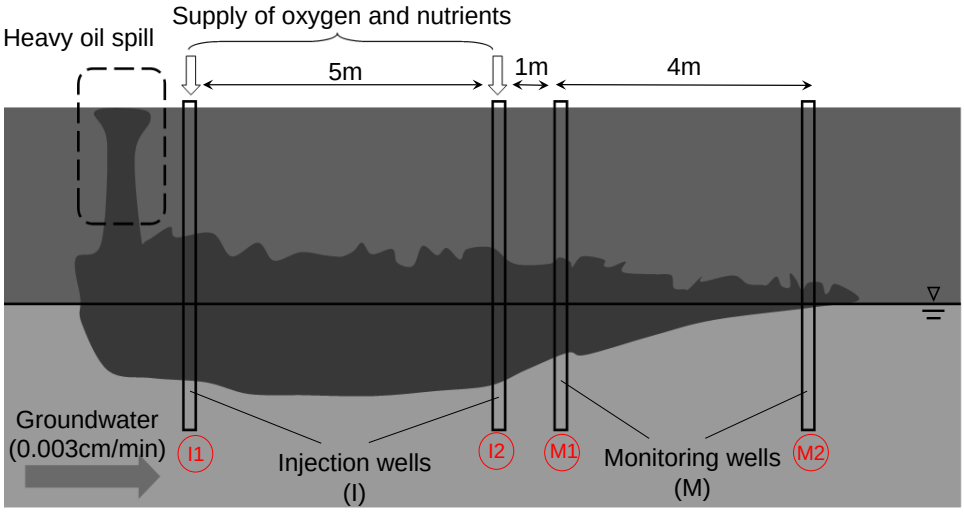

Figure 3 In-situ bioremediation

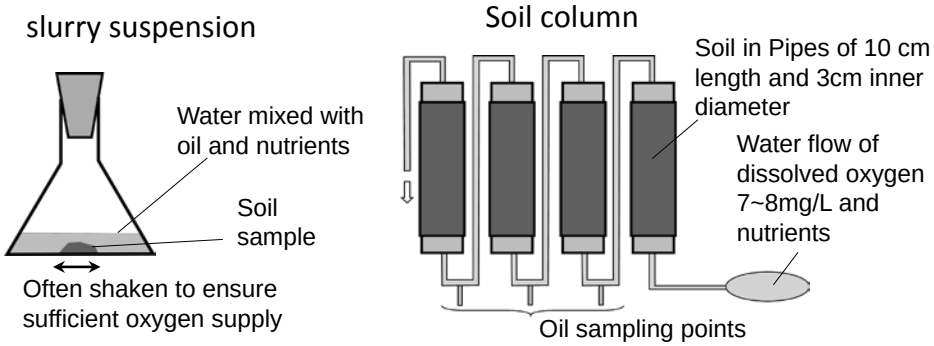

Figure 4 Laboratory experiment

4. NUMERICAL ANALYSIS OF THE BIOREMEDIATION

4.1 Model Establishment and Analysis Approach

Four transport models are optional in the environmental sub-system. For special environmental conditions, reasonable simplifications can be made. Herein, for the in-situ experiment, the release of oxygen and nutrients, as well as the sampling, were carried out in the saturated zone. Oil degradation may also occur in the capillary zone, but it was not investigated probably due to the cost and difficulty of implementation. In the laboratory experiment, all of the soil samples were also saturated, therefore, in this study, numerical analysis focuses on saturated soil, and water content is regarded as constant. In addition, the temperature of groundwater is usually relatively stable, so all of the temperatures are assumed to be the value of 15°C, and moreover,

oil is assumed not to move with groundwater during bioremediation. A crucial environmental factor is the amount of dissolved oxygen, which dominates in the column and in-situ experiments, hence, the oxygen transport model is activated and implemented in the analysis.

Oxygen transport in saturated soil is described using the following equation,

$$\varphi \frac{\partial \rho_{O2d}}{\partial t} = -A\tau_d D_0^d \cdot \frac{\partial^2 \rho_{O2d}}{\partial x^2} + Q_{O2} \tag{5}$$

where, φ: soil porosity; ρ_{O2d}: concentration of dissolved oxygen (kg/m^3); Q_{O2}: oxygen sink term due to oil degradation (kg/m^3/day); τ_d: tortuosity coefficients of dissolved oxygen transport in soil pores; D_0^d: oxygen diffusion coefficient in bulk water (m^2/day); and A: equivalent factor considering the acceleration effect of groundwater advection.

For the temperature and water factors, constants are assumed. The oil factor is represented as the following equation,

$$f_{CH}(\rho_{CH}) = \frac{\rho_{CH}}{K_{CH} X + \rho_{CH}} \tag{6}$$

where, K_{CH}: coefficient related to half-saturation of oil concentration effect; and X: microbial weight density in Eq. 2, therefore, $K_{CH} \bullet X$ represents oil concentration at the point when the oil factor becomes half of its maximum value. For a constant K_{CH} value and various X values, the function of the oil factor is plotted in Figure 5. With a constant microbial population, microbial activity will decrease as oil concentration decreases, and furthermore, with the same oil concentration, the oil factor value of large populations is lower than that of small populations. This is reasonable, because as the oil amount shared for an individual microbial decreases, the overall community activity will also decrease.

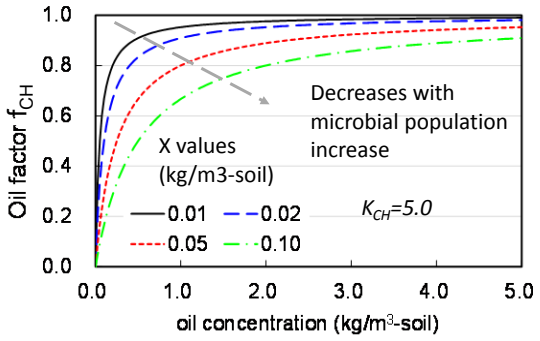

Figure 5 Oil influential factor

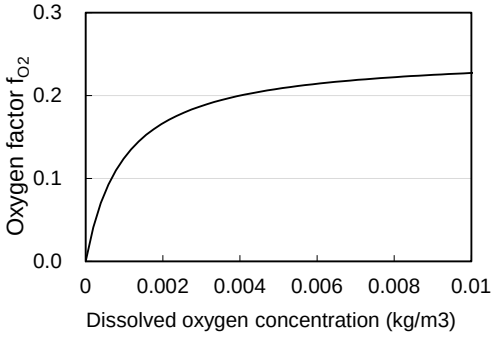

Figure 6 Oxygen influential factor

In the slurry experiment, soil particles were fully dispersed in the suspension. Because frequent shaking ensured sufficient oxygen around most of soil particles, microbial activity can be regarded to approximate the maximum aerobic condition, therefore, the oxygen factor in Eq. 3 is assumed to be 1.0. For the in-situ and column experiments, soil particles were compacted making it difficult for all of microbials to intake oxygen and achieve the maximum activity. The following equation is used to quantify oxygen factor,

$$f_{O2}(\rho_{O2d}) = P\frac{\rho_{O2d}}{K_{o2} + \rho_{O2d}} \tag{7}$$

where, P: the maximum activity in compacted soil conditions; and K_{o2}: half-saturation coefficient. K_{o2} represents the oxygen concentration at the point when the oxygen factor becomes half of P. The function of the oxygen factor is shown in Figure 6 where it can be seen that the oxygen factor increases with oxygen concentration. This trend is more obvious at the low concentration range.

The finite element method is used to deal with oxygen transport cases. For the in-situ analysis, the focus is on well I2 to the spot 10 meters downstream (Figure 7). In well I2, stable oxygen is supplied due to the release of ORC, which can be considered to be a Dirichlet boundary condition. Eight node isotropic elements with size 5 cm are used in the groundwater direction. The nodes in well I2 are restrained with a constant DO concentration value of 8 mg/L, which is the only boundary condition. The initial oil concentrations at the locations of I2, M1 and M2 are known in the experiment, therefore, the initial oil distribution is determined to be linear between each two of them. For the column experiment, a similar geometry model is established, but the length is much smaller (40 cm).

4.2 Analytical Results and Discussions

For the simplest case, the slurry experiment, the analytical results are shown in Figure 8 and compared with experimental data. Although overestimation existed at 4 weeks, generally the analysis was consistent with the experiment. It is revealed that if sufficient oxygen is supplied for varied initial oil concentrations ranging from 1,000 to 10,000 mg/kg, oil can be efficiently degraded in a short amount of time.

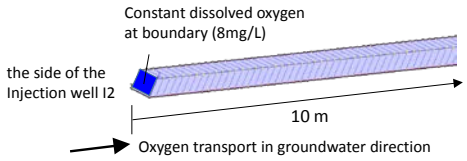

Figure 7 FEM model of the in-situ analysis

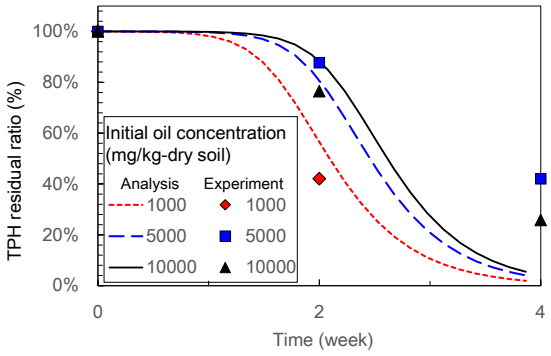

Figure 8 Slurry experiment and analysis results

The results of the column experiment and analysis are shown in Figure 9. It can be seen that oil degradation efficiency is much lower than that of the slurry experiment. After 60 days, including the spot 10 cm from the water inlet, less than 30% of oil was degraded. Moreover, the oil degradation rate decreased as the distance from the inlet increased. In the analysis, this tendency can be reasonably traced. The low degradation efficiency can be attributed to dissolved oxygen transport, and the available oxygen amount depends on the distance from the supply source. The distribution amount of dissolved oxygen from the analysis is shown in Figure 10.

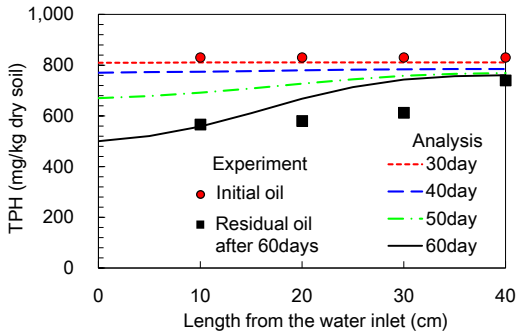

Figure 9 the column experiment and analysis results

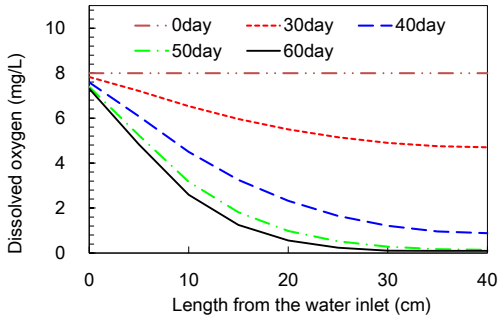

Figure 10 the analysis of dissolved oxygen

The results of the in-situ experiment and analysis are shown in Figure 11. In the experiment, only the data from wells I2, M1 and M2 were opened, so the data in the analysis is shown as a comparison. For I2, the initial concentration was not high (70 mg/L), and due to continuous oxygen supply, oil was effectively degraded. In the experiment, concentration after 1 month became zero. In the analysis, this process takes a longer time, but is completed within several months. For M2, which is 5 m from the injection well, the initial concentration is also not high (100 mg/L), but the degradation efficiency is much slower than that of I2. After 6 months,

concentration decreased to zero, but after that a tiny amount less than 10 mg/L was observed once. In the analysis, it takes around 1.5 years to decrease into a negligible level. Due to the distance from the injection well, oxygen was consumed, but could not be promptly supplied from the upstream, resulting in retardation of microbial activity. With regards to M1, which is 1 meter from the injection well, the initial concentration was very high (1000 mg/L). The experiment indicated that after 2 years the concentration decreased to tens of mg/L, appearing to be an effective degradation. The analysis shows a relatively faster degradation, and after 2 years the concentration becomes negligible. Based on the above discussion, it can be concluded that the overall tendency of in-situ bioremediation is to roughly reproduce the aspects of time and residual oil level. Even so, it should be recognized that the analysis largely simplifies in-situ conditions. Several factors that may influence the final result are not considered. For example, oil may flow with the pressure of groundwater, increasing oil concentration downstream. It is also probable that oil in the capillary zone sinks into the saturated zone. Rainwater percolation may be another source of oxygen supply. The transport of nutrient salts needed may also be taken into account. More sophisticated studies on those influences should be carried out in the future.

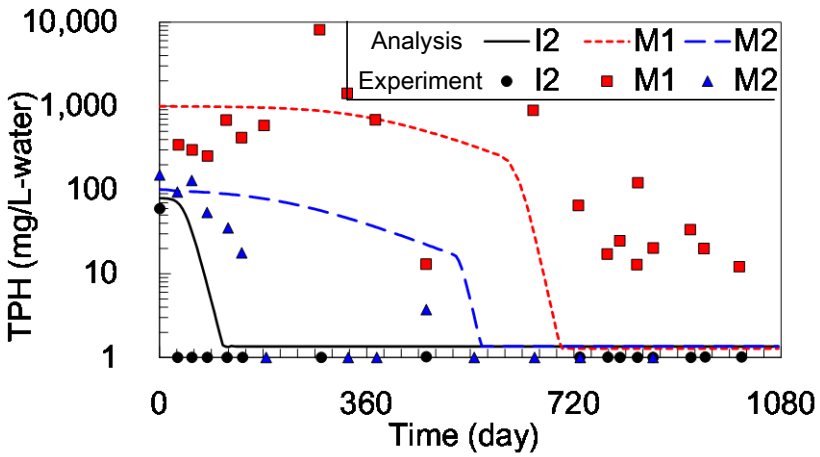

Figure 11 The results of the in-situ experiment and analysis

5. CONCLUSION

In this study, numerical analysis of the bioremediation of in-situ soil in the groundwater zone was conducted. A one-dimensional finite element model in the groundwater direction was established. Dissolved oxygen concentration was regarded as the most important environmental factor in this process, therefore, dissolved oxygen transport in saturated soil was simulated and

coupled with microbial activity. The nodes in the boundary are set to a constant value of dissolved oxygen concentration to coincide with oxygen supply from the injection well. The results were then compared with the measured data from the in-situ experiment. The results show that within three years, most of oil in the downstream groundwater direction can be effectively degraded, and the overall process can be reasonably reproduced in the analysis.

6. REFERENCES

Edwards F and Nirmalakhandan N. 1999. Modeling an airlift bioscrubber for removal of airphase BTEX. J. Environ. Eng. 125(11): 1062-1070.

Komilis D, Vrohidou A, and Voudrias E. 2010. Kinetics of aerobic bioremediation of a diesel-contaminated sandy soil: effect of nitrogen addition. Water Air Soil Pollut. 208(1-4): 193-208.

Lamy E, Tran T, Mottelet S, Pauss A, and Schoefs O. 2013. Relationships of respiratory quotient to microbial biomass and hydrocarbon contaminant degradation during soil bioremediation. Int Biodeterior. Biodegradation. 83: 85-91.

Luan Y and Ishida T. 2013. Numerical simulation on the bioremediation of oil contaminated soil using a microbiological reaction model. Proceedings of the 9th International Symposium on Social Management Systems, 2-4 December 2013, Sydney, Australia. Available from: http://management.kochi-tech.ac.jp/?content=ssmspaper.

Ministry of the Environment, Government of Japan. 2006. Countermeasure Guideline for Oil Contamination, Document B (*In Japanese*).

Tanaka H, Fujinaga A, Kiyoto M, Uragami H, and Sasamoto Y. 2006. In-situ bioremediation studies of oil contaminated soil (*In Japanese*). Annual Technical Report of Konoike Construction Co., Ltd. Available from: http://www.konoike.co.jp/solution/thesises/pdf/2006_civil_02.pdf.

IMPLEMENTATION OF THE SWRCB's LOW THREAT PETROLEUM UNDERGROUND STORAGE TANK (UST) CLOSURE POLICY AT NON UST SITES IN SANTA BARBARA COUNTY

Paul McCaw[1], Charles Lambert[2,3], Katherine Butler[4§], Rebecca Countway[3]
[1]*2125 South Centerpointe Parkway, Room 333, Santa Maria, California, USA, 93455,*[2]*100 Theory Drive, Suite 100 , Irvine, California, 92617, USA,* [3]*1608 Pacific Ave, Suite 201, Venice, California, USA, 90291,* [4]*241 N Figueroa St, Los Angeles, California, USA, 90012*

ABSTRACT

Santa Barbara County has a large number of historical and operating crude oil exploration and production facilities. The county's Land Use Element for restoration of properties in the former oilfields requires restoration of oil leases prior to final lease closure. The recent California State Water Resources Control Board (SWRCB) Low Threat Underground Storage Tank Case Closure Policy (LTCP) may be applicable to some of these sites. The primary purpose of this guidance is to establish consistent statewide case closure criteria for low-threat petroleum UST sites. There have been questions as to how to implement the guidance at non-UST petroleum sites (e.g. oil and gas production sites, above ground storage areas, tank farms, sumps, etc.), which guidance suggests may be possible for release scenarios with "attributes similar to those which this policy addresses." Implementation at non-UST petroleum sites requires additional considerations mentioned only briefly, or not at all in the guidance, such as:

1) The presence of ecological concerns/receptors at or near the site;

2) The presence of elevated levels of total petroleum hydrocarbon (TPH) that will be left in place in shallow soil, or in deeper soil where there is a high likelihood they will be brought to the surface, which may provoke stakeholder concerns. The LTCP does not address nuisance TPH issues for soil nor does it account for noncancer health effects associated with higher molecular weight environmentally persistent petroleum hydrocarbons;

3) The use of the site for residential development or other sensitive receptors (e.g. schools), or the presence of sensitive receptors adjacent to the site;

---

[1]Corresponding Author: Paul McCa*w*, 2125 South Centerpointe Parkway, Room 333, Santa Maria, California, USA, 93455; Tel: (805) 346-8359; Paul.McCaw@sbcphd.org

4) The presence of metals (e.g. arsenic, lead, nickel, vanadium) in excess of regional background concentrations; and

5) Sites where the cumulative cancer risk or noncancer hazard may be significant (e.g. multiple petroleum-related chemicals [such as toluene, xylenes, trimethylbenzenes, tert-butyl alcohol] just at the low-threat thresholds or screening levels).

In this paper, we describe additional steps to address these concerns and determine when additional site investigation, a human or ecological risk assessment, remedial actions, and/or a land use covenant may be required for non-UST petroleum sites.

1. Introduction

The primary purpose of the LTCP guidance (Cal/EPA, SWRCB, 2012) is "to establish consistent statewide case closure criteria for low-threat petroleum UST sites." The policy was designed to improve the UST program by focusing on high priority cases (drinking water or other human health related impacts, with product still in place) and developing "Path to Case Closure Plans."

Santa Barbara County has a large number of historic and operating crude oil exploration and production facilities, including some in residential areas. There has been interest from responsible parties in applying the LTCP at non-UST sites. These non-UST sites include former oil and gas production areas, above ground storage tank sites, tank farms, sumps, and former refinery locations. Implementation at other types of petroleum sites requires additional steps and considerations mentioned only briefly, or not at all, in the current guidance. Santa Barbara County Environmental Health Services (SBC EHS) has experience applying these additional considerations and believes there are examples where the LTCP can be applied to non-UST sites, however, they will typically require the responsible party to conduct additional environmental investigations to support the low-threat status.

2. Petroleum-Impacted Sites in Santa Barbara County

Oil and gas sites in Santa Barbara County and the associated chemicals of potential concern (COPCs) fall into several categories. Former and operating oil and gas leases are found throughout the county, and COPCs at these properties usually are limited to TPH, metals, and both non-carcinogenic and carcinogenic PAHs. In addition to these petroleum-related compounds, COPCs at abandoned

sumps and pipeline corridors may include chlorinated chemicals, organochlorine pesticides, and polychlorinated biphenyls (PCBs). Sites such as former tank farms, oil and gas separation plants, and small refineries often have an even more extensive list of COPCs, including the presence of TPH, metals, volatile and semi-volatile organic compounds, chlorinated compounds, dioxins, and PCBs. The area of impact for nearly all of these types of sites typically is greater than the 25x25 meter area to which the LTCP soil screening levels apply.

3. Conditions Excluding Application of the LTCP Guidance

There are certain conditions in Santa Barbara County which exclude application of the LTCP guidance. For example, if ecological concerns/receptors are present at or near the site, the LTCP guidance does not apply. Similarly, if elevated levels of petroleum hydrocarbons will be left in place in shallow soil, or in deeper soil at sites where development may bring them to the surface and possibly provoke stakeholder concerns, it would be difficult to leave the impacted soil in place. The LTCP does not address soil nuisance issues nor does it account for noncancer health effects associated with environmentally persistent petroleum hydrocarbons.

Additional conditions which also exclude application of the LTCP guidance include: if the site is or will be used for residential development or other sensitive receptors (e.g. schools); if sensitive receptors are located adjacent to the site; if metals (e.g. arsenic, lead, nickel, vanadium) exceed regional background concentrations; if the cumulative cancer or noncancer health risk is significant (i.e. multiple petroleum-related chemicals [e.g. benzene, toluene, xylene, trimethylbenzenes, tert-butyl alcohol, polycyclic aromatic hydrocarbons (PAHs)], if the presence is found to be just below the low-threat thresholds, the SWRCB Environmental Screening Levels [ESLs] for human health, and/or the USEPA's Regional Screening Levels [RSLs]), or if the impacted area is greater than 25 x 25 meters.

Currently, the LTCP does not include soil screening levels for direct contact with TPH. Cal/EPA's Department of Toxic Substance Control (DTSC) specifies TPH as a COPC and identifies a process to evaluate associated non-cancer risk (Cal/EPA, 2013). In addition, TPH has a low ecological threshold of concern for soil invertebrates (~1,000 mg/kg). TPH cannot be left in residential areas without further assessment [e.g. Human Health Risk Assessment (HHRA)], and TPH as crude oil may create a localized soil nuisance under the LTCP guidance obstructing the free use of property. Residual TPH previously has been the basis for litigation in Santa Barbara County, particularly in areas where homes have been built on former oil and gas lease properties.

4. A Complete Environmental Assessment – The Key to Non-UST Sites

In order to assess any oil and gas operation, a complete adequate environmental assessment is needed. The assessment should include a thorough historical review of TPH, volatile organic chemicals (VOCs), semi-VOCs (including PAHs via GC/MS-SIM), and metals in soil, as well as other potential COPCs such as PCBs, pesticides, and/or dioxins, depending on the site history. Assessment of soil gas should be site-specific and based on operational history, known and potential contaminant sources, and the results of soil investigations, in addition to planned future land use. Consultation with Santa Barbara County EHS is necessary to ensure all issues are satisfactorily addressed.

Important questions to consider when reviewing the results of the environmental assessment and considering LTCP applicability to the site include the following:

- Are metals greater than regional or site-specific background levels?
- Is TPH > 1,000 ppm in the shallow soil horizon?
- Are non-petroleum-related COPCs present?
- Do any of the petroleum-related COPCs exceed 0.25 of the USEPA RSLs?
- Is the site currently or in the future likely to be residential or sensitive use (e.g. school, hospital, etc.)?
- Are ecological receptors and/or significant habitat present?

If the answer is yes to any of these it is unlikely that the site would qualify for the LTCP without a site-specific HHRA and/or ecological risk assessment.

Houses built on former oil and gas leases in Santa Barbara County generally require a site-specific HHRA to support no further action and the ability to sell property without a deed restriction, and as such, these would not fall under the LTCP guidance. This does not include houses built on former sumps, but does apply to houses built on former oil lease areas where TPH was moved around by development. TPH is a heavy, weathered material present in highly variable concentrations, and is generally found in concentrations greater than 1000 ppm. Usually there are no ecological concerns, a limited vapor intrusion threat, and very few non-petroleum-related COPCs. However, there is a high level of public concern, as well as soil nuisance issues that must also be considered.

5. CONCLUSIONS

The following conditions make a site a good candidate for low-threat closure in Santa Barbara County:

1) Sumps or hydrocarbon-impacted soil beneath rights-of-ways, or at depth in recreational areas or other low-exposure potential situations;

2) Residual impacts will not obstruct free use of property or interfere with comfortable enjoyment of life or property;

3) Property owner agrees in writing to restrict future land use as appropriate; and/or

4) Agricultural or commercial/industrial properties with appropriate restrictions on future land use.

Application of the LTCP guidance at non-UST sites requires careful consideration of important issues to Santa Barbara County, including future land use, a complete environmental data set and property owner's rights to free and comfortable enjoyment of life and property.

5. REFERENCES

California Environmental Protection Agency, Department of Toxic Substances and Control (Cal/EPA DTSC). 2013. Preliminary Engangerment Assessment Guidance Manual. Interim Final. October.

California Environmental Protection Agency, State Water Resources Control Board (Cal/EPA SWRCB). (2012). Low-Threat Underground Storage Tank Case Closure Policy. November.

A RATIONAL APPROACH TO METHANE HAZARD ASSESSMENT

John Sepich[1§] and Stephen Marsh, Esq.[2]
[1]*Brownfield Subslab, San Antonio, TX,* [2]*McKenna Long & Aldridge, LLP, San Diego, CA*

ABSTRACT

Two quotations sum up the dilemma facing methane reform:

"It's easier to fool *people than* to *convince them that* they have been fooled." – Mark Twain, and

"It is difficult to get a man to understand something, when his salary depends upon his not understanding it." – Upton Sinclair.

A serious incident known as the Ross explosion in 1984 marked the general beginning of methane awareness among the populace of Los Angeles. "Methane Madness" came later when moderate and rather harmless levels of methane in the soil at Los Angeles' proposed Belmont Learning Center were made into a decade long media spectacle. Meanwhile the La Brea Tar Pits – a world tourist mecca for hydrocarbon seepage – was not even on the methane radar as far as the same media were concerned. The site was "grandfathered."

Misguided and inaccurate reporting of high profile methane issues has fooled many into believing that methane explosions are inevitable in widespread geographic areas, and that there is no way to know if particular sites are at risk or not. These erroneous beliefs have become entrenched in the public mind and memorialized in government regulations. A now thriving methane junk science and mitigation industry generates enormous revenue through a combination of professional fees, equipment, materials, installations, inspections, operations, maintenance and monitoring. Any change in the status quo could affect profits.

Actual hazard from soil gas is uncommon. Current practice involves widespread mitigation of thousands of sites with no methane hazard whatsoever, at great cost and no benefit. The factors that make methane hazardous are well established. It is important now to also make them "understood."

[§]Corresponding Author: John Sepich; 4007 McCullough Avenue #469, San Antonio, Texas 78212; Tel: (213) 500-0425; jesepich@gmail.com

This paper presents the science behind methane site risk assessment, and examines the progress that is being made in the various regulatory arenas, a conversation which must always include the San Diego County example.

Keywords: methane, media, politics, money, vested interests, junk science, profiteering, low risk, no risk, no action

1. INTRODUCTION – MEDIA, POLITICS, AND REGULATIONS

Media, politics, and even governmental regulations shape the public perception of methane hazard. In southern California, methane soil gas issues have been simultaneously exaggerated and ignored in the media.

Large areas of Los Angeles and adjacent communities lie on geologic formations containing natural gas and oil. Oil production in downtown Los Angeles began in the late 19th century, with deposits so shallow that the first wells were hand dug. Tar seeps and soil gas are ubiquitous in these areas. At Hancock Park in Los Angeles, the much visited La Brea tar pits have totally captured the public fascination with the extreme gas and tar seepage, as well as the fossil remains of giant ice age mammals. The park is open to the public daily, and schoolchildren on field trips enjoy the bursting tar and methane bubbles in the mastodon pond.

Not far from the La Brea tar pits, the 1984 "Ross explosion" near Third Street and Fairfax Avenue prompted the City of Los Angeles to enact much needed methane mitigation ordinances. Other southern California entities followed with new or updated methane codes.

Against this backdrop a few years later, Belmont Learning Center became a media sensation. The proposed downtown Los Angeles public high school had methane soil gas conditions which were unremarkable for the area, but for a variety of reasons including politics and money, the project had a high media profile. Methane became a ready surrogate for a great number of other issues surrounding the project, all political.

Ironically, while the infamous Belmont Learning Center methane debate raged, the public continued to visit and safely enjoy the complex of museums and park space surrounding and atop the profusely seeping gas and tar at Hancock Park just a few miles to the west with nary a media peep regarding that methane.

1.1 Ross: Methane as News. In 1984, thermogenic gases from the ground found a pathway through a cold joint in the concrete-slab-on-grade at a retail

clothing outlet (Ross) and ignited, apparently, from an electrical spark. The resulting explosion caused considerable property damage and a number of injuries. Fortunately, there were no deaths. Methane continued to flow from cracks in the parking lot for days after the explosion. Soil gas at the site was virtually 100% combustible by volume, mostly methane, and driven by subsurface pressure (Cobarrubias, 1992) measured at 20, and estimated at perhaps up to 40 pounds per square inch (psi) or over 1,000 inches of water column (inH_2O). The site is within the boundaries of the Salt Lake Oil Field, where abandoned and active hydrocarbon wells -- and perhaps some unknown borings -- exist. Geology includes complex faulting . Those injured in the incident brought suit against the City and other parties related to previous oilfield activities. There were differing theories regarding the cause of the incident, with plaintiffs claiming negligent oil operations and defendants claiming natural pathways and causes. The lawsuit was settled under terms not made public. The gas was thermogenic, meaning that it originated in high pressure zones deep in the earth rather than from shallow microbial action. Mitigation measures included passive relief wells and subslab venting, membrane, and electronic gas detection. The shopping center site continued to operate for a number of years after the explosion, and with the retro-fit mitigation measures in place, has since been redeveloped into luxury multi-family housing, which includes subterranean parking, and is built with normal methane mitigation.

1.2 Belmont: Methane as Politics. Powerful political interests drove the media to create the public perception that the Belmont Learning Center (BLC) site was heavily contaminated with both toxic wastes and methane, and could never be safely developed as a school; none of this was true (Kaplan and Sepich, 2010).

The BLC site was located at the edge of the old Los Angeles oilfield (see photographs below), which around the turn of the 20th century had over a thousand producing oil wells on it, but by the 1990's during the height of the Belmont publicity, the field had already been largely depleted for many decades.

Figure 1 - L.A. oilfield circa 1900 (Kaplan & Sepich, 2010).

Figure 2 - L.A. oilfield circa 1900 (Kaplan & Sepich, 2010).

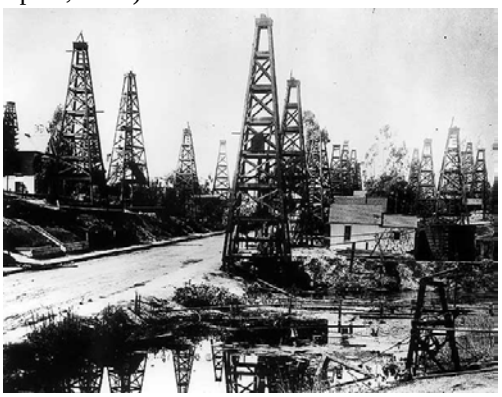

Old Belmont High School Never Had a Methane Incident. The Los Angeles Unified School District (LAUSD) operates public elementary and high schools throughout the City, including many schools within the boundaries of the several oilfields that blanket large portions of the City. Old Belmont High School was constructed in 1927 just blocks from the new BLC site and situated the same as the proposed Belmont Learning Center at the edge of the Downtown L.A. oilfield.

Union Avenue Elementary School Never Had a Methane Incident. Union Avenue Elementary School, of similar age and neighborhood as old Belmont, lies entirely over the old Downtown L.A. oilfield. Soil gas conditions at those two older schools – Union and old Belmont - are so similar to those at the controversial BLC that it can be said the sites are identical from a soil gas risk standpoint. Each of the older schools was built without any methane mitigation, since such science was unknown at their time of construction. Each operated continuously throughout the years without any history of soil gas problems, soil gas complaints, or soil gas incidents. Of course, a long history without methane problems does not guarantee against problems in the future; testing and scientific evaluation are required to evaluate risk.

Soil Gas at Proposed Belmont Learning Center was Identical to Other Older Schools in the Area. Testing of gases at the BLC site showed levels of methane (CH_4) well above the lower explosive limit, elevated carbon dioxide (CO_2), and varying concentrations of hydrogen sulfide (H_2S), which in at least one case was found in the range of tens of thousands of parts per million (ppm). None of the soil gases exhibited inherent pressure. The methane and carbon dioxide were established through isotopic testing to be a mixture of ancient thermogenic and modern microbial gases. The hydrogen sulfide appeared to be formed from reduction of dissolved sulfate in deep oxygen-depleted groundwater zones.

Analytical results showed that both the CH_4 and H_2S had been diluted with air and oxidized by methanotrophs (methane eating bacteria) and sulfur-oxidizing bacteria as they migrated to the surface, greatly reducing their amounts. Wells in the largely depleted oil field were not under excessive pressure, hence, the rate of release of CH_4 and H_2S was in equilibrium and due to their dilution and oxidation during migration, they did not present a danger to surface structures or to humans. Separate health risk analyses of soil vapors at the site showed no toxic or health hazards. Those are simply the scientific facts.

Political Interests Insisted that the Proposed BLC Would Not be Safe.
There were a number of political and other interests at play, which in some ways made Belmont the perfect media storm. The LAUSD was already under fire for poor performance of the educational system, and the methane issue was used quite effectively during this time period to shake up the administration. A great deal of public money was involved, the school's initial budget having been over $100 million. That budget more than tripled in final costs, in no small part due to the confusion over methane safety. The cost overages included funding of many investigative boards, discussion panels, special commissions, and their consultants. Political careers were made and lost. Opponents of an unrelated development, Playa Vista on the west side of the City, recognized the opportunity to transfer negative methane press from Belmont to the Playa Vista site, where methane had also been detected in the soil. Added to this were an abnormal number of individual players and simple gadflies whose reasons for opposing the project were not entirely clear. Many environmental professionals either remained silent or hopped on the bandwagon for a piece of the action. Interestingly, the neighborhood parents whose children would attend the school were always in support of the project. They lived in homes and apartments all around the campus atop soil gas conditions similar to those at the proposed school, many of them for generations. Allegations of incompetence and even criminal activity ultimately caused the District Attorney's office to conduct an investigation. The DA concluded that no criminal activity had occurred (Cooley, 2003).

Project Costs Multiplied. Eighteen years after the initial environmental investigations, the project was finally completed and opened for school in September of 2008, at a cost of nearly $400 million. After years of negative media, the name Belmont Learning Center (BLC) was so stigmatized that the school was successively rebranded Central High #11, then Vista Hermosa, and finally Edward R. Roybal Learning Center, all before it ever opened.

The Belmont Learning Center Site was Never Unsafe. Site testing and competent data evaluation has shown that the BLC soil gas conditions posed little and

probably no risk to the safety of the structures, students, teachers and maintenance personnel -- even without methane mitigation. But in the public perception the mention of Belmont Learning Center still evokes distaste and uneasiness.

1.3 La Brea Tar Pits: How could Methane be a Non-Issue Here? In 1863, Major Henry Hancock purchased the land in the mid-Wilshire area of L.A. known as Hancock Park. Tar from the property was sold to pave nearby roads. The site has long been known for its ice age fossils. In 1965, the Los Angeles County Museum of Art (LACMA) established its present home there. The somewhat newer Page Museum exhibits fossil finds from the site. Even during the height of methane madness in the media, there was never any negative publicity regarding the tar pits park and museums. In fact the tar pits have been and continue to be a great attraction to those students lucky enough to be within field trip range of the site. It is impossible to give any scientific reason why the media presented the Belmont Learning Center site as some sort of hell on earth while ignoring the real methane, the popular tar pits site -- the elephant in the room. Perhaps truth is the first casualty of politics.

1.4 Concentration and Radius-Based Methane Codes. The Ross incident prompted the City of Los Angeles to enact their methane codes and guidelines, which now require that new construction in many areas of the City be provided with methane mitigation measures. The code does not require mitigation for existing structures or for tar seepage, and does not rely upon evaluation of soil gas risk at sites. Since the code is readily accessed through the internet, it is frequently referenced with respect to methane soil gas issues at sites outside of the City. A number of methane codes in southern California pre-existed the Ross incident, with some related to sanitary landfill gas, and others focused on oilfields. Many of these other codes were revisited and revised in the wake of Ross. All of these codes are either zone/radius-based, or concentration-based:

- zone/radius-based – requirements are based upon the physical location of a property, such as within some prescribed methane zone, or within some distance of a landfill, oil well or other potential source of methane soil gas; and
- concentration-based – exceeding "action level" concentrations of combustible gas in soil gas testing, which triggers requirements for mitigation measures at the tested property.

Some codes combine zone/radius criteria with soil gas concentration action levels. Existing codes do not directly consider actual risk. Factors that determine methane risk were not well understood when the codes were enacted.

1.5 San Diego County – The Beginning of Enlightenment. In San Diego County, CA, during the late 1990's, a "flash" or ignition of combustible gas occurred in a utility trench excavation in the Rancho Bernardo area. Subsequent testing showed methane at hundreds of thousands of parts per million by volume (ppmv) in newly-compacted, engineered earth fill. All construction in these areas was halted for a period of time. An emergency ordinance was enacted (San Diego County, 2001) requiring methane mitigation under the slabs of new homes in these areas depending upon methane test results. Some already constructed homes were retrofitted with mitigation systems.

San Diego County faced with the same sensational news coverage that plagued the Los Angeles projects (Union Tribune, 2000). Retrofitting methane mitigation would cost $40,000 to $50,000 per home. Costs of this magnitude could not be passed on to consumers even in a luxury home market. One county supervisor's office offered that: *"We would not want someone to occupy a home … and go into their back yard and have a barbeque that would spark an explosion."*

As we will explain, there was never a methane hazard, the political situation was serious, and there was not sufficient science available to assist in decision-making.

Union-Tribune Newspaper Headlines Figure 3

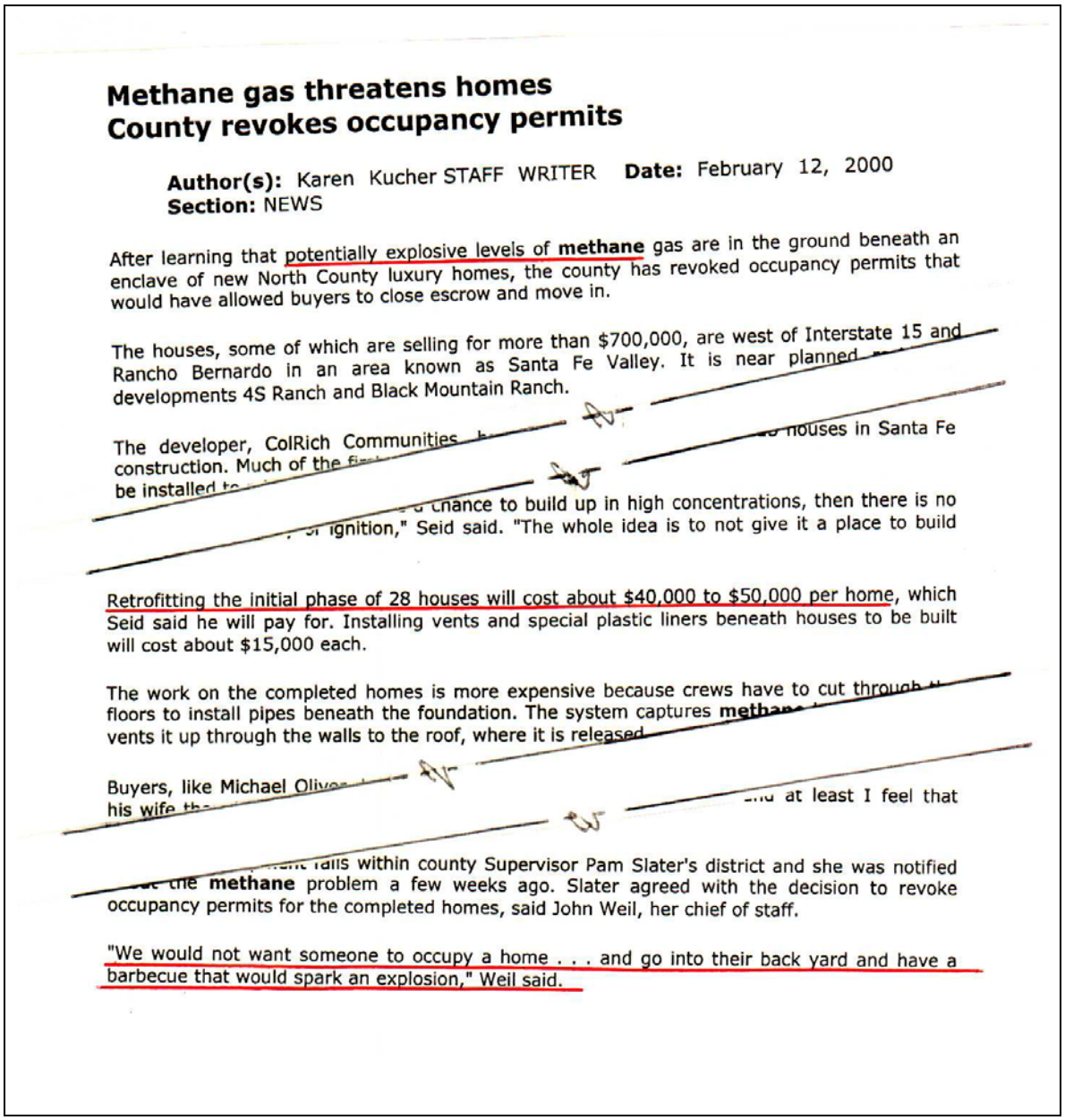

Methane gas threatens homes
County revokes occupancy permits

Author(s): Karen Kucher STAFF WRITER **Date:** February 12, 2000
Section: NEWS

After learning that potentially explosive levels of **methane** gas are in the ground beneath an enclave of new North County luxury homes, the county has revoked occupancy permits that would have allowed buyers to close escrow and move in.

The houses, some of which are selling for more than $700,000, are west of Interstate 15 and Rancho Bernardo in an area known as Santa Fe Valley. It is near planned [illegible] developments 4S Ranch and Black Mountain Ranch.

The developer, ColRich Communities, [illegible] houses in Santa Fe construction. Much of the [illegible] be installed to [illegible]

[illegible] chance to build up in high concentrations, then there is no [illegible] ignition," Seid said. "The whole idea is to not give it a place to build

Retrofitting the initial phase of 28 houses will cost about $40,000 to $50,000 per home, which Seid said he will pay for. Installing vents and special plastic liners beneath houses to be built will cost about $15,000 each.

The work on the completed homes is more expensive because crews have to cut through [illegible] floors to install pipes beneath the foundation. The system captures **methane** [illegible] vents it up through the walls to the roof, where it is released.

Buyers, like Michael Oliver [illegible] his wife [illegible] [illegible] at least I feel that

[illegible] falls within county Supervisor Pam Slater's district and she was notified [illegible] the **methane** problem a few weeks ago. Slater agreed with the decision to revoke occupancy permits for the completed homes, said John Weil, her chief of staff.

"We would not want someone to occupy a home . . . and go into their back yard and have a barbecue that would spark an explosion," Weil said.

San Diego County could have done what every other agency had done previously, and let their emergency ordinance stand. Concentrations of gas found in the soil were far greater than what was generally considered safe at the time. Either the costs of methane mitigation would be borne ultimately by potential homeowners, or perhaps some home building would be not economically viable.

The decision on the part of the County to further evaluate methane was not without much discussion and controversy. However, instead of institutionalizing the ordinance in perpetuity, an ad hoc committee of regional stakeholders – including developers, regulators, and technical professionals – was formed to determine whether the initial emergency code requirements were appropriate.

The committee was organized by Mr. Ivan Holler, then head of the County Building Department. The group brought to bear other science, which was being advanced in southern California outside of the committee. The inclusion of a wide range of stakeholders was critical in developing a complete understanding of not only the science, but also of the socioeconomic impacts of the emergency regulation.

> Enacting regulations to protect the public safety is an essential duty of government and is the highest form of public service. Enacting unnecessary regulations may also be safe, but can constitute a great disservice to the public when the regulations are merely a substitute for understanding.

The action by the County to further study and understand what factors result in an actual methane hazard was unique. The output of the committee prompted somewhat of a breakthrough for methane science and understanding, as discussed later herein.

2. THE EVOLUTION OF METHANE SCIENCE

There is a long history of man versus methane gas hazard, in and around swamps, coal mines, oilfields, pipelines, and sanitary landfills. Early heuristic methods of dealing with explosive gas issues have slowly given way to more scientific approaches. The coal mine canary became obsolete two hundred years ago with the invention of the Davy lamp, but nothing was known at that time regarding what specific concentrations of methane and other gases were actually hazardous. Nearly a century ago, the first electrical gas detector was invented. Within a year of this development, and armed with such new equipment, H. F. Coward published his treatise on methane concentrations that can actually explode in air, which is still the landmark paper on the subject. Now we have a plethora of solid state, flame ionization, infrared, GPS-equipped cavity ring-down spectrophotometers, and other highly sensitive and reliable electronic gas sensors with which to measure gas *concentrations*. Still, there has been a dearth of knowledge regarding the nature of gas movement through the soil, the dynamics of gas intrusion into structures, and what factors other than concentration make soil gas hazardous at structures. However, in just the past decade or two, our knowledge of how to assess methane soil gas hazard has unfolded. **We are now able to establish with a great degree of certainty whether sites with methane soil gas pose a hazard or not.** Below is a step-by-step explanation of how and why.

2.1 First, Some Definitions.

Types of Methane, Defined by Origin. Methane soil gas may be microbial or thermogenic, or a "mixed gas" combination of these.

- Thermogenic methane is formed from ancient organic materials at great depths and pressures underground. Sometimes it seeps to the surface.
- "Microbial" methane, loosely and somewhat ambiguously referred to as biogenic methane[1], is formed from the anaerobic microbial decomposition of shallower buried organic materials.

Soil Gas Compositions. Microbial gas is made up primarily of methane and carbon dioxide, and perhaps some trace compounds. Thermogenic gas may contain large quantities of methane, some higher-order hydrocarbons, and possibly traces of other chemicals. All methane has a molecular composition of CH_4 -- one carbon atom and four hydrogen atoms.

Determination of Origin. Laboratory testing of the isotopic ratios of the carbon

[1] Both thermogenic and microbial methane are formed from biomass, so in that sense they are both biogenic. The term microbial is unambiguous.

atoms and the isotopic ratios of the hydrogen atoms can further identify the genesis of the methane molecules (see "Methane Isotopes Road Map" figure below).

Whole Gases, Defined."Whole gas" refers to either microbial or thermogenic gas found in the soil *undiluted* by air (i.e. nitrogen, oxygen, and other atmospheric gases).

Whole Thermogenic Gas: Methane, ethane, propane, butane, pentane, and possibly traces of hydrogen sulfide, carbon dioxide, or other compounds.

Whole Microbial Gas: Methane, carbon dioxide, and perhaps trace sulfur compounds and various chemical contaminants.

Figure 4 – Methane Isotope Roadmap

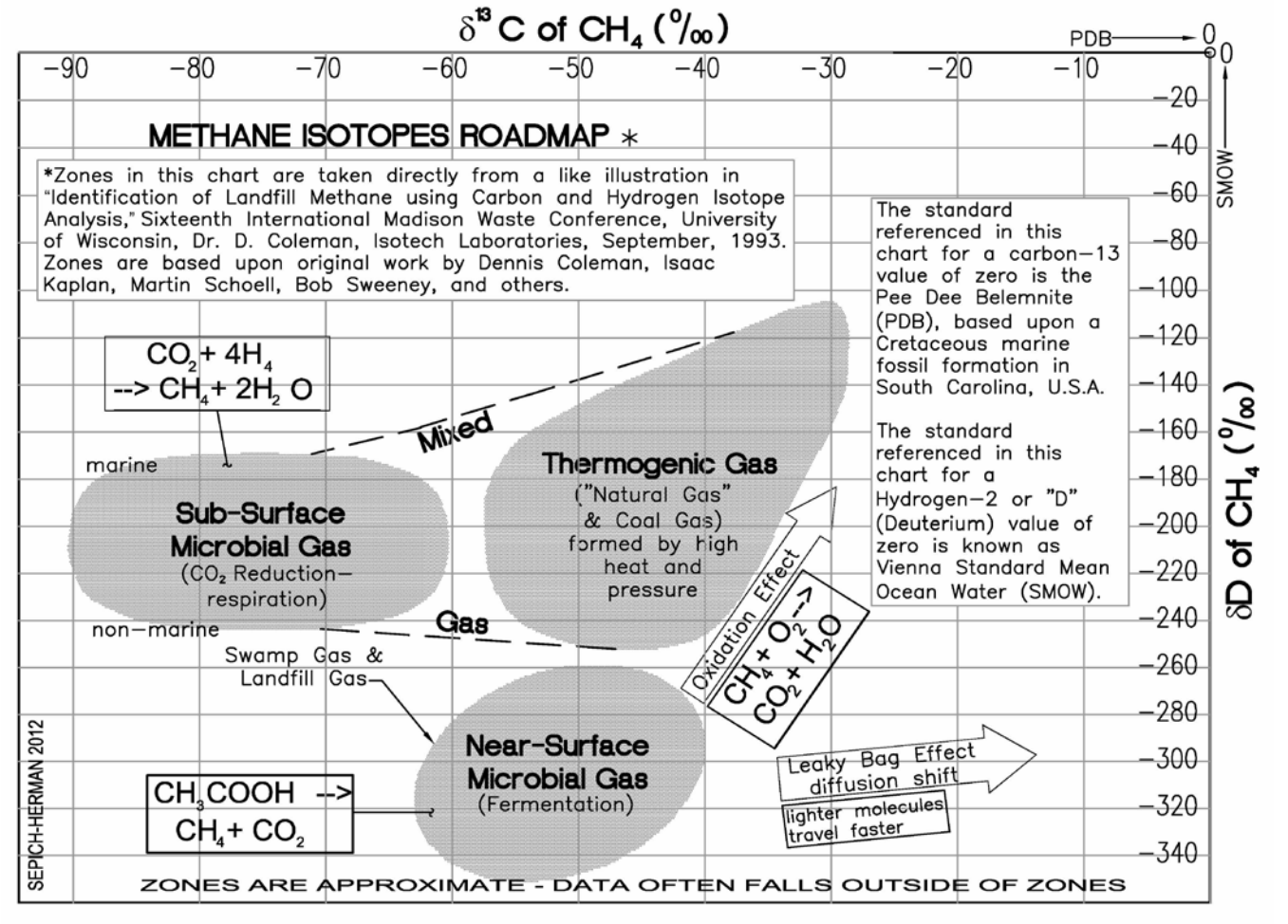

Figure 11 – Google Image

2.2 Historic Management of Coal Mine Gas.

The history of combustible methane gas management and hazard control is long. Some of the more interesting developments included the use of the following technology.

Canaries were found to be more susceptible than humans to such conditions as low oxygen and carbon monoxide, and were taken down into mines as an early form of gas detector.

If a canary passed out, a dangerous situation might exist. Often two canaries were used (100% redundancy).

The Davy Lamp (RKI, 2001). In 1815, the Englishman Sir Humphry Davy invented what became known as The Davy Lamp.

The device was an oil lamp with the flame contained within a glass sleeve, and most importantly, having a flame arrestor.

High flame meant methane; low flame meant low oxygen.

Methane and The Wheatstone Bridge (RKI, 2001). Dr. Oliver Johnson, while working for Standard Oil Company of California (now Chevron), responded to a need to prevent explosions in storage tanks on oil and gasoline tankers.

In 1926, he demonstrated in the laboratory that:

- Hot platinum wire catalytically oxidizes flammable gases at low concentrations;
- The hot wire experiences increased temperature and increased electrical resistance during oxidation of combustible gas; and
- A second hot wire not in the gas stream may be used as a reference filament, with resistance change measured using a modification of the Wheatstone bridge[2] to deflect a meter.

The First "Gas Detector" (RKI, 2001).

In 1927 this same Dr. Johnson introduced the first practical production model of the LEL meter, called the "Standard Oil Electric Vapor Indicator."

The unit had two meters: one for reading gas concentration and another for monitoring sensor voltage.

[2] Invented by Samuel Hunter Christie in 1833, and improved and popularized by Sir Charles Wheatstone in 1843, an electrical circuit used to measure an unknown electrical resistance by balancing two legs of a bridge circuit, one leg on the unknown component, and was initially used for soils analysis and comparison.

2.3 Quantifying Methane Explosive Limits / Cowards Triangle.

Figure 5 – Methane Explosive Limits

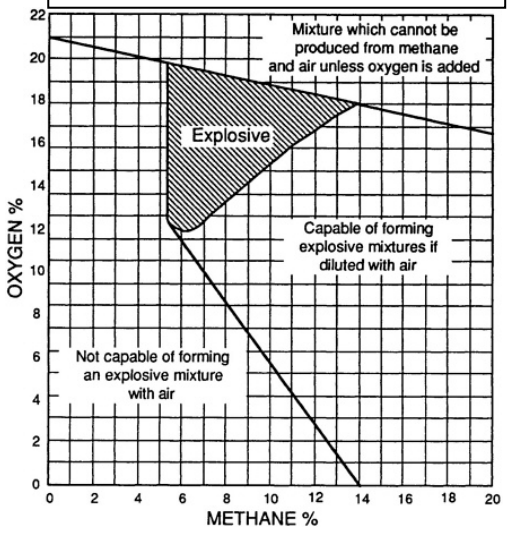

In 1928, just the next year after the production of Oliver Johnson's gas detector, H.F. Coward published his landmark paper in the Transaction of the Institution of Mining Engineers detailing the combustibility of various atmospheres containing methane gas. A modern version of "Coward's triangle" is pictured in the inset at right (NASA, 1994). The information revealed in this paper is still pertinent today. Methane consultants and regulators routinely refer to the combustibility parameters calculated by Coward. The lower explosive limit (LEL) of methane in air is approximately 5% by volume (v/v), and the upper explosive limit (UEL) is about 14% v/v. For an explosion to happen, methane must be

- between the LEL and UEL;
- in a confined space; and
- with a source of ignition (flame, spark, or auto-ignition temperatures).

Below its LEL, methane cannot ignite, combust, burn, flash, or explode, regardless of pressure or other conditions. Above its UEL, air methane is not combustible due to the lack of oxygen. We also know that in the soil methane does not explode or propagate a flame, regardless of concentration or oxygen mixture, due to the small dimension of the pore spaces between soil particles – the soil is effectively a flame arrestor.

2.4 Methane Measurement Units:

For the uninitiated, the various units used to express methane gas concentrations can be confusing. Methane gas concentrations are sometimes expressed as percent volume (i.e. methane in air), sometimes as a percentage of the LEL, and sometimes in parts per million by volume. A value of 100% LEL is the same as 5% v/v, and is also the same as 50,000 ppmv. Table 1

Table 1 – Converting Methane Measurement Units

%CH4	PPMV	% LEL	REMARKS
0.00001	0.1	-	laboratory
0.0005	5	0.01	flame ionization detector
0.05	500	1	catalytic detector accuracy
1.25	12,500	25	indoor air action level
5	**50,000**	**100**	**lower explosive limit (LEL)**
14	140,000	-	upper explosive limit (UEL)
100	**1,000,000**	**-**	**pure methane**

above may help to navigate these units.

2.4.1 Soil Gas Testing.

Much has been written on soil gas test methods. A full discussion of these techniques is beyond the scope of this paper. Existing zone based regulations and Phase 1 environmental reports (ASTM, 2013) identify sites potentially impacted by methane. Phase 2 field testing (ASTM, 2011) may measure methane and perhaps other vapors at a site. Testing may be subsurface, surface, or interior. Methane concentrations, pressures, and other parameters may be defined for a site so that methane risk may be assessed (Sepich, 2012).

Unlike health risks due to chronic exposure from other soil vapors (i.e. VOC's), methane poses safety risks during instantaneous exceedances of the lower explosive limit in indoor air.

VOC's are normally without inherent pressure. Methane may possess inherent gas pressure in the soil, yielding flows of the gas into confined spaces that far exceed diffusive - advective phenomena. Evaluation of methane soil vapor risk involves different considerations than the evaluation of VOC soil vapor risk.

2.4.2 How Does Soil Gas Get into Buildings? (Sepich, 2011)

The intrusion of subsurface vapors into confined, habitable spaces is normally an iterative process caused by a variety of mechanisms, which may include:

- diffusion;
- advection; and
- pressure driven flow.

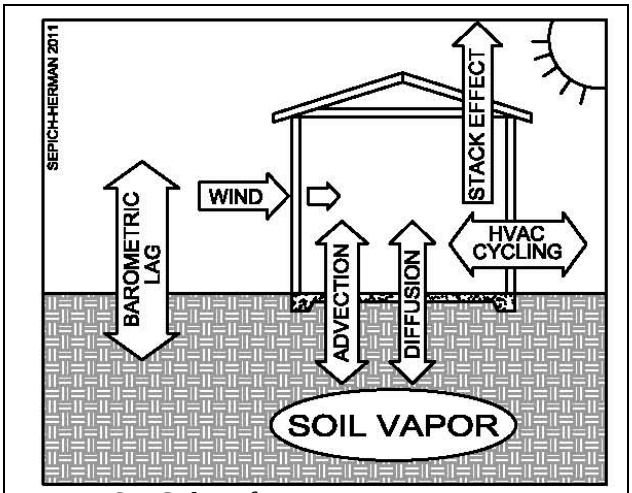

Figure 6 – Subsurface Intrusion

Diffusion is a relatively weak phenomenon whereby molecules move from areas of higher concentration toward areas of lower concentration. This slow process by itself is generally not considered responsible for any significant quantities of methane intrusion across slabs and into buildings. The term "diffusion" is sometimes loosely used to also include "advection."

Advection is the transport of molecules along with the flow of a greater medium, such as methane vapors carried by general movement of soil pore air. Advective

flow across building slabs is due to barometric pressure fluctuations, temperature differentials between buildings and soil, temperature differentials between buildings and outdoor air (stack effect), pressure differentials caused by the on-off cycling of building ventilation systems, wind, and other factors. Advective flow may be a significant factor in VOC intrusion, but not for methane because of the greatly different concentrations of concern (percent volume range for methane versus, for instance, parts per billion / parts per trillion volume ranges for some VOC's).

Convection is properly defined as the sum of diffusion and advection.

Pressure driven flow (Sepich, 2008) may result from introduction of gas under high pressures into the soil matrix. Normally, the soil gas expands away from the pressurized source until the gas concentration is diluted by air, at which point the pressure decreases. In some cases, the higher permeability escape pathways for pressurized soil gas are of limited volume and are directional so that the gas may perhaps escape to atmosphere, or in the worst case, to some confined space receptor whilst still retaining some of its origin pressure at the point of escape or entry. The potential for pressurized flow of soil gases is suggested in field investigations when the subsurface pore space matrix is filled almost entirely with the soil gas to the exclusion of air (oxygen/nitrogen+).

VOC's they may pose a risk at receptor structures even without pressure in the soil vapor, due to their ultra-low concentrations of concern.

Methane soil gas incidents are characterized by pressurized flow, due to high volumes and concentrations required for combustion hazard.

- Inherent or "Genesis" Gas Pressure. Knowledge of the origin of gas in the soil is useful in determining whether the soil gas is diluted or not. Gas may originate from thermogenic or microbial sources, or pipelines.
- Groundwater Pressurization of Gas. Below groundwater, small volumes of soil gas may be pressurized by the groundwater column above.
- De-pressurization. Soil gas pressure may be lost as the gas moves away from a pressurized source.
- Re-pressurization. Soil gas may be re-pressurized by rising groundwater, development of perched water above, or anthropogenic activities such as compressed air injection into soil that can occur during drilling or remediation.

Pathways into buildings from the soil can include cracks in slabs, unsealed space around utility conduit penetrations, the annular space inside of dry utilities (electrical, communications), elevator pits (particularly those with piston wells), basement sumps, and other avenues.

Barometric Lag. Atmospheric pressure variations may cause shallower or more permeable soils to breathe, and may cause "apparent" pressures and vacuums in deeper or less permeable soils. Apparent pressure must not be confused with "inherent" or source pressure.

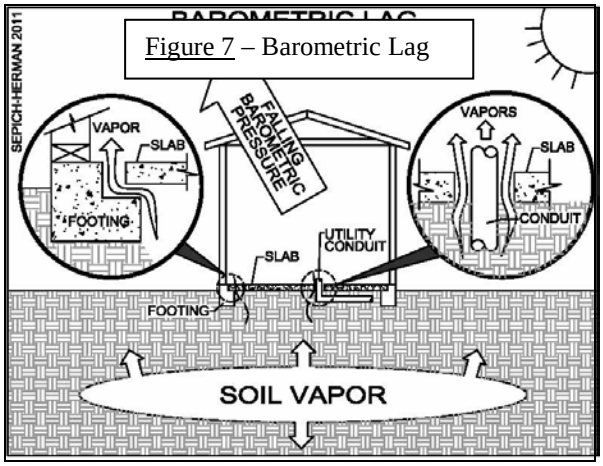

Figure 7 – Barometric Lag

Precipitation. Increased soil pore moisture is associated with decreased effective permeability.

Attenuation. Vapor concentrations "attenuate" or decrease in concentration when *diffusing* from soil to building interior. Unpressurized soil vapors normally decrease about a thousand fold in concentration from the soil to the building interior, a phenomenon which was modeled by Johnson & Ettinger more than twenty years ago. Pressurized soil gas may not conform to this model (figure 6 at right from Sepich, 2008).

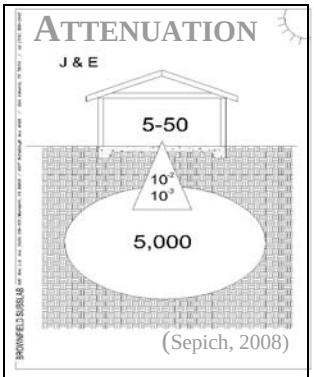

Figure 8 - Attenuation

When is Methane Soil Gas Hazardous? There are now answers to this question.

Concentration/Volume/Pressure. Methane soil gas must flow in sufficient volumes, under pressure, at concentrations above the LEL (lower explosive limit), and through complete pathways to receptors where attenuation is insufficient to dissipate gas concentrations to levels below the LEL.

There is no inherently unsafe methane concentration in the soil. One million parts per million methane in the soil is not inherently unsafe, when there is no gas source pressure.

2.5 Darcy's Law: Based upon his observations of groundwater behavior in France, Henry Darcy in 1856 published his landmark, "*Les Fontaines Publiques*

De La Ville De Dijon." This document has been a standard for engineers for centuries for the calculation of groundwater flow (Darcy, 1856).

2.5.1 Darcy's Law and Soil Gas Flow: Darcy's equation can also be used to model the flow of gases through the soil matrix. According to Darcy, **Q = KIA**, where Q is the flow of water; K is a dimensionless coefficient based upon the water permeability of the soil; and I is the "hydraulic gradient" for water (the difference in elevation between the beginning and end points of flow divided by horizontal distance); and A is the cross-sectional area of flow. Now let us utilize Darcy for gas flow in soil.

Figure 9 - Philip B. Bedient, Civil and Environmental Engineering, Rice University, power point slide.

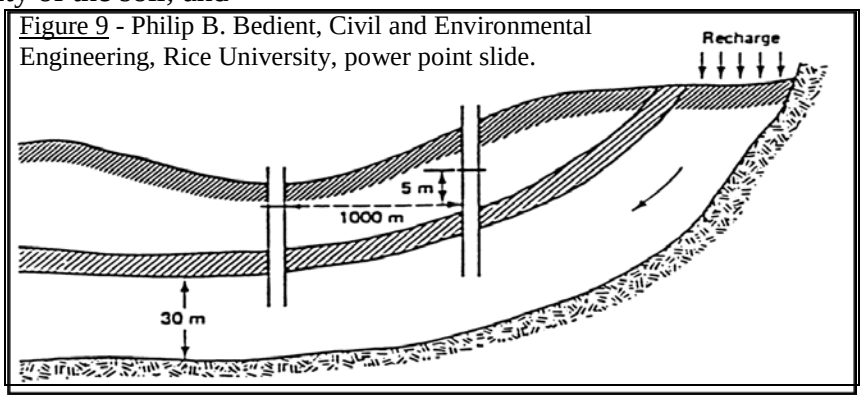

- **A** *(m^2 or ft^2)* – cross-sectional area of vapor flow in the soil matrix (a larger total flow), or slab cracks (a smaller total flow);
- **Q** *(m^3/sec or ft^3/sec)* – soil vapor flow;
- **K** *(m/sec or ft/sec)* – air permeability coefficient varying with soil type [water K's must be converted to air or gas K's, and also adjusted for moisture (less conservative) or not adjusted for moisture (more conservative)]; and
- **I** *(dimensionless)* – hydraulic (vapor) gradient, which in the case of soil gas vertical upflow would be the difference in soil gas pressure at depth as compared to atmospheric pressure divided by depth (see sketch above).

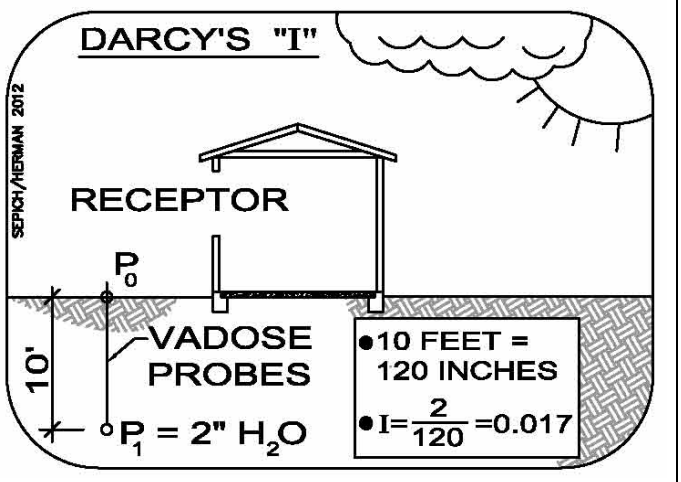

Figure 10 (Sepich 2012)

2.5.2 Flow Diminishes as Distance Increases. Barometric fluctuations may alternately push and pull gas in a shallow area underneath a building slab. The "gradient" diminishes rapidly with depth, and the associated soil gas flows are small as distance or depth increases. This is illustrated below. When the soil gas is not from a pressurized source, an intermittent vacuum due to falling barometric pressures quickly depletes the immediate soil matrix of gas within the radius of influence, and then recharges that same soil with air as the barometric cycle reverses. This push-pull process is not an efficient or major force in the movement of methane soil gas.

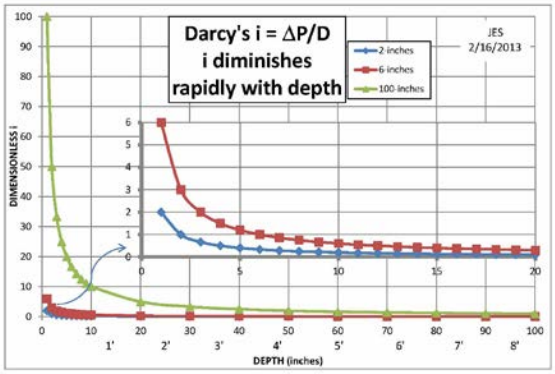

Figure 11 – Darcy Graph

2.6 Attenuation of Soil Gas Intrusion. At the exact point where soil vapor enters a structure, it is un-attenuated. Attenuation inside a structure is related to air exchange rates. See illustration:

- Q = Flowrate;
- V_B = Building Volume;
- AER =Air Exchange Rate;
- C = Vapor Concentration;
- $Q_1C_1 + Q_2 C_2 = Q_3C_3$; and
- $Q_3 = V_B$ x AER
- If $C_1 = 0$, then:
- $C_3 = C_2Q_2 / (V_B$ x AER)

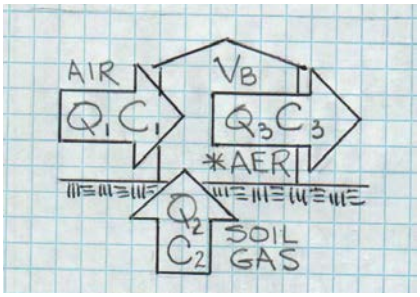

Figure 12 (Sepich, 2012)

AER's may vary from several per hour to several per day, depending upon structure and ventilation.

2.7 Gas Intrusion as Predicted by the Johnson & Ettinger Model. The United States Environmental Protection Agency (USEPA) J&E soil vapor intrusion mathematical model (Johnson & Ettinger, 1991) suggests that for soil vapor without source pressure, concentrations found inside habitable structures are normally attenuated by factors of hundreds or thousands (10^{-2} to 10^{-3}) below the methane concentrations found in the underlying soil . The J&E model and variations of it are used

There is no methane soil gas concentration that could model *by diffusion - advection* to reach a hazardous building air interior concentration.

extensively by environmental regulatory agencies everywhere. Methane has a lower explosive limit of 5% by volume (50,000 ppmv). If we assume an unpressurized source soil gas concentration of 1,000,000 ppmv, and use only a 10^{-2} attenuation factor, the interior methane concentration would be 10,000 ppmv or 1% by volume, or 20% LEL. Using a 10^{-3} attenuation factor, the interior methane concentration would 0.1% by volume, or 2% LEL (USEPA, 2003).

2.8 Gas Intrusion / The MTRANS* Model. During the late 1990's and early 2000's, elevated levels of methane were found at residential subdivisions constructed on former dairy lands in Riverside and San Bernardino Counties. The methane was microbial, formed from manure in the soils and urine leachate in shallow groundwater. Building officials desired to know the level of hazard which the methane might pose to the new upscale homes. Methane in the soil was measured at concentrations of up to hundreds of thousands of parts per million by volume (ppmv). The MTRANS model considered previous work such as the 1992 USEPA Johnson & Ettinger soil vapor intrusion model, and a 1999 University of Alabama groundwater movement standard known as MODFLOW (*Methane Transport Model, Applied Geokinetics, 2002).

2.8.1 MTRANS Modeling Results: Input to the model included soil density and permeability, rate of subsurface gas generation, number and width of floor slab cracks, rate of air exchange between the interior and the exterior of the structure, the air pressure in the interior of the structure, the barometric pressure on the exterior of the structure, and the degree to which barometric pressure fluctuates by time of day and weather. Elements of the modeled structure included the building interior, the concrete slab, the perimeter footing, the upper sand unit beneath the slab, the moisture barrier between the upper and lower sand, and the soil type below and adjacent to the structure. In addition to dairy farms, high risk sites were also modeled including leaking oil wells and sanitary landfills.

Methane soil gas generated at dairy sites was shown to be low in volume with no associated pressure. The study concluded that hazardous concentrations of methane would not accumulate inside the wood frame residential structures on dairy sites even under unmitigated worst case scenarios and that, ***"methane mitigation measures for structures built on former dairy land where no other sources of methane have been identified do not appear to be warranted."***

Actual soil gas attenuation field data collected in the 1990's at structures built upon a variety of methane impacted sites was compared with and validated mathematically

Modeling of the leaking oil well and sanitary landfill sites, called "high risk" sites in the MTRANS study, showed interior methane concentrations approaching the lower explosive limit of the gas using 10" H_2O pressure.

modeled attenuation factors.

See Table 2, next page.

2.8.2 Gas Intrusion: MTRANS Field Data. Field data was assembled as part of the MTRANS study (see Table 2, below). Measurements included concentrations of up to 1,000,000 ppmv soil vapor (i.e. "whole gas") correlated to respective indoor air methane concentrations in existing unprotected buildings at various southern California sites. Pressures observed during the investigations were not more than two-inches of water, attributed to barometric lag and minor source over-pressure phenomena.

Table 2 -- MTRANS
Comparison of Interior Air Monitoring Results for Mitigated and Unmitigated Homes

site	General Location	Date of Construction	Maximum Subsurface Methane Concentration (ppmv)	Source of Methane**	Gas Mitigation Improvements Installed?	Number of Homes or Buildings	Maximum Interior Methane Concentration (ppmv)
1	Yorba Linda	1997	370,000	biogenic (oilfield)	No ----- Yes	165 ---- 140	45 ppmv ---------- 38 ppmv
2	Century City	1970	960,000	Thermogenic (oilfield)	No	4	18 ppmv
3	San Diego	1999	205,000	biogenic (other)	No ----- Yes	15 ----- 36	34 ppmv --------- 38 ppmv
4	Corona Valley	1999	135,000	biogenic (dairy)	No	3	15 ppmv
5	Corona Valley	1999	450,000	biogenic (dairy)	No ------- Yes	3 --- 77	45 ppmv --------- 30 ppmv
6	Corona Valley	1999	17,000	biogenic (dairy)	No	3	27 ppmv
7	Corona Valley	2000	270,000	biogenic (dairy)	No	105	38 ppmv
8	Corona Valley	1999	25,000	biogenic (dairy)	No	3	35 ppmv
9	Los Angeles	1930 - 1985	1,000,000	Thermogenic (oilfield)	No	20	65 ppmv
10	Huntington Beach	1950 - 1960	500,000	biogenic (other)	No	45	115 ppmv
11	Chino	1995	350,000	biogenic (dairy)	No	23	15 ppmv

2.9 Attenuation / Modeled: J&E modeling over a wide range of input conditions (low to high soil vapor concentrations, coarse to fine soils, etc.) results in soil gas attenuation predictions in the 10^{-2} to 10^{-3} range.

2.10 Attenuation / Field: The 1990's soil gas versus indoor air data showed attenuation in the 10^{-3} to 10^{-4} range.

Field results were more conservative – showing greater attenuation – than modeled results.

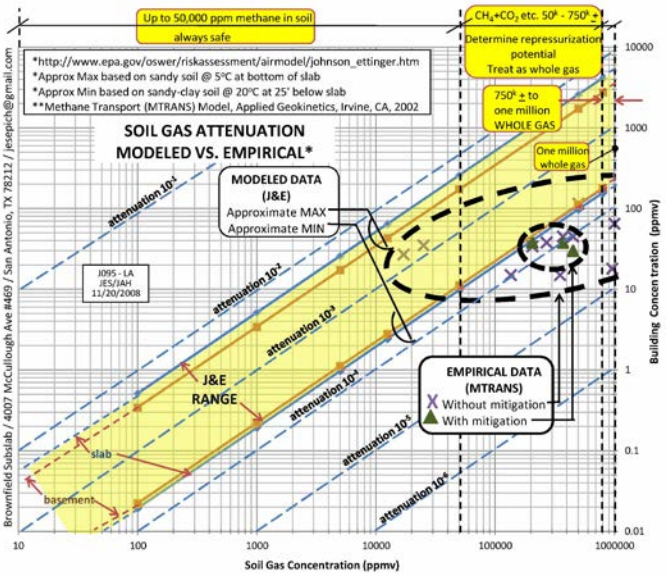

Figure 13 (Sepich, 2012)

2.11 Microbial Gas vs. Time: Anaerobic microbial action upon organic material in the soil is characterized by several stages of activity (see figure 12 below). The first stage of this process is actually aerobic, until all available oxygen is consumed, and involves the production of carbon dioxide. Subsequent stages are anaerobic, and involve the fermentation of methane and carbon dioxide from the biomass. Just as landfill biomass is consumed in the model, organic feed stock in the soil declines in mass as the microbial decomposition proceeds, leaving methane generation rates in general decline with time. The time frame for peak methane production after initial deposition of organic material varies, but is generally considered to be within the first several years, depending upon specific circumstances.

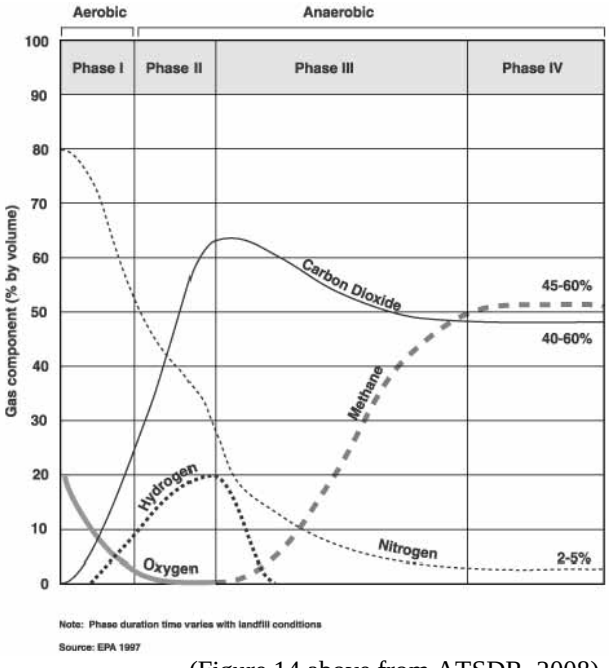

(Figure 14 above from ATSDR, 2008)

2.12 USEPA LandGEM: The LandGEM model (USEPA, 2006) is used to calculate the rate of decomposition of biomass. The LandGEM model uses a theoretical first-order kinetic model under anaerobic conditions to estimate decomposition rate and annual emissions over a user specified time period. A full description of the model and its workings is given on the USEPA website under its LandGEM model documentation, particularly the effect of moisture on decay rates. The importance of this model is that it can be used to quantify the time frame during which the anaerobic fermentation process produces methane, based upon site-specific conditions at sanitary landfills.

2.13 Methane Oxidation in Aerobic Soil Zones: In shallow soils where oxygen is present, methane may be oxidized by bacteria called methanotrophs. This tends to reduce the amount of methane reaching the surface. This process can be recognized by isotopic comparison of methane and carbon dioxide from deeper zones, with the methane and carbon dioxide from shallower zones.

2.14 The San Diego County Methane Study. A "flash" or combustion of gas without an explosion during construction of a utility trench was subsequently determined to be the result of non-methane hydrocarbon vapors from a fuel spill. A leaking fuel tank had previously existed near the location. The tank had been removed from the area some years before the trenching, but now the soil vapor testing also showed elevated methane. The emergency methane ordinances were in place and it was imperative to determine the source.

2.14.1 No Obvious Methane Sources. Research showed that there were no oil fields or sanitary landfills nearby any of the areas where high levels of methane occurred in the soil, nor were any leaking natural gas (utility gas) mains identified. Subsurface testing consisted of taking vapor rather than soil samples. Isotopic analyses of the gas indicated that it was a microbial (sometimes called biogenic) product of the anaerobic fermentation of organic material. It was observed that elevated levels of methane soil gas were widespread, and were even present in some older subdivisions which had been constructed up to 40 years prior. The methane was not found in cut areas, but was found generally in fill areas of greater than ten-foot depth. The methane was less prevalent in fill areas of less than ten-foot depth. Further studies included evaluation of the organic content of the various soils. There were unanswered questions.

2.14.2 Seminal Studies Related to Barometric Effects on Soil Gas. In order to better understand the phenomena, the late Dr. Richard Bell, professor emeritus and former chair of the Department of Chemical Engineering at the University of California at Davis, was consulted. He set up a weather station at

one of the development home sites with high soil gas concentrations. Data was taken and recorded initially over a thirty day time period, including barometric pressure variations, temperatures, wind direction and velocity, soil gas concentrations at various depths, and other parameters. The conclusions of the study were that barometric pressure fluctuations were a critical factor in soil gas concentrations in the shallow soil, but that deeper than about ten feet the barometric fluctuations had little or no effect in most soils. The rate of change of barometric pressure was more important than the absolute barometric pressure.

Historically, soils engineers specified a maximum of 5% organic material for engineered fill. A maximum of 2% became the norm in the early 1970's. Compliance is achieved by visual inspection. Plant debris is hand picked, or the earth is rejected where hand picking is not possible. Current southern California practice is to specify no more than 1% organic material. But these geotechnical limits on organic material are for foundation purposes only. Too much organic material in the soil can result in foundation movement and damage.

Soils utilized in engineered fill are normally well mixed and moisturized, and then compacted. Anaerobic processes require and consume moisture in the production of methane and carbon dioxide. Very small amounts of organic material in the soil can result in the production of anaerobic microbial gases for years after placement and compaction. MTrans data showed that levels of organic material in soil as low as 0.4% by weight could produce elevated levels of methane identical to those encountered in the field (hundreds of thousands of ppm).

2.14.3 San Diego County Ad Hoc Committee. While the MTRANS work modeled dairy sites (with manure and other organics in soil and groundwater), the San Diego issue of mass-graded sites (engineered fill) was very similar. Microbial (biogenic) methane soil gas conditions are quite common, but the presence of methane is not usually recognized and is seldom hazardous.

2.15 DTSC Biogenic Methane Model. The State of California Department of Toxic Substances Control (DTSC) regulates methane soil gas at public school sites in California. Recognizing the importance of utilizing multiple variables in assessing methane soil gas risk, DTSC promulgated, “Guidance Prepared for the Evaluation of Biogenic Methane in Constructed Fills and Dairy Sites,” which included a mathematical model (DTSC, 2011). DTSC considered such established models as Johnson & Ettinger in their work, but emphasized soil gas pressure in their calculations. The guidance addresses methane at sites limited in extent, with organic material of known origin and relatively low generation rates, and consequently, low volumes of methane; although, in some cases, the absolute concentration of methane can be quite high and may show strong seasonality.

California's semi-arid climate generally includes half a year of rainy season and half a year of dry season, which leads to marked variations in available moisture in the shallow soil. Soil moisture content tends to be more stable at greater depths. Fermentation of organic matter is moisture limited. Wetting and drying of a (non-irrigated) fill may result in variations in methane concentrations with time. The document suggests that an ideal case would be to measure pressure during the onset of a storm front with a substantial drop in barometric pressure, such as winter storms or summer thunderstorms. It is also noted that the most difficult time to sample is often during the late summer when the soil is at its driest, and there is little variation in barometric pressure.

The guidance presents a spreadsheet to calculate the intrusion rate of a well-characterized methane source in order to decide whether it poses a risk to the structure or inhabitants. Use of the model allows that if soil gas pressure measurements are not available, a default value of the maximum likely pressure differential, here considered to be 6 inches of water column, may be used. Despite potentially high methane soil gas concentrations, the low volumes are commonly insufficient to present a risk of explosion or fire.

Actual results will vary depending upon all input parameters, but a soil gas concentration of 1,000,000 ppmv methane may require a soil gas pressure of 10 inches of water to drive interior air concentrations to 500 ppm methane. At higher pressures, soil vapors behave as compressible fluids, but qualitatively, the model results are valid (i.e. increasing soil gas pressure = increasing risk). For gas flow from the soil matrix, considerable soil gas pressure is required for hazard to result inside a typical building space, even at high soil gas concentrations. This is consistent with available information regarding actual incidents of fire and explosion in buildings.

2.16 Risk Evaluation Database. Methane soil gas can pose safety issues related to fire and explosion. Methane is not toxic, and methane soil gas is not associated with health risk. Trace contaminants of toxic chemicals may be present with methane soil gas, say near a sanitary landfill, and this issue must be addressed separately from the methane safety issue. Pressureless concentrations of methane soil gas are greatly attenuated from soil to building. A number of factors should be considered in evaluation of potential risk from methane soil gas.

Elements Suggesting Soil Gas Hazard at Common Structures.

- Large pressurized source of concentrated gas;
- High permeability complete pathways;

Soil Gas Concentration vs. Pressure and Flow.

- Methane at high concentrations may be driven by source pressure;
- Low methane concentrations are driven only to diffusion and advection*

*exception – repressurization as from rapidly rising shallow groundwater

Site Testing for New Development.

- Simple soil matrix testing usually adequate for undeveloped sites.

Site Testing at Existing Development.

- Conceptual Site Model (CSM) very important.
- Monitor "pre-entry" concentrations in pathways at/near existing receptors.
- Interior near-floor and in-wall sweeps useful.

Existing and New Development.

- Pro-active mitigation may optimize cost and schedule.
- More extensive site testing and characterization is useful to the site if pro-active mitigation is not desired, and if project budget and time schedule will allow.

2.17 Flow Chart. Tiered Approach Risk Management: A chart (figure 13 on right) outlines a tiered approach to identify methane issues requiring immediate action, situations requiring further methane study, and sites where no further action is required.

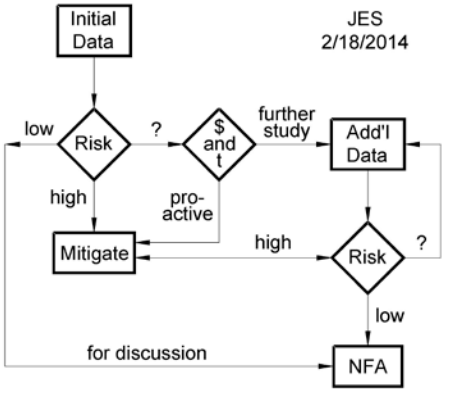

Figure 14

2.18 Building Mitigation Alternatives.

2.18.1 New Buildings. For new buildings, methane mitigation measures are rather simple, and usually include subslab venting and subslab barrier membrane. These methods are in wide use, and the design and installation techniques are well established. Venting should include a highly-permeable layer below the slab, with good connectivity to a redundant vent-riser system.

For methane mitigation, satisfactory results have been achieved using 6-mil low-density polyethylene (LDPE) visqueen. Ten-mil high-density polyethylene (HDPE) sheet is also widely used. Joints are taped rather than lapped, and a system of conduit boots, trench dams, and dry-utility conduit seals is also included. Government codes often require membranes of up to 40, 60, and even 100-mil thickness. These are generally unnecessary

Because unpressurized gas has been shown not to pose a problem to common habitable structures, a building is provided with a proper subslab venting ("depressurization") system is theoretically safe from methane, even without a membrane.

from a methane permeability standpoint. Heavier material does hold up better against construction damage. Smoke testing is routinely used on all membrane types and thicknesses to test for and repair leaks prior to constructing slabs.

2.18.2 Existing Buildings. For existing buildings, methane soil gas mitigation often takes the form of pathway plugging and/or soil gas venting. Preferential pathway plugging is effective against pressurized soil gas flow. Ambient ventilation of non-conditioned space is also an option. If necessary, a methane vent pipe can be jacked under an existing building. Sometimes existing buildings are retrofitted with membrane and vent piping.

All risk can be mitigated at existing buildings through various retrofit options.

Pathway Plugging – Slab Crack and Cold Joint Grouting. Methane soil gas, if pressurized, can enter a structure in significant quantities through cracks and cold joints in slabs. Flame ionization detector (FID) interior air monitoring, with attention paid to areas near the floor, can identify points of soil gas entry. Crack grouting, when necessary, may be accomplished using mastic or silicone materials.

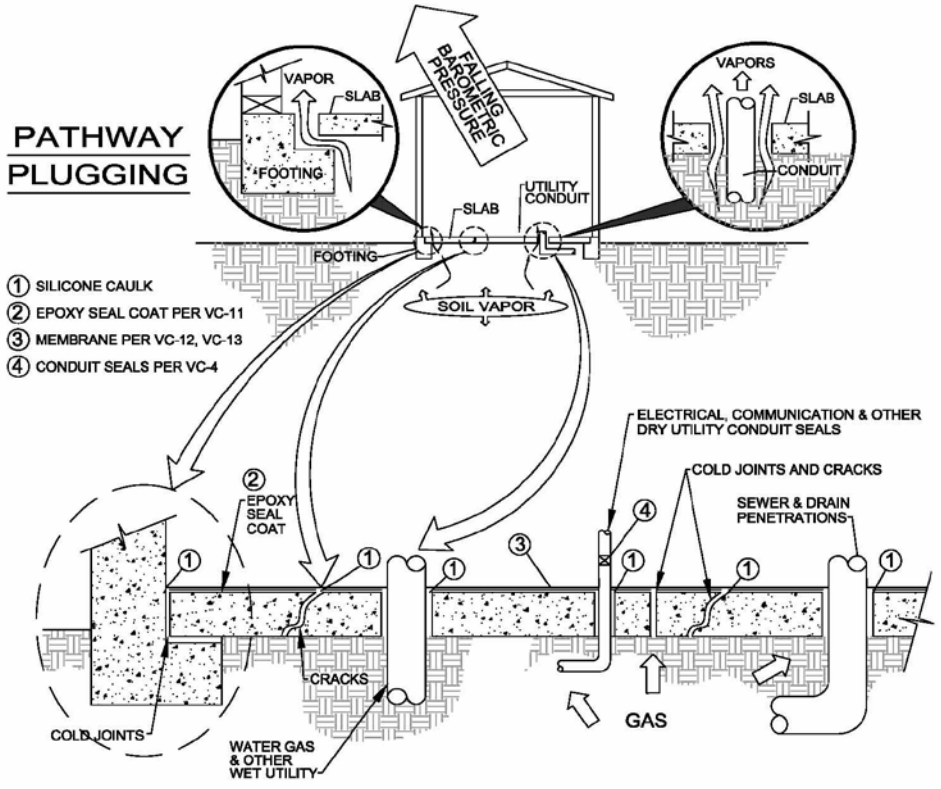

Figure 15 – Pathway Plugging (Sepich-Herman, 2014)

Trench Dams. Soil gas may flow through the more permeable sandy backfill of utility trenches, preferentially over perhaps less permeable native materials. Offsite soil vapors may enter a property from the street and find entry into a structure at the locations where utilities enter the building from the soil. Trench dams are useful for sealing off soil gas flow that occurs outside of and around buried pipes. The normal method of accomplishing trench dams for existing buildings is to locate the underground piping and excavate it. Then, an impermeable backfill is installed for several feet of the trench just outside the footprint of the structure, as shown in the "Trench Dam" sketch.

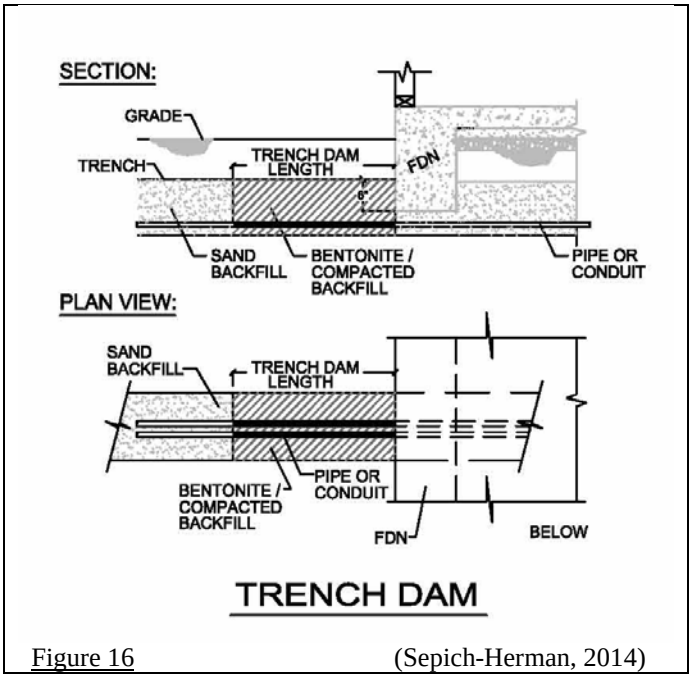

Figure 16 (Sepich-Herman, 2014)

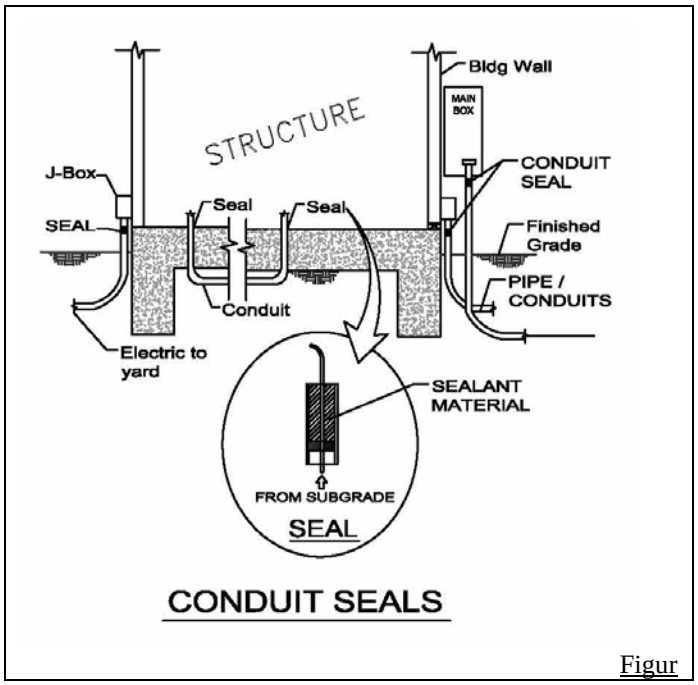

Figur

Conduit Seals. Conduit seals are intended to stop methane soil gas flow from traveling inside of "dry utility" pipes and conduits, and subsequently finding pathways to the building interior. Dry utilities include electrical, telephone, and other utility conduits. Conduit seals may be installed in existing services by caulking with mastic and/or silicone material.

e 17 (Sepich-Herman, 2014)

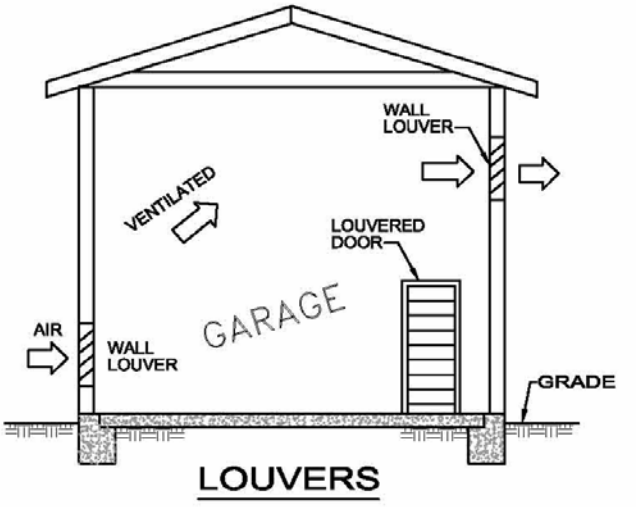

Figure 18 (Sepich-Herman, 2014)

Louvers. For non-conditioned spaces (i.e. without heating and air conditioning), wall louvers provide good mitigation against soil vapor build-up. This method is commonly used in garages.

Subslab Venting. Retrofitting existing structures with a subslab vent pipe is relatively straightforward using common boring and / or jacking techniques. Shop perforated pipe is inserted from a jacking pit, as shown

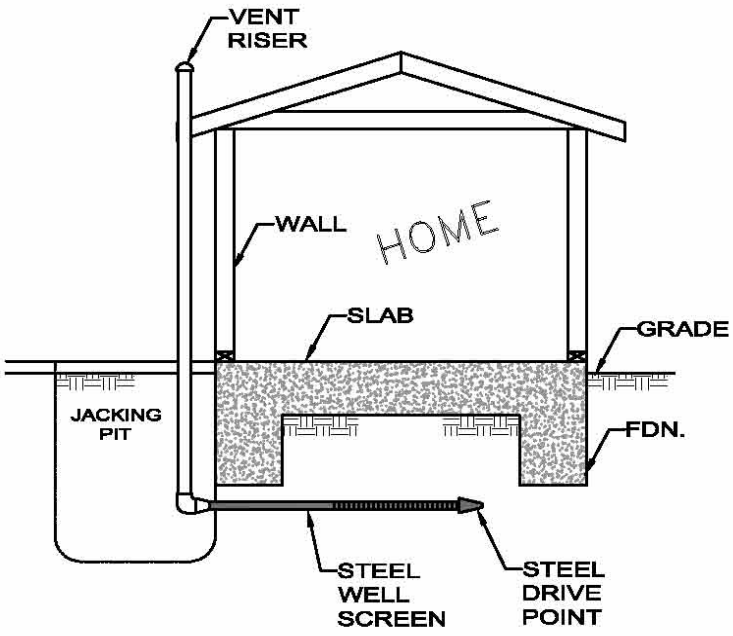

Figure 19 (Sepich-Herman, 2014)

in the illustration in figure 18. Then, the subslab perforated pipe is connected to non-perforated vent risers to a location above the roof of the house. These systems are generally passive, but can be made active by adding a fan, if necessary. The purpose of these systems is to insure against pressure in the soil.

2.19 Discussion. Field investigations and testing can determine whether methane gas exists in the soil, and if so, whether the gas may exhibit inherent pressure (i.e. pressure apart from barometric and advective forces). When gases are present in higher concentrations, or if pressures are measured or predicted in the soil, then proactive mitigation measures are sufficient for protection.

After rudimentary testing, most sites are seen to be either obviously safe (the great majority of sites), or obviously unsafe (a small minority of sites).

- Unsafe sites should be mitigated; and
- Questionable sites may be studied further, or simply mitigated in the interest of time and money.

- When no gas or lower gas levels are found, and when the gas will not be pressurized, buildings do not need methane mitigation.

2.19 Most Obvious Data Gaps in Existing Practice.

No existing methane codes require laboratory testing to determine whether gas is thermogenic or microbial, or whether the gas is from some pressurized source.

- Thermogenic gas is commonly associated with a large pressurized source, such as underlying oil fields or even leaky utility gas piping;
- Microbial gas can be associated with some large pressurized source such as a sanitary landfill; and
- Microbial gas in the soil is ubiquitous, and in many cases, is generated locally with no large pressurized source, and hence little or no potential for gas hazard.

Failure to differentiate between gas sources and potential pressures and volumes means that all soil gas is assumed to pose great hazard.

An owner or environmental consultant may perform testing over and above minimum code test requirements, but the test results will not be useful if regulators have no guidelines explaining how the results should affect mitigation requirements. Owners have no reason to spend extra money on testing when no benefit could accrue. The factors which make methane soil gas hazardous are well established; however, until they are also well understood, costly mitigation will continue to be required where there is no methane hazard.

3. EVOLUTION OF METHANE REGULATIONS RESULTS AND DISCUSSION

3.1 Action Levels. In environmental science, the term "action level" typically refers to some condition at or beyond which remedial or corrective measures must be implemented.

Methane Action Levels: Methane action levels may be based upon scientific principles, or they may be arbitrary. Action levels may refer to methane conditions in a confined / habitable space, or methane conditions in the soil. Most methane codes for new construction on undeveloped sites identify action levels based upon the *concentration* of methane found in the soil at a building site. Early regulations used the methane LEL concentration as a soil gas action level (RCRA, 1976). Today, some agencies prescribe methane soil gas action levels in low ppmv (Los Angeles, 2004).

Issues: Ultra low methane soil gas action levels are presumably safer, but are not based upon any engineering or scientific criteria. Sustainable methane pressures and flow volumes are as important as methane concentrations, but are less often cited in regulations. Determination of methane origin, which can be critical in assessing risk, is not required by any known code at this time. Methane soil gas issues at existing development are generally ignored except when permits are sought for new work or remodeling.

3.2 Science vs. Law. Vapor concentrations *attenuate* dramatically when diffusing from soil to building interior. Minor atmospheric and advective phenomena do not result in appreciable flows in otherwise unpressurized soil gases. When government agencies set soil-gas “action levels” at the same or lesser concentrations than building interior-air concentrations of concern, the resultant laws ignore the science surrounding attenuation phenomena.

3.3 Closing the Gap between Science and Regulations. Methane regulations in many jurisdictions are decades old and have not been updated to reflect advances in the understanding of soil gas intrusion. If based upon science, soil gas action levels can be set two or three orders of magnitude higher than indoor air concentrations of concern for unpressurized soil gas. Pure methane (100% by volume) is less than two orders of magnitude greater than the lower explosive limit for the gas. This begs the question of, “what other parameters are important in evaluating risk?” Along with soil gas concentration, soil gas pressure is the most important parameter to consider in evaluating risk.

3.4 San Diego County Ordinance Repeal: Nearly six years passed between the enacting of the ordinance in 1998 and its repeal in 2005. The timeline

is shown in the following illustration.

Figure 20 - **HISTORY OF METHANE IN SAN DIEGO**

1999	Methane gas first discovered in soil gas in San Diego Housing Developments.
Early 2000	General panic ensued (Belmont School) – DEH refused to take oversight.
2000	Methane Technical Workgroup formed by San Diego County Building Department
2001	San Diego County adopted Methane Testing Ordinance on interim basis. – Based on Los Angeles and Orange County Ordinances (e.g. oil wells).
2001-2002	Numerous methane test studies throughout San Diego and Riverside Counties.
June 25, 2002	MTRANS Methane Gas Migration Model – Concludes methane from dairy sites will not accumulate inside structures at hazardous levels – even in worst case scenarios and in the absence of mitigation
2003/2004	Methane Gas Migration Model released to the public.
2004	San Diego County Methane Technical Workgroup reconvened.
April 2005	San Diego County Methane Ordinance repealed.

The San Diego County case represents a unique instance where an effort was made to define the necessary science as a part of the regulatory process. The work done there and the knowledge gained were applied directly to methane action levels; and in April, 2005, the County of San Diego repealed the County ordinance which required methane gas testing and mitigation on mass graded lots within the unincorporated areas of the County. The repeal of the County's methane ordinance was based on the following:[13]

"In 2000, elevated concentrations of subsurface methane gas were detected at developments constructed on mass graded projects in San Diego County. At that time there was a lack of adequate testing data that could confirm the actual source of the methane gas, the amount of trapped subsurface gas, or the potential

risk of methane gas intrusion into an enclosed structure and possible ignition of that gas. Based upon the information that was available at the time, San Diego County Board of Supervisors adopted an ordinance on July 11, 2001 requiring methane gas investigations and mitigation guidelines.

"1) the gas was not under pressure; 2) the gas was found almost exclusively in engineered fill soils; 3) the gas was found only in small volumes; and 4) the source of the subsurface methane gas is associated with the natural degradation of organic matter.

"Because the subsurface methane gas is not under pressure and is associated with small amounts of organic material in engineered fills, the potential risks are much lower than with other types of occurrences, such as landfills or oil wells. This determination was supported with the completion of a computer modeling, which found that despite the numerous layers of conservatism built into the simulations (e.g. a constant methane gas generation rate, high number of cracked slabs and non-gastight moisture barriers, absence of sub-slab venting, high gas concentrations, and low interior pressure) the model showed that potential hazardous concentration of methane would not accumulate on the interior of a structure, even under worst-case scenarios in the absence of methane mitigation measures. Based upon the science available, methane mitigation measures for structures located on mass graded sites do not appear to be warranted."

3.5 DTSC Soil Gas Pressure Model.

The State of California Department of Toxic Substances Control (DTSC) mathematical model for determining risk from microbial methane soil gas (DTSC, 2011) built upon J&E, and further refined the San Diego findings. The model specifically enables the use of soil gas pressure to determine risk, in addition to the normal soil gas concentrations, soil types, and other parameters utilized in J&E. The DTSC model shows that considerable soil gas pressure is required for hazard to result inside common building spaces. This is consistent with available information regarding actual incidents of fire/explosion in buildings.

3.6 Proposed Regulatory Framework.

The table below suggests methane concentrations and pressure action levels for a variety of circumstances (Eklund, 2011). The action levels are also arbitrary, but are consistent with actual observations by professionals in the field. No methane incidents (fire or explosion) are known or have been documented that are inconsistent with the suggested values in the table.

Table 3. Decision Matrix for Methane in Soil Gas and Indoor Air

Shallow Soil Gas Conc. [a]	Indoor Air Concentration			
	None Available	<0.01% (i.e. <100 ppm)	0.01 to <1.25%	≥ 1.25%
<1.25% to 5%	No further action	No further action	No further action [b]	Immediately notify authorities, recommend owner/operator evacuate building
>5% to 30% [c]	No further action unless ΔP >2 inches H_2O [b]	No further action unless ΔP >2 inches H_2O [b]	No further action unless ΔP >2 inches H_2O [b]	Immediately notify authorities, recommend owner/operator evacuate building
>30% [c]	Collect indoor air data	Evaluate on case-by-case basis	Evaluate on case-by-case basis	Immediately notify authorities, recommend owner/operator evacuate building

Footnotes:
[a] Maximum methane soil gas value for area of building footprint.
[b] Landowner or building owner/manager should identify indoor sources and reduce/control emissions. If no sources are found, additional subsurface characterization and continued indoor air monitoring are recommended.
[c] The potential for pressure gradients to occur in the future at a given site should be considered.

General Notes:
1. Table is intended for sites with existing buildings. To address future development, no further action is required if the shallow soil gas concentration is <30% and ΔP <2 inches H_2O.
2. If the combined soil gas concentrations of methane and carbon dioxide are ≥90%, mitigation should be considered.

3.7 ASTM.

On a number of fronts, developments are occurring that will make it easier to declare sites safe. ASTM International is developing a standard practice for evaluating potential hazard due to methane in the vadose zone (ASTM, 2014). This standard will provide a simplified approach for evaluating site methane hazard based upon methane concentrations, volumes, pressures, and other factors. Suggested action levels and pressures will reflect actual hazard.

The ASTM standard is intended to streamline stakeholder decision making and avoid endless testing. Sites can be quickly found to be safe, or alternately they can be immediately provided with proactive mitigation using the ASTM guidelines.

Extensive site testing is most necessary when mitigation is not preferred. For those projects where it is not desired to mitigate, and as long as time and resources are available, any amount of additional testing may be done.

4. CONCLUSIONS

4.1 When Confusion Reigns: Considerations other than science will always dominate decision-making if the scientific principles are not well known and understood. Bad science makes bad laws. Junk science is widely used to

confuse the lay person – or the jury (Park, 2000). At methane sites with no actual risk, all that is required for loss of property value is the widespread perception of hazard, not actual hazard. This nuance of law has been widely exploited.

4.2 Risk Can be Evaluated: Methane incidents are extremely rare, and sites with high risk are easily identified with current science. Sites with very low risk are also easily identified. Most sites, even with high concentrations of methane soil gas, have de minimis risk from combustible soil gas if there is no pressure.

4.3 All Risk can be Mitigated: When methane risks are identified, mitigation is routine with current best practices, even for high risk sites.

4.4 Mitigation is not Always Necessary: Sites which are determined to have low or no risk do not need mitigation.

4.5 Progress: It has been several years since San Diego County rescinded its methane requirements related to microbial gas at engineered fill sites. The County has had no negative issues following repeal of the ordinance. The DTSC "Biogenic Gas" guidelines are a further advancement and clearly show that elevated pressures of soil gas are necessary to pose hazard to common structures. The ongoing development of an ASTM methane standard is hoped to additionally benefit those stakeholders in determining methane site hazard and expediting mitigation alternatives. Determining the genesis of soil gas (whether gas is thermogenic or biogenic, and whether from a local or remote source) can greatly enhance the environmental professional's ability to assess risk at a site.

4.6 Further Goals: The now well established science of soil gas intrusion phenomena must be widely discussed and understood. Guidelines and standards need to be revised and to allow decision makers to:

- put aside arbitrary action levels, and
- utilize science-based assessments of soil gas hazard.

4.7 Epilogue: Galileo's peer reviewers would have had him dead for suggesting that the earth revolves around the sun. As we become accustomed to new ideas, they gradually lose their strangeness. When technical professionals utilize best available knowledge to make supportable recommendations, the result can be enlightened action. It would greatly benefit all stakeholders, including property owners and regulators, if science-based methane standards were to be universally adopted.

5. REFERENCES

Applied Geokinetics, 2002. Methane Transport (MTRANS) Model, Volumes 1 and 2. Irvine, CA.

ASTM, 2011. E-1903 Standard Practice for Environmental Site Assessments: Phase II Environmental Site Assessment Process. ASTM International, West Conshohocken, PA.

ASTM, 2013. E-1527 Standard Practice for Environmental Site Assessments: Phase I Environmental Site Assessment Process. ASTM International, West Conshohocken, PA.

ASTM, 2014. WK32631. Practice for Evaluating Potential Hazard Due to Methane in the Vadose Zone. ASTM International Subcommittee E50.02, West Conshohocken, PA.

California Environmental Protection Agency, Department of Toxic Substances Control, June 2011. Evaluation of Biogenic Methane. CA/EPA/DTSC, Sacramento, CA.

Cobarrubias, J.W., 1992. Methane Gas within the Fairfax District, Los Angeles. Engineering Geology Practice in Southern California, Association of Engineering Geologists, p. 131-143.

Cooley, S., March 2003. District Attorney's Final Investigative Report: Belmont Learning Complex. Los Angeles, CA.

Darcy, H., 1856. Les Fontaines Publiques de la Ville de Dijon. Dijon Academy of Science, Art and Literature, Paris, France.

EPA, 2008, Chapter 2: Landfill Gas Primer - An Overview for Environmental Health Professionals. Landfill Gas Basics. ATSDR, Atlanta, GA.

Eklund, B., 2011.Proposed Regulatory Framework for Evaluating the Methane Hazard Due to Vapor Intrusion, Table 3, page 12. American Waste Management Association, Pittsburg, PA.

Ettinger, R. and Johnson, P. 1991. Model for Subsurface Vapor Intrusion into Buildings. United States Environmental Protection Agency, Washington, D.C.

Kaplan, I. R. and Sepich, J. E., March 2010. Geochemical Characterization, Source, and Fate of Methane and Hydrogen Sulfide at the Belmont Learning Center, Los Angeles. Environmental Geosciences, Volume 17(1).

Los Angeles, City of, 2002. Ordinance No. 175790, Appendix D, City of Los Angeles Methane Seepage Regulations. City of Los Angeles, CA.

NASA, 1994. Subcommittee on Spacecraft Maximum Allowable Concentrations, Committee on Toxicology, Board on Environmental Studies and Toxicology, Spacecraft Maximum Allowable Concentrations for Selected Airborne Contaminants, Volume 1. National Research Council, Washington, D.C.

Park, R. 2000. Voodoo Science. Oxford University Press.

Resource Conservation and Recovery Act (RCRA), 1976. Code of Federal Regulations (CFR) 40, part 258.23(a)(1) and 258.23(a)(2).

RKI Instruments, 2001. Gas Detection History Power Point. Union City, CA.

San Diego County, July18, 2001. Ordinance No.9364, An Ordinance Adding Chapter 3 to Division 6 of Title 8 of the San Diego County Code Related to Testing Requirements for Methane Gas on all Projects with Mass Grading. San Diego, CA.

Sepich, J.E., 2008. Hazard Assessment by Methane CVP – Concentration/Volume/Pressure (Everything You Heard About Methane Action Levels Was Wrong). Paper A-008, Proceedings of the Battelle Sixth International Conference on Remediation of Chlorinated and Recalcitrant Compounds, Monterey, CA.

Sepich, J. E., September 2011. VOC Practice –Toxic Soil Vapor Identification, Assessment, and Mitigation. ASCE, Amarillo, TX.

Sepich, J.E., 2012. CH4 Practice – Methane Soil Gas Identification and Mitigation, A Boots on the Ground Primer. ASCE, San Antonio, TX.

Union Tribune, February 12, 2000. Methane Gas Threatens Homes, County Revokes Occupancy Permits. San Diego, CA.

United States Environmental Protection Agency, June 2003. Users Guide for Evaluating Subsurface Vapor Intrusion into Buildings. (Johnson and Ettinger model), Office of Emergency and Remedial Response, Washington, D.C.

United States Environmental Protection Agency, May 2006. Landfill Gas Emissions Model (LandGEM) Version 3.02 Users Guide. Office of Research and Planning, National Risk Management Agency, and Clean Air Technology Center, Research Triangle Park, NC.

USING TEMPERATURE MEASUREMENTS IN CONJUNCTION WITH BIODEGRATION MODELS TO EVALUATE IN SITU BIOREMEDIATION

Robert E. Sweeney[1§] and Shankar Subramanian[2]
[1]*707 Howell Avenue, Etna, CA, 9602,* [2]*URS Corporation, 100 S. Wacker Drive, Suite 500, Chicago, IL 60606*

ABSTRACT

Temperature measurements made down existing wells can be used in conjunction with *in situ* biodegradation models to evaluate depth, areal extent, and relative magnitude of biodegradation of petroleum hydrocarbons in the soil. During aerobic biodegradation, the rates of petroleum hydrocarbon degradation and O_2 loss, along with CO_2 and heat production, are all related. Heat generated from biodegradation is used to raise the temperature of soil, as well as being dispersed through the soil by heat transport processes. As a result, temperature maxima, or thermal anomalies (deltaT), are developed within the biodegradation layer of the soil. The magnitude of deltaT can be used to estimate the minimum rate of biodegradation in the soil. For sites where *in situ* bioremediation is being carried out by soil vapor extraction (SVE), air sparge (AS), or *in situ* chemical oxidation (ISCO), temperature measurements can also be used to identify the depth and areal extent of remediation. By comparison of thermal anomalies between wells from active remediation areas and those where natural attenuation is occurring, the effectiveness of remediation for enhancing the rate of biodegradation can also be evaluated.

In this paper, the general conceptual model for using temperature measurements to evaluate biodegradation of petroleum hydrocarbons will be used to discuss temperature measurements collected at several different locations. Methods for identifying thermal anomalies due to biodegradation of hydrocarbons will be presented. Examples will be shown where the temperature method is used to evaluate the effectiveness of SVE operations for enhancing the rate of biodegradation in the soil. Another example will be shown where the temperature method is used to document biodegradation that occurs outside the area of air flow at an AS operation.

Keywords: Hydrocarbons, Biodegradation, Temperature, Remediation, SZNA, PVI

[§]Corresponding Author: Robert E. Sweeney, Environmental & Petroleum Geochemistry, PO Box 694, Etna, CA, USA, 96027; Tel: 530-467-3972; rsweeney@sisqtel.net

1. INTRODUCTION

Aerobic biodegradation of hydrocarbons is an important process involved in lowering the risk for petroleum vapor intrusion (PVI) and methane hazard, as well as increasing the ability of *in situ* remediation for removing hydrocarbon contamination from soil. Different types of vapor transport/biodegradation models can be used for PVI risk (DeVaull, 2007), methane hazard assessments (Amos and Mayer, 2006), and determining the rate of source zone natural attenuation (Johnson et al., 2006). Though these models are used for different applications, the objectives are similar - they provide a method to estimate the depth, areal extent, rate, and sustainability of the biodegradation of hydrocarbons in the soil. In this paper, the potential for the temperature method (Sweeney and Ririe, 2014) to aid in these determinations will be discussed for each type of model.

Recent studies (USEPA, 2013) have shown that aerobic biodegradation significantly reduces the risk of PVI at petroleum-impacted sites. For UST sites, biodegradation removes PVI risk from groundwater sources deeper than 5 feet and for LNAPL sources deeper than 18 feet. For both PVI and source zone natural attenuation (SZNA), LNAPL sources are considered to be in direct contact, or in close proximity, to groundwater (Johnson et al., 2006). LNAPL sources at non-UST sites (e.g. refineries, tank farms, and large releases from pipelines and ethanol spills) may have a higher potential PVI risk due, in part, to methane generation or the presence of petroleum-contaminated shallow soil (Sweeney et al., 2013). As a result, one of the challenges for PVI risk assessment is to assure that no risk exists due to the presence of shallow soil contamination. Although methods such as PID analyses, geologic logs, and soil sampling exist for this purpose while drilling wells and bore holes, the temperature method may provide an alternative solution that can be used later after wells have already been completed.

For source zone natural attenuation (SZNA), the presence of shallow petroleum contamination can also complicate the determination of the rate of source removal. Presently, source removal is generally determined by one of two different field methods. The first method uses soil vapor sampling to determine the oxygen concentration gradient (Johnson et al., 2006), and calculates the rate of source removal on the basis of oxygen flux to the source. This method requires the installation of soil vapor points and the determination of the effective diffusivity (De) of oxygen through the soil. Field measurements can be used to determine soil diffusivity (De) for oxygen (Lundegard and Johnson, 2006); however, soil diffusivity at most sites is estimated from soil type or water/air porosity of the soil (Millington and Quirk, 1961). An alternative approach (Sihota

et al., 2011) is to determine the flux of CO_2 diffusing out of the soil using a flux chamber. For this method, the contribution of CO_2 due to decaying plant material is removed on the basis of the carbon-14 content of the sample. However, the contribution of CO_2 derived from shallow hydrocarbon contamination and/or other older geologic material in the soil (DeVaull, 2007) is still included in the estimate of CO_2 derived from the source. The presence/magnitude of the thermal anomaly at the source may provide documentation of source removal without complication from organic matter in the overlying vadose zone.

Soil vapor extraction (SVE) and air sparge (AS) involve advective flow of air through the soil, thus increasing the rate of *in situ* biodegradation (Johnson, 1998). The rate of biodegradation from AS can be estimated for the 'area of influence' from measurements of SVE gas flow rate and concentrations of O_2 and CO_2 in the gas. For AS/SVE systems, some of the air injected into groundwater will dissolve in to the water and potentially be transported laterally before removal through biodegradation. As a result, the area for which biodegradation occurs and removes soluble hydrocarbons may extend beyond the area of airflow through the soil (Adams and Reddy, 2003). Pulsing the air injection maximizes oxygen mass transfer in the water and reduces hydrocarbon rebound post AS (Yang et al., 2006). Temperature measurements in wells adjacent to air sparge operations could provide documentation of biodegradation resulting from lateral transport of oxygen from the air injection area.

Field measurements from several sites with different environmental issues will be presented in this paper. The results will be discussed in terms of providing additional insight on the distribution and magnitude of biodegradation in the soil at petroleum-impacted sites.

2. MATERIALS AND PROCEDURE

2.1 Field Methods

Two different field procedures were used to make temperature measurements down existing monitoring wells. The thermistor or probe/cable method was used to determine temperature profiles for different wells at a particular time of the year. For this method, it is important to include an upgradient background (i.e. no soil contamination) well for comparison to wells within the area of soil contamination. The sensor method (Johnson et al., 2005) is used to monitor temperature changes with time. Using either method, temperature measurements are made on either a 2-foot or 5-foot vertical spacing, depending on the depth of the well. The temperature sensors were usually retrieved/replaced in the well at the time of groundwater monitoring and sampling events.

2.2 Temperature Probe Method

Temperature probes are calibrated and dried before placement into wells. Starting near the surface, the probe is lowered to a given depth in the well and allowed to equilibrate with the temperature of the soil surrounding the well. The routine procedure used at most sites was to wait 3 minutes before taking a temperature measurement in the vadose zone, and 1 minute for groundwater measurements. During this time interval, the temperature of the thermistor approaches that of air in the well at that depth. The high heat capacity of soil versus air retains the well air temperature near that of the soil.

2.3 Temperature Sensor Method

Three types of Thermochron 'iButton' temperature sensors (Johnson et al., 2005) were used in this study. Each type covers a different temperature range, with the least precise 'G' type covering the total range expected at environmental sites. The iButton sensors are placed into a rubber holder and attached to PVC pipe or tygon tubing for deployment down wells. The tubing/pipe is connected to the bottom of the well cap so that the well can be tightly sealed to minimize leakage of air while temperature measurements are being made. The sensors are waterproofed using petroleum or silicon-based grease. In addition, the sensors are covered with a rubber coating for protection during installation/retrieval. Under normal conditions, over 95% of iButton sensors deployed yielded reliable temperature data.

The temperature sensors appear to be routinely stable for up to a three-month deployment in the subsurface. Several iButtons deployed at depths below 30 feet have yielded over 2000 hourly readings that did not change at the 0.1°C sensitivity level. Certain iButtons, however, were determined to not be properly calibrated at the factory and a consistent error up to 0.4°C occurred during deployment. Sensor calibration is routinely checked by collecting ambient temperature measurements before and after installation in the well. Since using this practice, the temperature data from about 5 % of sensors were determined to be out of calibration by 0.2°C or more, and the field measurements were corrected accordingly.

2.3 Estimation of Rate of Heat Generation during Biodegradation

Heat released during the oxidation of organic matter follows thermodynamic principles, even when the reaction is mediated by biologic activity. For hydrocarbons, the general oxidation equation below can be used to calculate heat released from individual molecules:

1) $$C_xH_y + (x + ¼ * y) * O_2 = x * CO_2 + ½ * y * H_2O$$

Where: x = # carbon and y = # of hydrogen atoms in the molecule

Using equation 1 and the standard heat of formation of molecules, the heat released from different gasoline molecules can be calculated. Heat released from the combustion of gasoline and kerosene ranges from about 45 to 50 kJ/g. For field studies, the heat released during aerobic oxidation of petroleum products is assumed to be 48 kJ/g-hydrocarbon ($H_{hydrocarbon}$), and 15 kJ/g-oxygen (H_{oxygen}).

2.4 Heat Generation and Vapor Transport/Biodegradation Model

Fick's first law (equation 2) provides the basis for calculating the flux of oxygen through the soil, and can be used (Johnson et al., 2006) to calculate rates of hydrocarbon removal from soil. To calculate the flux of oxygen, field data is needed to determine the concentration gradient (dC/dz). For biodegradation at the aerobic/anaerobic (A/A) interface (Davis et al., 2009), 'dC' equals the oxygen concentration at the top boundary (atmospheric) as oxygen is depleted at depth 'z' (the A/A interface). Based on this model, heat released during biodegradation will occur within a narrow depth window. The rate of heat generation in the soil (G-bio) can be calculated by multiplying the rate of oxygen flux by the amount of heat released during oxygen removal (equation 3):

2) Flux-oxygen (mg/m^2-hr) = De * dC/dz

Where: De is the effective diffusion coefficient (m^2/hr)
dC/dz is the concentration gradient (mg/m^4)
dC = concentration of oxygen in air (mg/m^3)
dz = depth of the A/A (m)

3) G-bio: Rate Heat Generated (J/m^2-hr) = O_2 Flux (mg/m^2-hr) * H_{oxygen}

Where: H_{oxygen} = 15 kJ/g or 15 J/mg

Under steady state conditions, heat generated from biodegradation will be transported up (Heat Flux-up), down (Heat Flux-down), and laterally. The rate of Heat Flux-up from the A/A will be a function of the temperature gradient and the thermal conductivity of the soil (equation 4):

4) Heat Flux-up (J/m^2-hr) = k * dT / dz

Where: k = thermal conductivity of soil (J/m-hr-K)
dT/dz = thermal gradient (degrees K or C/m)

If a site factor (SF) is used to represent the fraction of heat generated that is transported to the surface (Heat Flux–up/Heat Generated), then dT can be related to De by equation 5:

5) $dT = De * [dC * H_{oxygen} * SF] / k$

The temperature difference (dT) in equation 5 can be replaced by deltaT determined from field measurements, and the value of thermal conductivity (k) can be estimated from soil type, ranging from about 1.2 (dry soil) to 2.5 (moist soil) J/m-sec-K (de Vries, 1963). The term SF is considered to be site specific, and is significantly affected by source depth and groundwater flow rates. If SF is assumed to be 1, then deltaT in the soil would represent the minimum rate of biodegradation. Figure 1 shows the plot of deltaT versus De for SF=1, where De is represented by soil porosities (Millington and Quirk, 1961).

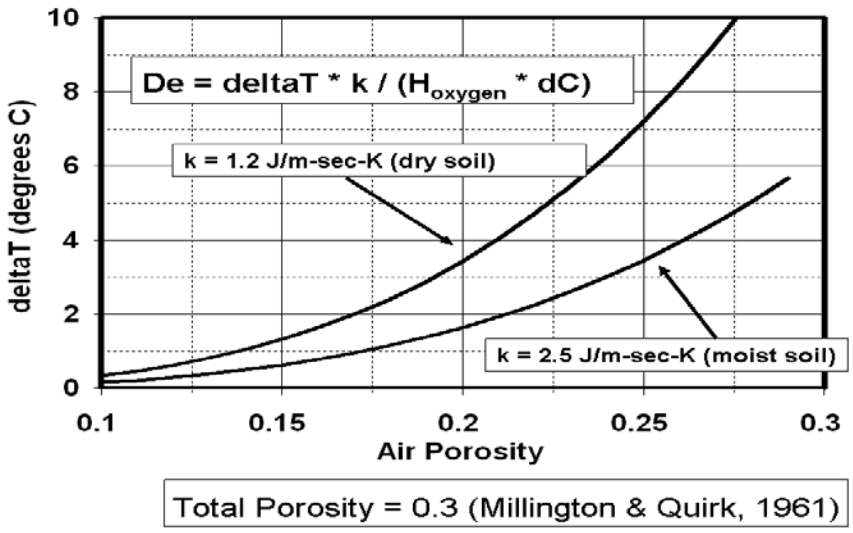

Figure 1. Relation between deltaT and De (SF=1). This plot can be used to determine the minimum rate of biodegradation at the source.

2.5 deltaT from Temperature Probe Measurements

Figure 2 shows the plot of temperature vs depth for 4 wells from a former service station site in Central California. Groundwater is at about 20 feet depth, and the site is presently being used as a car wash. At this site, a significant LNAPL source exists along the western boundary, with one of the wells from the study being located in a grassy area overlying LNAPLs. A second well is located mid-site in a cemented area, and two wells are located in a grassy area on the eastern boundary of the site (no contamination). One of the background wells is located adjacent to the present day car wash. An arrow is shown in Figure 2 for the mean

annual atmospheric temperature for the area. Soil temperatures reflecting the annual atmospheric fluctuations will have a mean annual temperature equal to that of atmosphere, and a range in temperature that decreases with depth (Van Wijk and de Vries, 1963). At a depth of 20 feet, the annual range in temperature due to atmospheric fluctuation will only be few °C (Sweeney and Ririe, 2014). The temperature for the well in clean soil on the east side of the site is consistent with that projected from heat exchange with the atmospheric temperature. The lower temperature of the groundwater for the well adjacent to the car wash was later determined to be due to leakage from the car wash facility. Water leakage also created groundwater mounding at this location.

As shown in Figure 2, deltaT for the well on the west side of the site is about 2 °C higher than the background well on the east side of the site. Using a thermal conductivity value of 2.5 J/m-sec-K and SF=1, De is calculated to be 0.004 m^2/hr. Using equation 2 and the source at 20 feet, this corresponds to an oxygen flux of about 200 mg/hr-m^2.

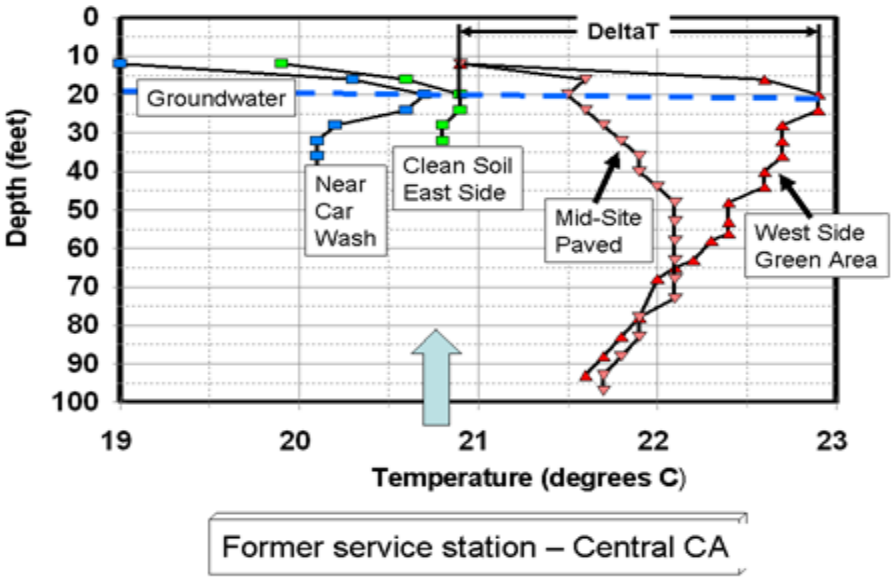

Figure 2. Plot of temperature probe measurements, showing deltaT for the west side well and an arrow indicating approximate groundwater temperature in equilibrium with the atmosphere.

2.6 deltaT from Temperature Sensor Measurements

Sensors are generally used in areas where interest exists for the change in the rate of biodegradation with time. For areas where active remediation is to occur, sensors are placed at several depths down the wells before, or during, the operation. For PVI or SZNA studies, sensors are placed near the top of groundwater (i.e. source depth) and at depths above or below the source.

At one former service station location in Southern California, temperature sensors were used to monitor temperature changes for about 1 ½ years. Figure 3 shows the temperature measurements obtained at 20 feet of depth, near the top of groundwater. The sinusoidal temperature change throughout the year reflects temperature exchange with the atmosphere. For the background well, the mean temperature for the year is similar to that for the atmosphere, indicating the lack of anthropogenic or geologic contribution to soil temperature at the site. For the smear zone well, deltaT remained about 2 °C throughout the year.

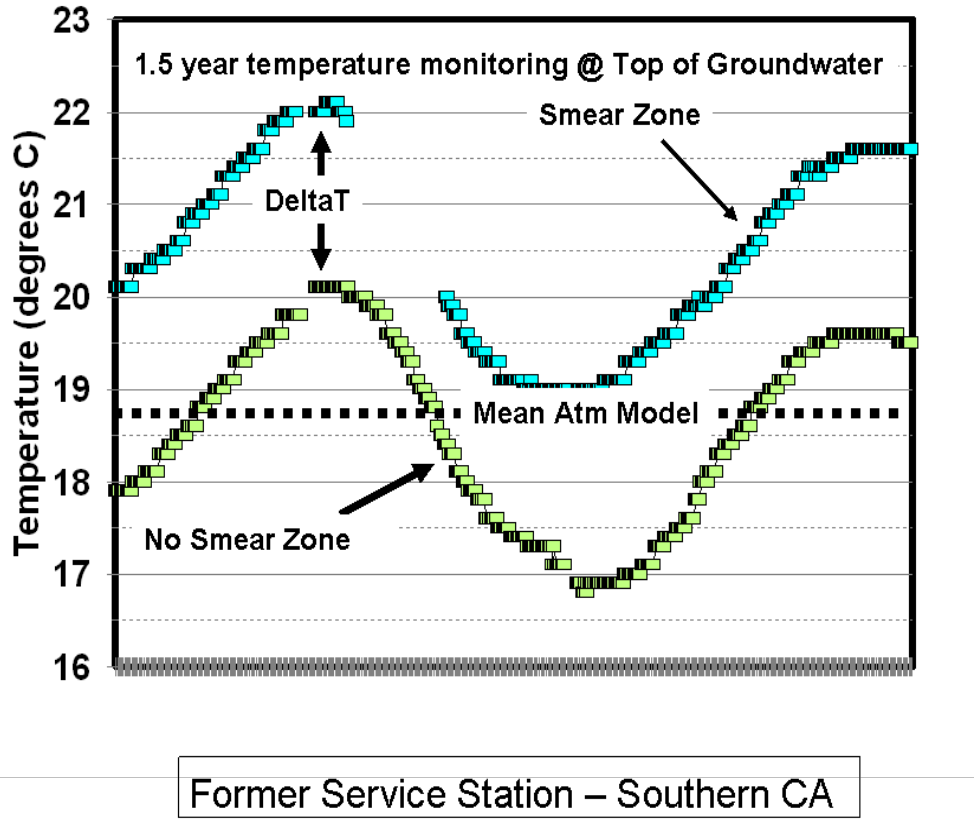

Figure 3. Plot of temperature versus time for sensors placed at the top of groundwater in background and smear zone wells. The value for deltaT is consistently about 2 °C.

2.7 Temperature and Soil Vapor Oxygen Concentration

Temperature measurements have been included in a study of biodegradation processes occurring at a former refinery site in the north-central United States. Within the non-remediated monitoring natural attenuation (MNA) area, the temperature and oxygen profiles both indicate that biodegradation is occurring in the source near the top of groundwater (Figure 4). The temperature profile was measured in the fall when the surface temperature is lower than the soil at depth. The temperature profiles for several other wells in the MNA area showed similar temperature maxima near the top of groundwater at this time of year. For vapor profiles, the oxygen concentration in the MNA area generally decreases linearly with depth to the source. As shown in Figure 4, oxygen diffusion to the source results in biodegradation and generation of heat, which will be lost by transport away from the source. It is only the portion of heat conducted to the surface that is used to estimate the minimum rate of oxygen flux to the source.

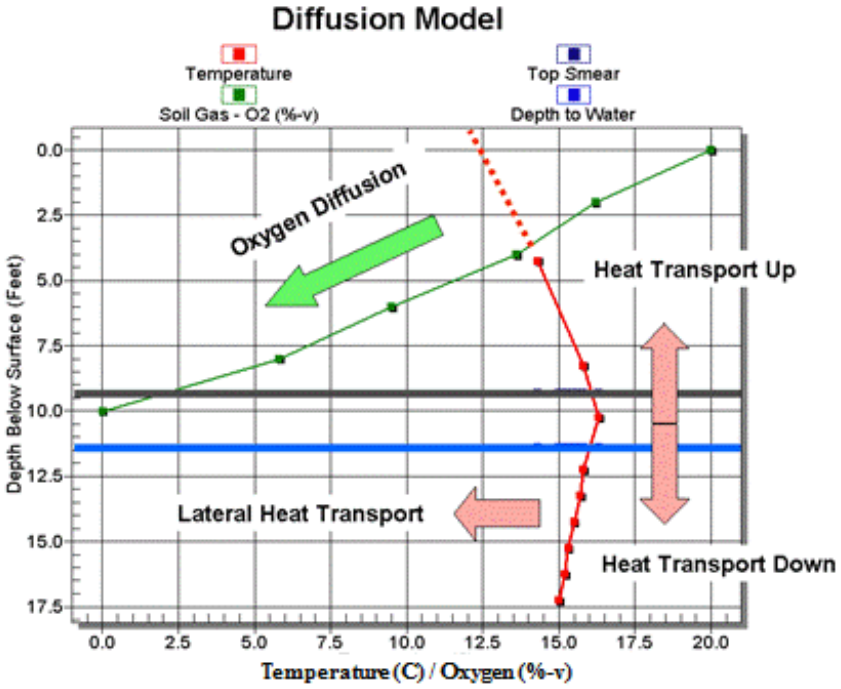

Figure 4. Plot of oxygen concentration and temperature versus depth for MNA area.

Adjacent to the MNA area, soil vapor extraction is being carried out as part of the remediation operation at the site. Though the soil column can be less than 10 feet over the smear zone, the radius of influence for the extraction wells is greater than

100 feet. The oxygen concentration profiles at soil vapor locations in the SVE area are different (Figure 5) from those in the MNA area. Air circulation through the soil retains a high oxygen concentration in vapor near the top of the source. The temperature profiles in the SVE area are similar to those in the MNA area, but have a larger temperature maxima due to the enhanced rate of biodegradation resulting from advective air flow.

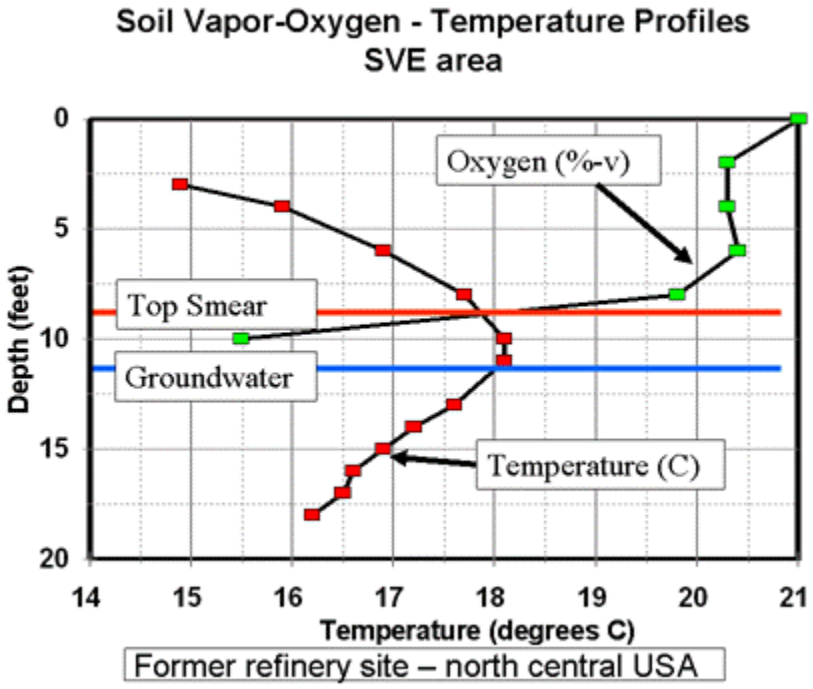

Figure 5. Plot of oxygen concentration and temperature versus depth for SVE area.

2.8 Temperature Anomalies in MNA and SVE areas

Although temperature anomalies in the soil can only be used to estimate the minimum rate of biodegradation, they can be used to evaluate the relative importance of biodegradation across a site. As mentioned above, a temperature study was carried out in adjacent areas where MNA and SVE were being used as

remediation options. Groundwater monitoring across both areas in the spring (May) and the fall (November) included *in situ* measurements of temperature near the top of groundwater. Figure 6 shows the plot of temperature measurements collected in the spring and fall of 2010 for wells in both areas, and two upgradient background wells in uncontaminated soil. The temperature measurements for the background wells are consistent with the atmospheric model for the site (mean annual temperature = 12.5 °C), with groundwater in the fall having a higher temperature than in the spring. In general, the temperatures for MNA wells are 1 – 4 °C higher than background wells, with some of the lower temperature locations being in an area of a more developed, near-surface silt layer. Groundwater temperature within the SVE area is in general higher than the MNA area; however, several SVE wells do have temperatures similar to those for the MNA wells. These wells are from locations within the part of the SVE area that may no longer need active remediation.

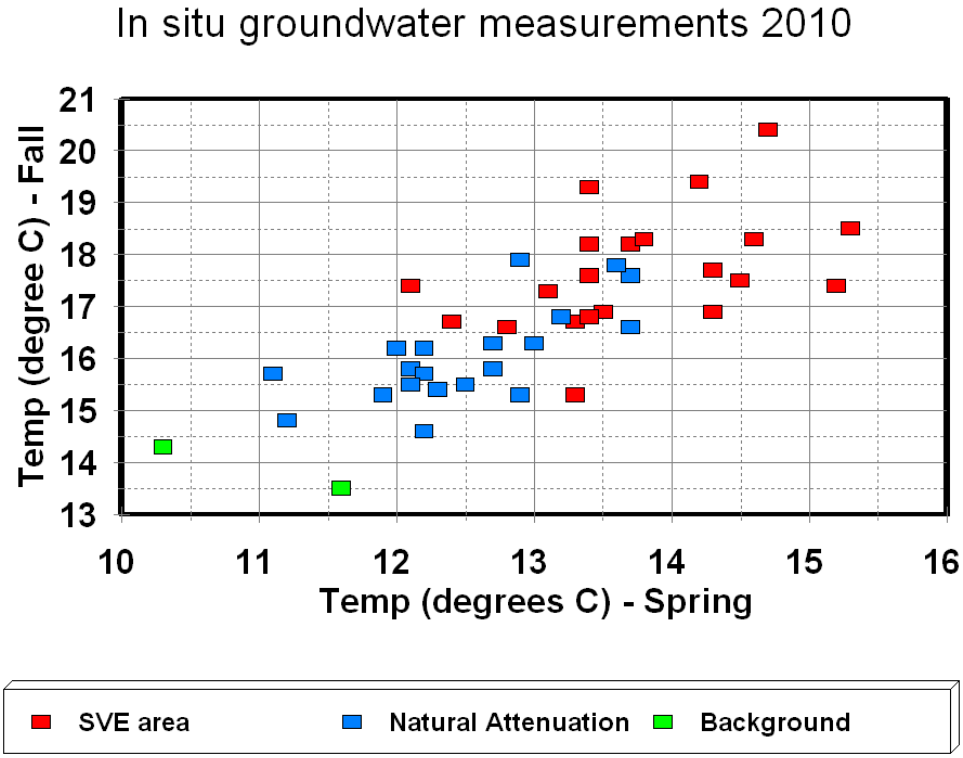

Figure 6. Plot of fall versus spring groundwater temperature for wells from former refinery site.

2.9 Temperature and Vadose Zone Biodegradation of Gasoline

A significant gasoline release occurred at a former service station in Southern California. Since the release, the depth to groundwater has decreased from about

30 feet bgs in 1988 to the present depth of about 70 feet bgs, smearing gasoline throughout the soil column. Extensive AS/SVE remediation since 1996 has removed most of the volatile hydrocarbons from the soil. However, significant benzene concentrations still exist in groundwater in the known area of residual gasoline, and at a well (MW-13) located about 100 feet downgradient on the other side of a highway. Figure 7 shows the temperature profiles for the background well (MW-12) and two monitoring wells (MW-7 and MW-8) located in the area with residual gasoline.

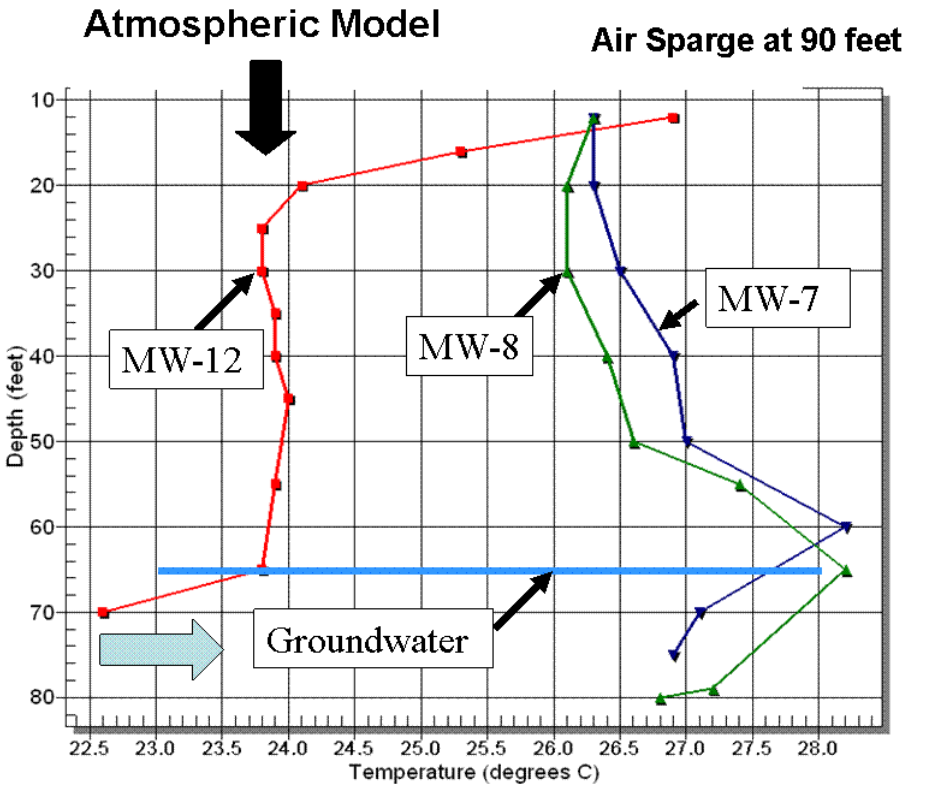

Figure 7. Plot of temperature versus depth for upgradient background well MW-12 and monitoring wells MW-7 and MW-8 in the area of residual gasoline. The atmospheric model temperature and groundwater flow direction are shown.

The vadose zone temperature for soil at the background location is consistent with mean annual atmospheric temperature. Groundwater flowing into the site is cooler than the overlying soil temperature, but increases by over 4 °C within the residual gasoline area. Soil temperature in the residual gasoline area is over 2 °C higher than the background location. Temperature maxima for wells MW-7 and

MW-8 correspond to the depth of residual TPH in the soil between 55 and 65 feet bgs. The higher soil temperature in these wells is attributed to previous AS/SVE remediation operations, with the temperature maxima indicating the depth where biodegradation is presently occurring. Even though the remediation operation involves the introduction of air into groundwater at 90 feet of depth, the temperature anomaly occurs in the vadose zone at the depth where residual TPH exists.

Temperature sensors were placed at different depths in the downgradient well with elevated benzene (MW-13). Figure 8 shows the plot of temperature measurements taken from June 20 to August 7, 2008 from sensors placed in the vadose zone at 55 and 65 foot depth, and within groundwater at a 75 foot depth. The temperature anomaly at 65 feet bgs in the vadose zone indicates that residual gasoline exists in the soil at this depth and that air flow through the vadose zone occurs due to the SVE system located across the street. Since gasoline is considered to be present at MW-13, the current footprint of an air sparge operation on the other side of the street is considered not to be effective for removing benzene from groundwater in the downgradient well.

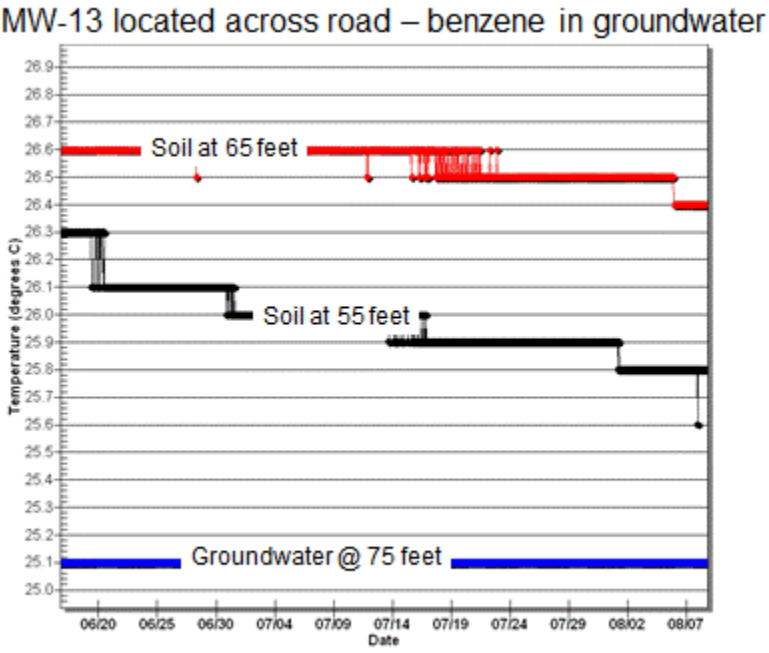

Figure 8. Plot of temperature from June 20 – Auguest 7, 2008 for 3 depths in MW-13. The temperature maxima at 65 feet is consistent with gasoline being present in the soil, and is probably the source for benzene in groundwater.

2.10 Temperature and Biodegradation from Air Sparge

Groundwater and vadose zone temperature measurements were conducted during and after air sparging, and soil vapor extraction system (AS/SVE) operations at a former refinery in north-central USA. The temperature measurements were made to determine the importance of biodegradation for removing BTEX and MTBE from a 30-foot thick smear zone that extends below groundwater at a depth of about 30 feet bgs. Air was injected through a number of wells screened between 60 - 70 feet bgs, and air was extracted from wells screened from 20 - 30 feet bgs. Groundwater was monitored from a set of wells screened between 45 and 50 feet bgs. The air sparge system was operated for 2 ½ years and terminated in March 2010. Figure 9 shows a map of the area and a general outline of the operation. Temperature measurements were made in wells shown on the map, including ASMP-11 located within the air sparge area, G-417 located about 90 feet upgradient, and AS-2 located approximately 80 feet downgradient from the area of influence. For comparison, temperature measurements were also made at G-35, which was located 750 feet southeast from the air sparge area.

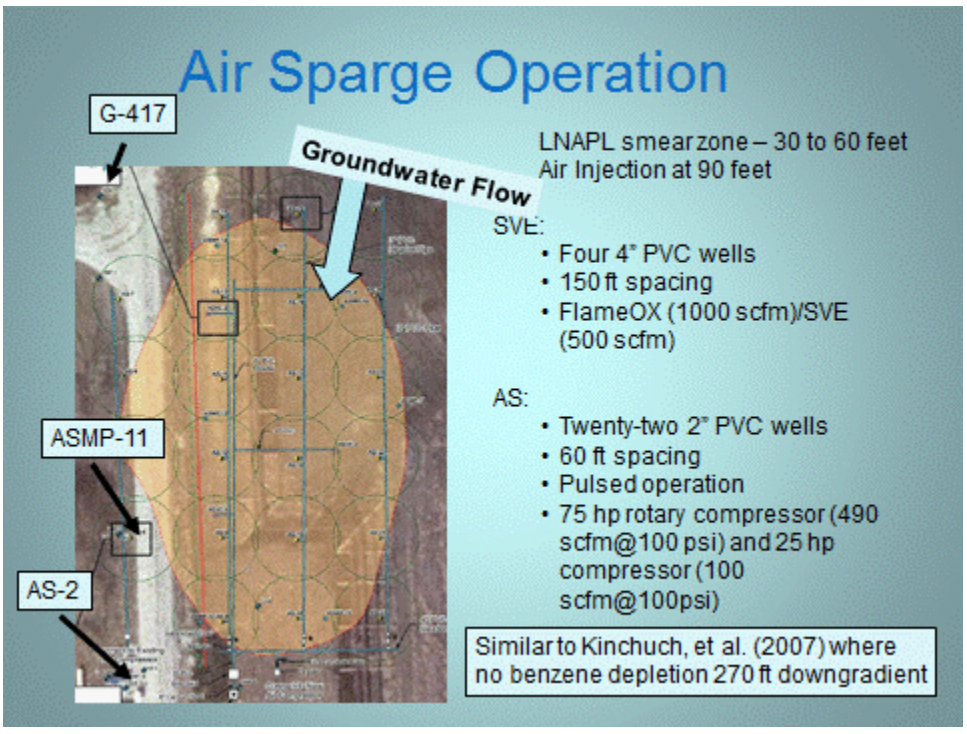

Figure 9. The location of wells within and outside air sparge area.

Prior to air sparge, the average groundwater concentrations in the air sparge area for MTBE and benzene were 7,200 µg/L and 11,000 µg/L, respectively. After air sparge, the concentrations were reduced to < 100 µg/L, and remained low during rebound monitoring for the next two years. Figure 10 shows the temperature profiles for the wells shown in Figure 9.

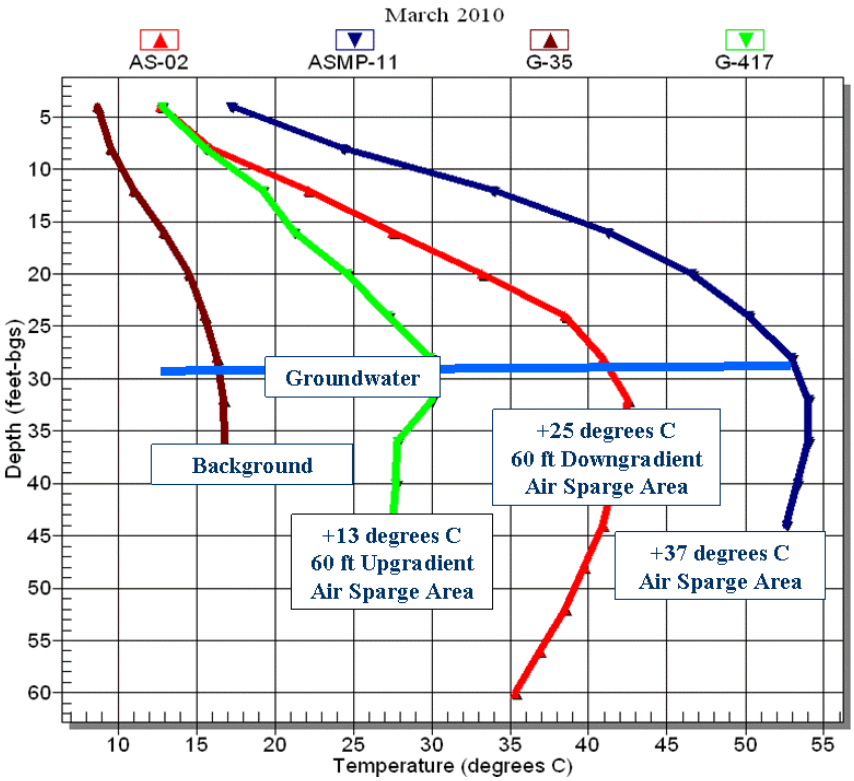

Figure 10. Temperature profiles for background well G-35, upgradient well G-417, downgradient well AS-02, and well ASMP-11 located within the air sparge area.

The high temperatures present in wells surrounding the air sparge operation are considered to be due to aerobic biodegradation from the injection of air into groundwater. At ASMP-11, the temperature near the top of groundwater exceeds the limit for mesophilic petroleum degraders (Johnson et al., 2011). This demonstrates that the transition from mesophilic to thermophilic petroleum degraders can be accomplished during air sparging. AS-02, located downgradient from the air sparge area, has groundwater temperatures about 25 °C higher than background. The high temperature is considered to be due to lateral transport of heated water from the air sparge area and/or *in situ* biodegradation due to lateral transport of oxygen in groundwater. For comparison, Klinchuch et al. (2007) did not observe the removal of benzene downgradient from an air sparge operation that was very similar to this site. Both sites had high 'oxygen demand' soil (i.e.

thick smear zone). The 13 °C temperature anomaly at G-417, however, occurs at a location upgradient from the air sparge area. At this location, the high temperature groundwater must be due to biodegradation from oxygen supplied from the air sparge system.

3. CONCLUSION

Temperature measurements in the subsurface at environmental sites can be made nonintrusively down pre-existing wells. The information obtained can potentially be used to aid in determining the extent and magnitude of aerobic biodegradation of hydrocarbons in the soil. It is important to consider the presence of alternative heat sources at the site, and verify whether or not temperature in the soil for the area is due to heat exchange with the atmosphere and/or contributions from anthropogenic or geologic sources.

For PVI or SZNA sites, biodegradation at/near the source will result in a measurable thermal anomaly indicative of the minimum rate of biodegradation at the source. Biodegradation in overlying shallow soil would limit the rate of oxygen transport to the source, and could eliminate the thermal anomaly at the source. For *in situ* bioremediation, temperature measurements can be used to evaluate the effectiveness of AS or SVE systems by comparing temperature anomalies developed in the soil from remediation to those at locations where biodegradation is occurring from natural attenuation processes. Temperature measurements made down wells can also be used to determine the lateral and vertical extent of bioremediation across an area, and show whether biodegradation from AS/SVE is occurring in groundwater and/or in the vadose zone.

4. REFERENCES

Adams, J.A. and K.R. Reddy 2003. Extent of Benzene Biodegradation in Saturated Soil Column During Air Sparging. Ground Water Monitoring & Remediation 23 (3), 85 – 94.

Amos, R.T. and K.U. Mayer 2006. Investigating Ebullition in a Sand Column using Dissolved Gas Analysis and Reactive Transport Modeling. Environ. Sci. Technol. 40, 5361 – 5369.

Bekins, B., F.D.Hostetler, W.N. Herkelrath, G.N. Delin, E. Warren and H.I. Essaid 2005. Progression of Methanogenic Degradation of Crude Oil in the Subsurface. Environmental Geoscience 12 (2), 139-152.

Davis, G.B., B.M. Patterson, and M.G. Trefry 2009. Evidence for instantaneous oxygen-limited biodegradation of petroleum hydrocarbon vapors in the subsurface. Ground Water Monitoring & Remediation 29(1), 126-137.

DeVaull, G.E. 2007. Indoor vapor intrusion with oxygen-limited biodegradation for a subsurface gasoline source. Environmental Science and Technology 41 (9), 3241-3248.

de Vries, D.A. 1963. Thermal properties of soils. In Physics of Plant Environment, ed. W.R. van Wijk, 210 235, Amsterdam: North-Holland Publishing Company.

Johnson, A.N., B.R. Boer, W.W. Woessner, J.A. Stanford, G.C. Poole, S.A. Thomas, and S.J. O'Daniel. 2005. Evaluation of an inexpensive small-diameter temperature logger for documenting ground water river interactions. Ground Water Monitoring and Remediation 25(4), 68-74.

Johnson, C.D., J.J. Plumb, B.S. Robertson, M.G. Trefrey, T.P. Bastow, and J.A. Lancaster. 2011. Internal heat generation as a design consideration for in situ biosparging of petroleum hydrocarbons. 4th European Bio Remediation Conference 1D41.

Johnson, P. C. 1998. An Assessment of the Contributions of Volatilization and Biodegradation to *In Situ* Air Sparging Performance. Environmental Science and Technology 32, 276-281

Johnson, P., P. Lundegard, and Z. Liu. 2006. Source zone natural attenuation at petroleum hydrocarbon spill sites – 1: Site-specific assessment approach. Ground Water Monitoring and Remediation 26 (4), 82-92.

Kinchuch, L.A., N. Goulding, S.R. James and J.J. Gies 2007. Deep Air Sparging – 15 to 46 m beneath the Water Table. Ground Water monitoring & Remediation 27(3), 118 – 125.

Lundegard, P.D. and P.C. Johnson. 2006. Source zone natural attenuation at petroleum hydrocarbon spill sites– II: Application to a former oil field. Ground Water Monitoring and Remediation 26 (4), 93-106.

Ma, J., W.G. Rixey, G.E. DeVaull, B.P. Stafford and P.J.J. Alvarez 2012. Methane bioattenuation and implication for explosive risk reduction along the groundwater to soil surface pathway above a plume of dissolved ethanol. Env Sci Tech 46, 6013-6019.

Millington, R.J. and J.P. Quirk. 1961. Permeability of porous solids. Transactions of the Faraday Society 57, 1200-1207.

Sihota, N.J., O. Singurindy, and K.U. Mayer. 2011. CO2-effux measurements for evaluating source zone natural attenuation rates in a petroleum hydrocarbon contaminated aquifer. Env Sci. Tech. 45, 482-488.

Sweeney, R.E., S. Subramanian, and D. Tsao. 2013. Methane Generation in Groundwater and Transport to the Vadose Zone. International Symposium on Bioremediation and Sustainable Environmental Technologies, June 10-13, Jacksonville, Fla.

Sweeney, R.E. and G.T. Ririe 2014. Temperature as a Tool to Assess Aerobic Biodegradation of hydrocarbons in Contaminated Soil. Accepted for publication Groundwater Monitoring & Remediation

USEPA 2013. Evaluation of empirical data and modeling studies to support soil vapor intrusion screening criteria for petroleum hydrocarbon compounds. EPA 5101R-13/001.

Van Wijk, W.R. and D.A. de Vries. 1963. Periodic temperature variations in a homogeneous soil. In Physics of Plant Environment, ed. W.R. Van Wijk, 103-143.

Warren, E., B. Bekins, N. Sihota, P. Cambell-Swarzengki. 2011. Unsaturated zone temperature increase due to aerobic methanotropic activity. GSA Annual Meeting, October 10, Minneapolis, Min.

Yang, X., S. Subramanian, T. Dull, T. Tunnicliff, and G. Jeviak. 2006. Pulsed Air Sparging for MTBE and TBA Source Zone Remediation. NGWA 2006 Petroleum Hydrocarbons and Organic Chemicals in Ground Water ®: Prevention, Assessment, and Remediation Conference Proceedings.

QUANTIFYING HYDROCARBON POLLUTION IN SOILS USING MID-INFRARED FOURIER TRANSFORM SPECTROSCOPY

Sayed Salman Tabatabai[1§], Marleen F. Noomen[2], David G. Rossiter[2]
[1] M.Sc. Alumnus, Department of Earth System Analysis, Faculty of Geo-Information Science and Earth Observation, University of Twente, No 31, Majd 28.1 St. Majd Blvd., Mashhad, 9184885115, Iran, [2]Department of Earth System Analysis, Faculty of Geo-Information Science and Earth Observation, University of Twente, Hengelosestraat 99, 7514 AE Enschede, The Netherlands

ABSTRACT

Environmental protection agencies require rapid and quantitative analysis of oil and other hydrocarbon spills in the environment. Most of the studies so far have focused either on the traditional time consuming chemical methods or on the visible-near infrared spectroscopy. Although several studies proved the strengths of mid-infrared range and diffuse reflectance infrared Fourier transform spectroscopy to detect the hydrocarbon fundamental vibrations, they have not considered the effect of natural soil moisture and soil grain size. This study considers these effects as well as spectral transformations on the detectability and quantifiability of the pollution. Reflectance of polluted samples were measured in the laboratory over the 4000 to 400 cm^{-1} wavenumber range. Reflectance spectra were correlated to soil pollution quantity by partial least squares regression. The lowest detectable limit of motor oil in soils, regardless of grain size and water content, was 1 weight percent. The quantification limit in the worst case was about 5.7%. Except for the coarse grained soil, the predictions had R^2>77%, even with water contents as high as 20%. Predictions in fine and mixed grained soils were shown to be significantly more accurate than the coarse grained ones.

Keywords: hydrocarbon, soil pollution, mid-infrared, Fourier transform spectroscopy, partial least squares regression

§ Corresponding Author: Sayed Salman Tabatabai, No 31, Majd 28.1 St. Majd Blvd., Mashhad, 9184885115, Iran, Tel: +98-915-1240392; tabatabai28990@alumni.itc.nl

1. INTRODUCTION

Hydrocarbon pollution and oil spills have become a serious environmental challenge in recent centuries. The rapidly growing global economy demands oil-producing countries to extract and transport large amounts of oil and oil-based products. This may result in hydrocarbon leakages to the environment. These leaks can occur in different stages of extraction, transportation, and storage of hydrocarbons. Soil pollution endangers the food chain and poses a threat to ecological systems (Fine et al.,1997). The United States Environmental Protection Agency (EPA) has reported 14,000 oil spill incidents annually only in the United States (EPA, 2011).

Most soil investigations and quality assessment methods are based on physicochemical laboratory techniques (Viscarra Rossel et al., 2006). Methods for the quantification of total petroleum hydrocarbon (TPH) are complex, expensive, and time-consuming (Schwartz et al., 2009; Forrester et al., 2010). Some of these methods, namely “purge and trap” and “headspace”, use chemicals to extract the hydrocarbon from soil (TPHCWG, 1998), and hence the soil and its integrity is affected by the test itself (Janik et al., 1998; Stenberg and Viscarra Rossel, 2010). The chemicals used in or produced by these methods are also hazardous to the environment (Graham, 1998; Nanni and Demattê, 2006; Stenberg and Viscarra Rossel, 2010). Due to their complicated procedures and instrumentation requirements, these methods cannot be used in-situ or in the field, thus are not usable over large areas (Forrester et al., 2010). An extensive review of these methods, their application domain, and limitations can be found in Graham (1998) and TPHCWG (1998).

As an alternative to traditional methods, remote sensing in general and spectroscopy in particular have been shown to provide quick and relatively inexpensive methods of investigating soil pollution. One of the first laboratory spectroscopic studies was by Cloutis (1989), who used visible (Vis) and near-infrared (NIR) spectroscopy to determine the fundamental absorption features of major hydrocarbons in these spectral ranges. Nguyen et al. (1991) later used diffuse reflectance infrared Fourier transform spectroscopy (DRIFTS) to characterize soils both mineralogically and also by quantification of organic constituents, including hydrocarbons.

Previous studies suggest that H-C fundamental molecular vibrations are typically excited in the mid-infrared (MIR) region of the spectrum, and that this range is sensitive to some other soil constituents that lack absorption features in Vis-NIR ranges (Hazel et al. 1997; Reeves et al. 2001; van der Meer et al. 2002). Hazel et al. (1997) showed that the MIR data is able to simultaneously quantify soil hydrocarbon (HC) and moisture content, as well as other soil constituents. The

MIR region has also shown to be intrinsically more sensitive than the NIR to molecular information with narrower and increased absorption (Janik et al., 1998; Stenberg and Viscarra Rossel 2010). Forrester et al. (2010) further showed that TPH and natural soil organic materials can be differentiated based on MIR spectra. A recent study by van der Meijde et al. (2012) used MIR and thermal infrared (TIR) laboratory spectroscopy to model the hydrocarbon concentration in clays using partial least squares regression (PLSR) and step-wise multiple linear regression (SMLR). They also investigated the applicability of several airborne sensors with bands in MIR and TIR for hydrocarbon detection over large areas.

Using MIR DRIFTS combined with PLSR has also been shown to generally produce more accurate predictions of different soil constituents and pollutions than NIR (Bertrand et al., 2002; Viscarra Rossel et al., 2006; Forrester et al., 2010; Stenberg and Viscarra Rossel, 2010). A review of the predictions by Vis, Vis-NIR, NIR, and MIR diffuse reflectance spectroscopy (DRS) comparing their prediction success for several chemical, physical and biological soil properties is reported by Stenberg and Viscarra Rossel (2010).

The few spectroscopic studies of the MIR range so far have ignored the effect of natural soil moisture and soil grain size in the detection and quantification of pollution; therefore, in this study we incorporated the effects of these factors, as well as spectral transformations on the detectability and quantifiability of the pollution. We developed a method to quantify the amount of an abundantly used hydrocarbon (motor oil) in three soil materials in varying moisture conditions using laboratory MIR DRIFT spectroscopy. The aim of this study is to determine the lowest detectable limit of oil pollution in soil, and the effect of soil particle size and varying moisture content on the quantification of motor oil pollution using MIR DRIFT spectra.

2. MATERIALS AND METHODS

2.1 Sample Preparation

Three soil materials were used in this study:

1. Fine sand (<0.5 mm fraction), mainly consisting of quartz particles;

2. Coarse beach sand (0.5-2.0 mm fraction), mainly consisting of weathered granitic minerals; and,

3. A 1:1 mixture of the aforementioned soil materials to produce a more complex system, both in terms of particle size and mineral composition of the particles.

To prepare the first set of samples, 20 g of air dried coarse, fine, and mixed soils were weighed and poured into opaque glass containers. Distilled water was added to each container to moisten the soils at one of two proportions: 10 and 20 wt%. Soil and water were then mixed thoroughly in order to moisten the soils homogeneously as possible, both as coatings on the grains, and as filler in the intergranular pore spaces. Shell Helix™ 15w-40 mineral motor oil was then added in six different concentrations. The moist soil and the oil were mixed thoroughly to ensure that each sample was a homogeneous mixture of soil, water, and oil. Containers were then closed firmly by air-tight caps to prevent evaporation. Sample composition is shown in Table 1.

Table 1. Soil samples prepared for measurements

Soil Material	Water Content (wt%)	Pollution Concentration (wt%)
Fine	10	0
		1
		2
Coarse	20	4
		8
		12
Mixed		20

2.2 Spectral Measurements

Each sample was scanned with a Bruker Vertex 70 ™ spectrometer to obtain its MIR DRIFT spectrum. Measurements were done in the whole mid-infrared range: wavenumbers of 4000-400 cm^{-1} (2.5-25 μm) in 1866 overlapping bands. Since the samples were composed of materials in solid and liquid states, a spectral resolution of 4 cm^{-1} was chosen for the measurement, which is expected to give the highest resolution with the lowest noise level for these material states (Smith, 1996).

For each measurement, the sample container was opened, the moist soil and the oil were mixed thoroughly (since some separation may have occurred after sample preparation), and a small portion of homogeneous material was applied on the measuring container. The surface of the sample was smoothed to reduce the effect of grain size orientation on the spectral measurement. Before measuring the sample, a background spectrum was measured on a specular mirror with maximum reflectance.

For the background measurements, the amplitude was manually set to the highest value possible to acquire the best reading. The sample container was then placed in the DRIFT setup of the spectrometer and the amplitude was set manually to the highest level possible for the sample measurement. The amplitudes differed depending on the amount of reflected energy received from the sample, which was dependent on the amount of water (high absorption, less reflected energy), pollution concentration (more oil, more reflectance), and soil grain size (coarse soil particles causing more light dispersion than the fine particles).

The measurement container was then rotated 180 degrees to account for the brightness difference caused by different orientation of the soil particles and a second measurement was made. Each sample was measured at least twice, and some samples were randomly chosen for more measurements to ensure that preparation procedures and sampling introduced no significant error in the resulting spectra.

2.3 Data Analysis

Based on the recommendations of Clark and Roush (1984), the continua of the spectra were removed (Huang et al., 2004) in order to normalize and isolate the absorption features. The first derivatives of the spectra were calculated in order to amplify the detectability of subtle changes in spectra (Low and Mark, 1970).

Since spectroscopic data by its nature has a high amount of correlation between the bands, Partial Least Squares Regression (PLSR) was chosen for data analysis. This method relates two data matrices (response and predictors) in a multivariate linear model, while also modelling the matrix structures, similar to principal components analysis (PCA). PLSR is able to find relations between data matrices with high amounts of noise and multi-collinearity. It is also advantageous in its ability to increase the model parameters precision by increasing the number of observations (Wold et al., 2001). It can explain more variance with fewer components compared to PCA, the results are easy to interpret, and the computation time is relatively short (Stenberg and Viscarra Rossel, 2010).

The data were reorganized by matrix transposition, assigning the reflectance of all spectra as predictors and the known pollution concentrations as responses. The “pls” package (Mevik and Wehrens, 2007) of the R Project for Statistical Computing was chosen for analysis due to the simplicity of use, open source, free

license, analytical power, and robustness. The PLSR was performed on the data using a leave-one-out (LOO) cross-validation method and the root-mean-square error of prediction (RMSEP), coefficient of determination (R^2), calibration and validation measured vs. predicted values, as well as loading effect per wavenumber and component were plotted.

3. RESULTS

3.1 Detection

Figure 1 shows the MIR reflectance spectra of the motor oil used in this experiment. Two prominent absorption features occur at 2958 and 2925 cm^{-1} and two less prominent at 1463 and 1377 cm^{-1}. These values are similar to the fundamental absorption features of hydrocarbons reported in the studies of Nguyen et al. (1991), Hazel et al. (1997), Dominguez-Rosado and Pitchel (2003), Stuart (2004), Reeves (2012), and van der Meijde et al. (2012).

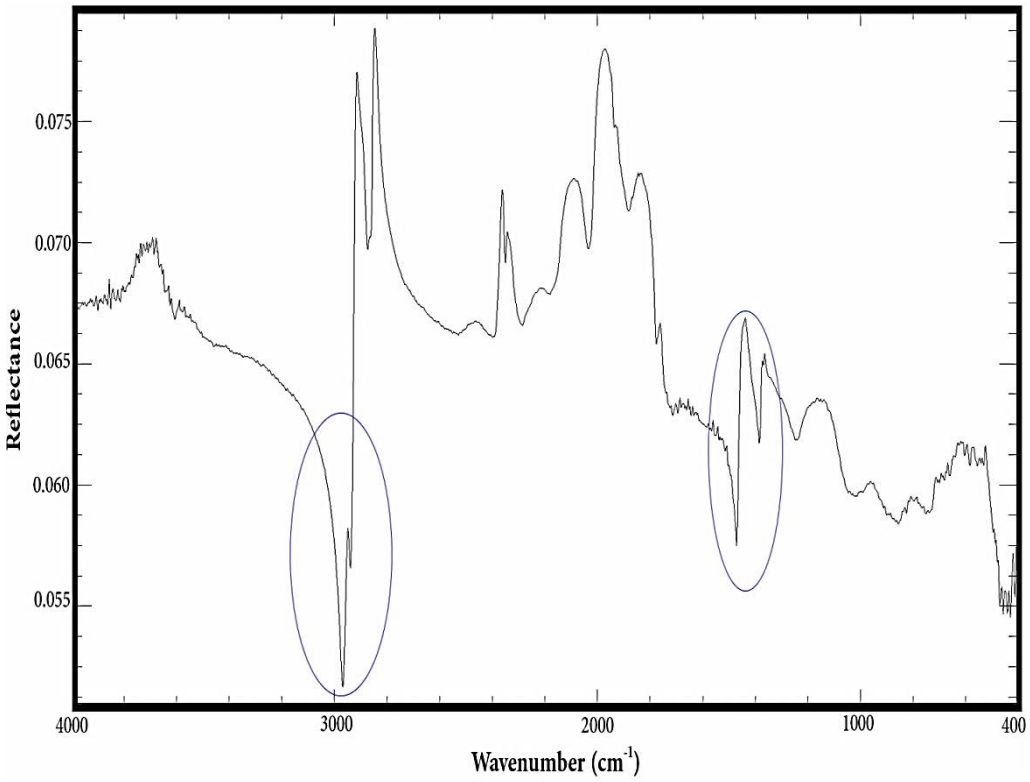

Figure 1. MIR spectra of the motor oil used to pollute the samples

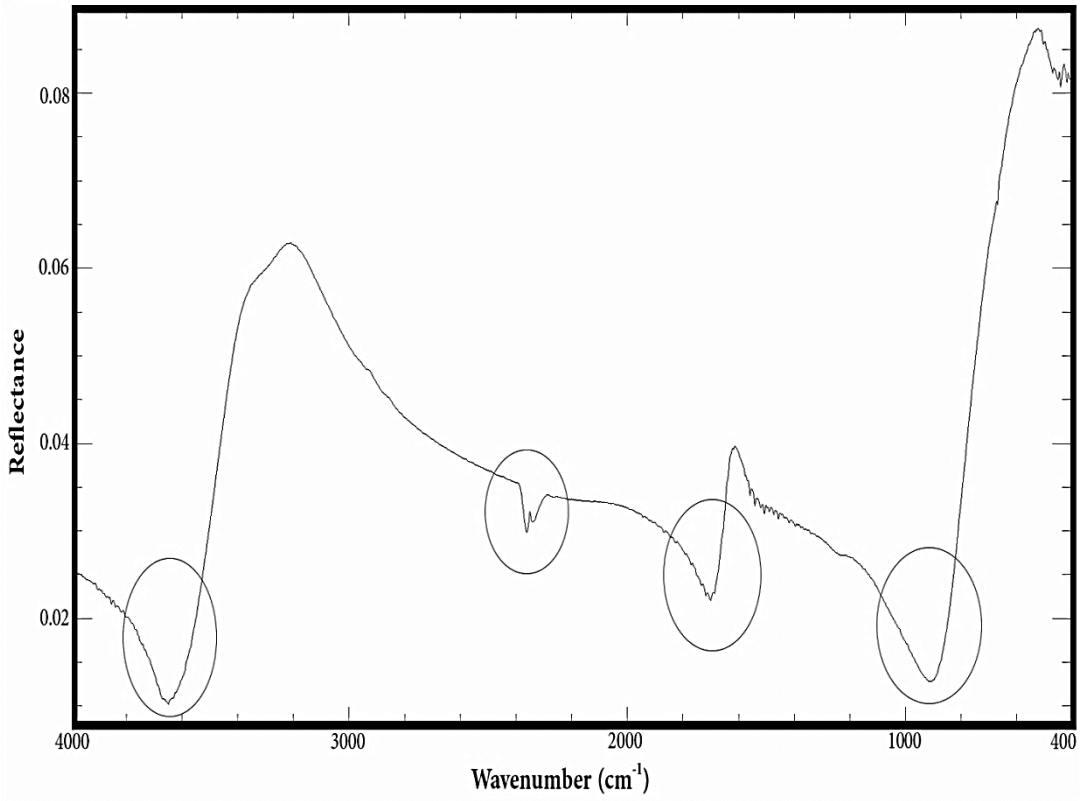

Figure 2. MIR spectra of distilled water

The spectrum of distilled water was also measured. As shown in Figure 2, the significant absorption features are in 3650, 2360, 2340, 1700, and 908 cm^{-1}, with the deepest being at 3650 cm^{-1}. These wavenumbers do not coincide or overlap with the major absorption features of oil.

The spectra of the polluted samples (Figure 3) showed absorption features with wavenumber ranges of 2970-2860 cm^{-1}, becoming more distinct with increasing amount of added oil. This is in accordance with the deepest absorption feature of the pure oil end-member. The second deepest absorption feature of the oil end-member could also be identified in the polluted samples at 1465 and 1377 cm^{-1} (Figure 4), however, these were not as clear and distinct as the previous features.

The significant hydrocarbon absorption features were clearly visible from 1% pollution in all three soil materials, with both 10% and 20% water contents. This means that motor oil pollution in the soil can be detected with a minimum concentration of 1% without any statistical analysis.

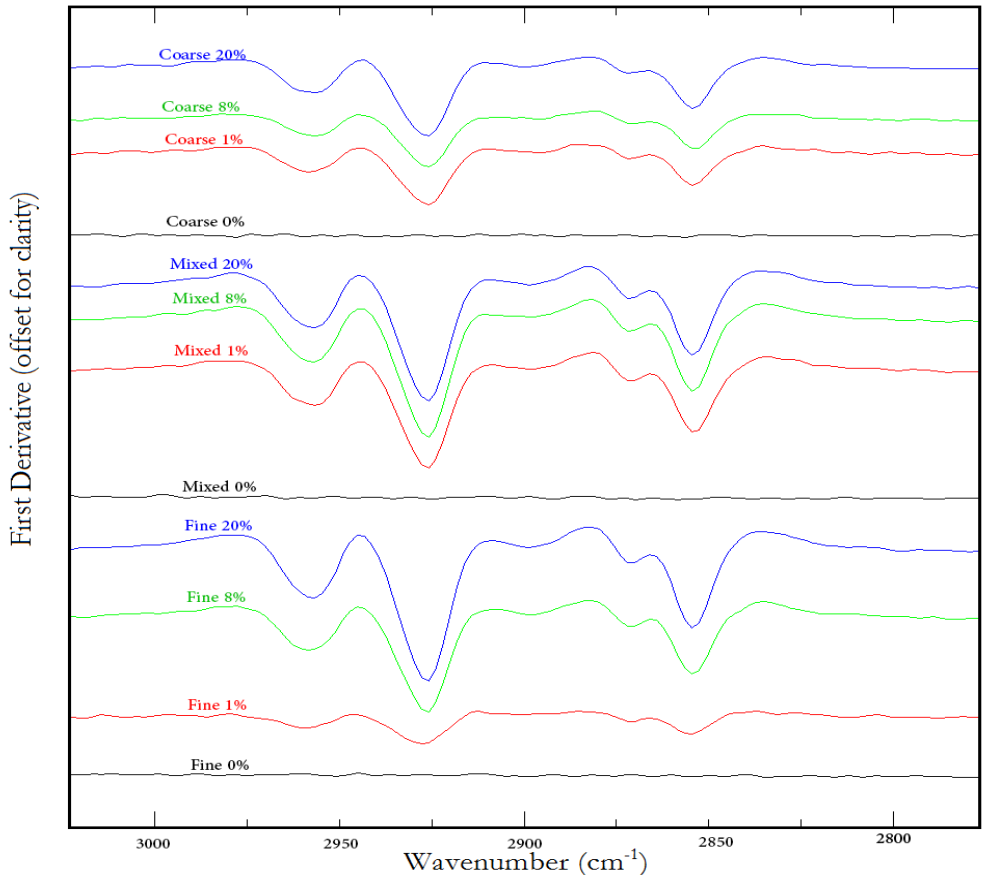

Figure 3. The effect of increasing pollution (in %) on the three soil materials spectra with 20% water content (3000-2800 cm^{-1})

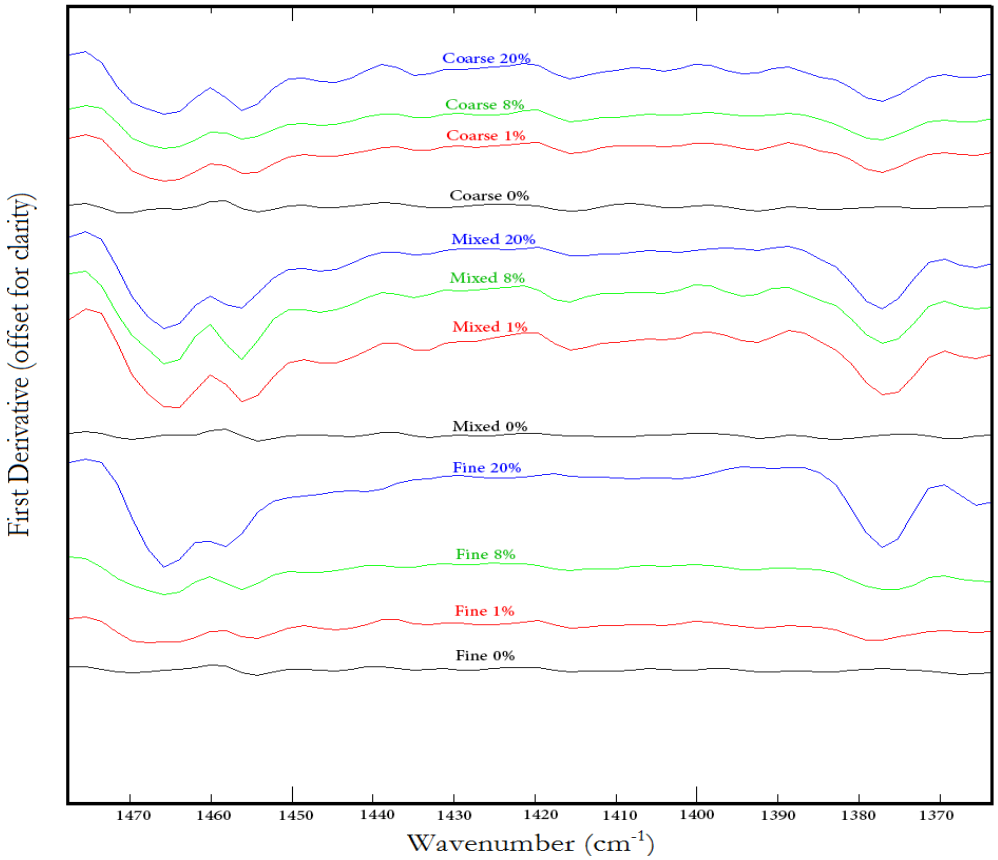

Figure 4. The effect of increasing pollution (in %) on the three soil materials spectra with 20% water content (1480-1370 cm^{-1})

3.2 Quantification

The whole spectral range in the mid-infrared (4000-400 cm^{-1}) in 1866 bands was used to relate the reflectance value in each band with the amount of oil present in the samples. PLSR was first run once to determine the highest variance explanation with the least number of components. The smaller the number of components and the greater the variance explanation, the stronger and more robust the model.

The analysis was done on the untransformed spectra and its corresponding reflectance values, as well as the continuum removed and the first derivative of the spectra.

3.2.1 PLSR Results for the Untransformed Spectra

The PLSR prediction results on the whole MIR range (4000-400 cm^{-1}) untransformed spectra for each soil material with different oil concentrations and different water contents (i.e. one PLSR per soil material per water content) are presented below.

For the 10% water in the fine soil, both calibration and cross validation R^2 results increased up to five components, although, the highest increase was in the first two (Figure 5). This results in the explanation of 93% of the variance both in the training and validation sets. This was in conformity with the results of RMSEP as a function of the number of components, which has the minimum value (less than 2%) with 5 components (Figure 6).

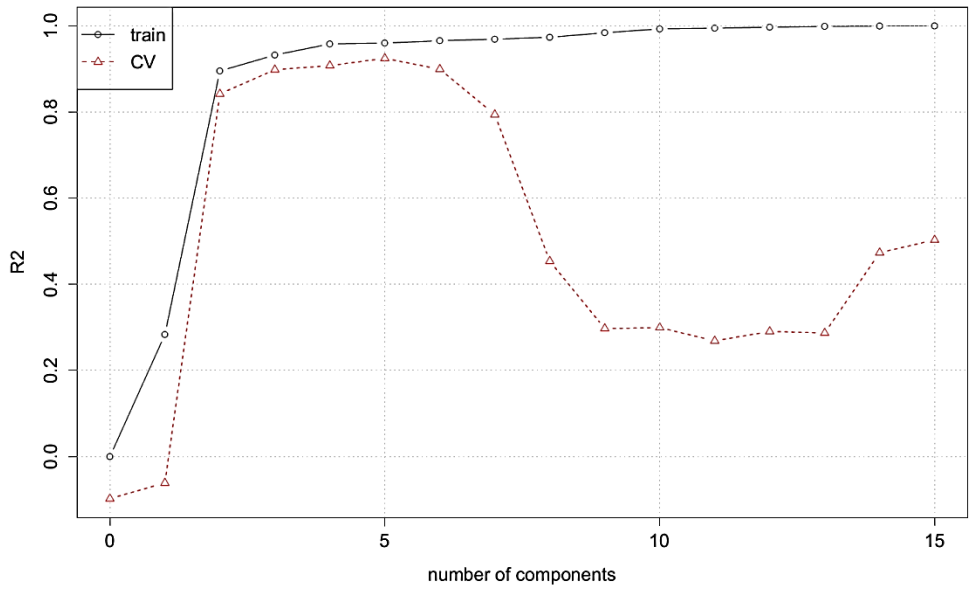

Figure 1. R^2 for the fine grain samples with 10% water content for the whole MIR range of the untransformed spectra

Figures 7 and 8 show the R^2 and RMSEP results of the same soil material as above (fine grained) with the same pollution concentrations, but with increased water content to 20%. The PLSR ability to predict the amount of pollution was reduced substantially with increased water content.

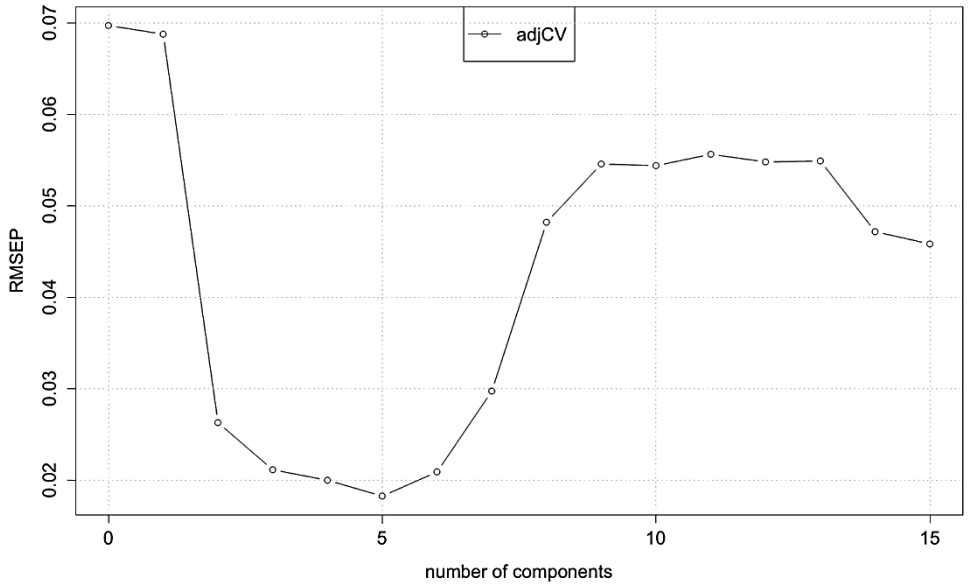

Figure 2. RMSEP for the fine grain samples with 10% water content for the whole MIR range of the untransformed spectra

The R^2 of the training set and the cross validation increased up to the second component at about 82% and RMSEP decreased to 2.7%. Starting from the next components, cross validation R^2 was increased and RMSEP decreased with increasing number of components. This is evidently a weaker result compared to the soils with 10% moisture.

The loading values indicate the most important wavenumber ranges in the prediction by PLSR. The fine grained samples with 10% water content (Figure 9) had the largest loading values in their first component (76.4% of loading effect) in a broad range between wavenumbers 3000 to 2000 cm^{-1} and a narrow range of 1280 to 1000 cm^{-1}. The latter wavenumber range is in agreement with the hydrocarbon fingerprint range reported in previous studies (Stuart, 2004; van der Meijde et al., 2012; Reeves, 2012). The second sample set with 20% water content had 49% of loading effect by the second component and showed exactly the pattern of the first component of the previous set (Figure 10).

The data from coarse grained and mixed grained soils were also processed in the same manner and the results are summarized in Table 2.

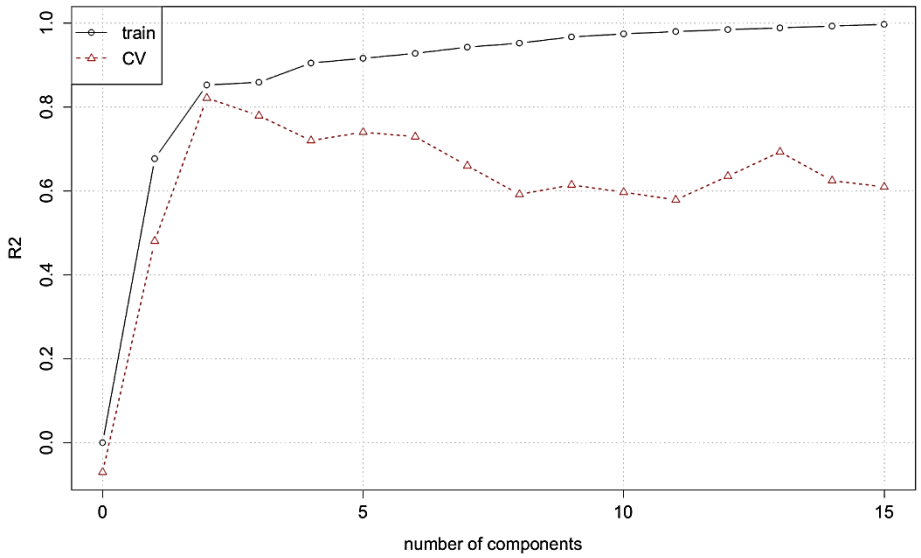

Figure 3. R^2 for the fine grain samples with 20% water content for the whole MIR range of the untransformed spectra

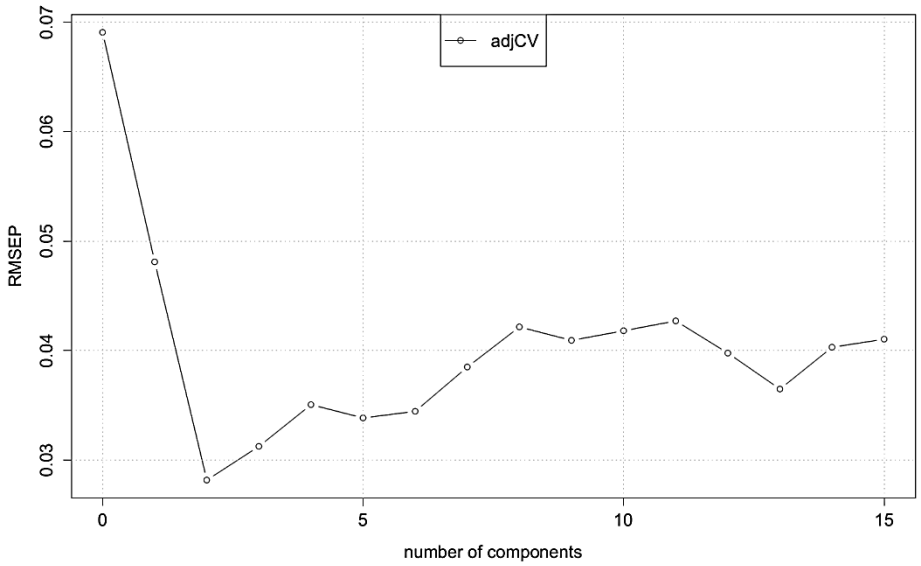

Figure 4. RMSEP for the fine grain samples with 20% water content for the whole MIR range of the untransformed spectra

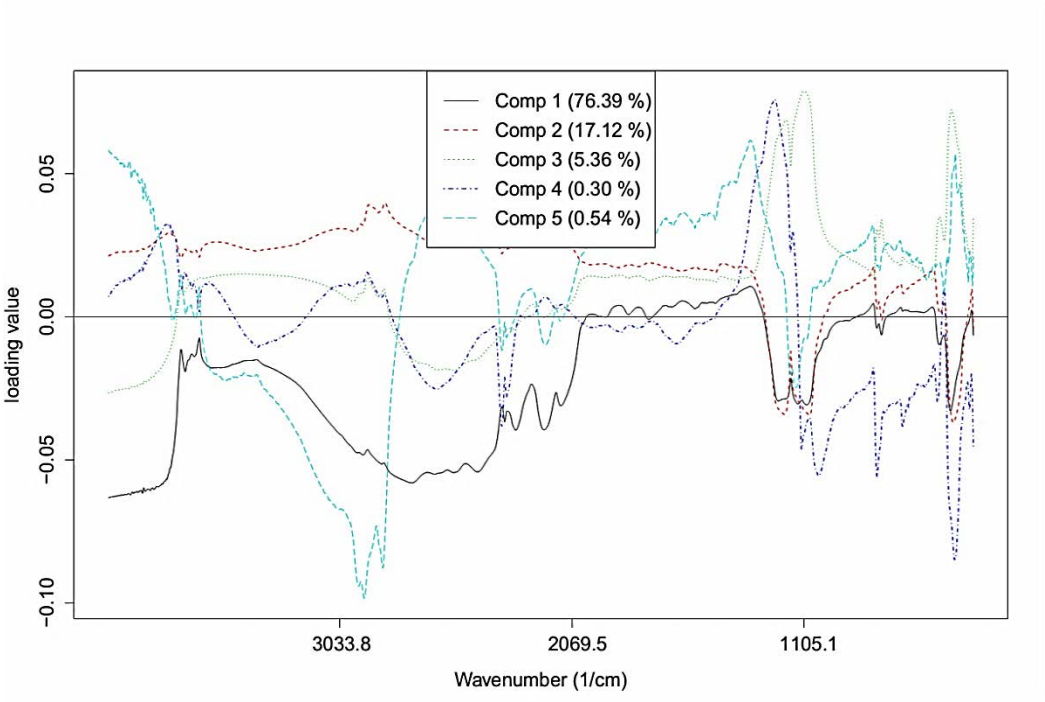

Figure 5. Loadings of the spectra for the fine grain samples with 10% water content for the whole MIR range of untransformed spectra

Table 1. The output summary of PLSR on the untransformed whole spectra of different samples

Sample	Fine 10%	Fine 20%	Coarse 10%	Coarse 20%	Mix 10%	Mix 20%
No. of Factors	5	2	7	8	4	7
R^2 %	93	82	88	25	92	77
RMSEP %	1.8	2.8	2.3	5.7	1.9	3.2
Max. Load. (cm^{-1})	3000-2000, 1280-1000	1280-1000	1280-1000	2970-2860	1280-1000	2970-2860, 1280-1000

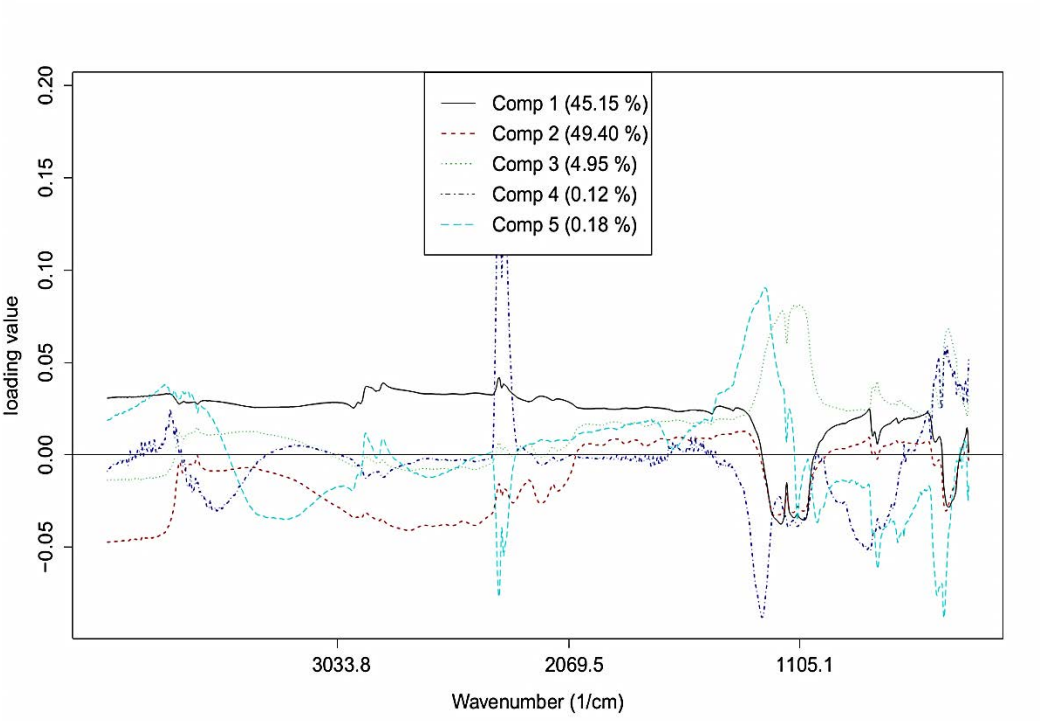

Figure 6. Loadings of the spectra for the fine grain samples with 20% water content for the whole MIR range of untransformed spectra

3.2.2 The Continuum Removed and First Derivative Spectra

Tables 3 and 4 summarize the PLSR results of the continuum removed and first derivative MIR spectra for all of the three soil materials with different water contents and pollution levels. On average, the continuum removed spectra produced slightly better variance explanation compared to the first derivative (73.0% compared to 72.1%); however, both were weaker than the average untransformed spectra results (R^2=74.6%)

Table 2. The PLSR output summary of the continuum removed spectra of different samples

Sample	Fine 10%	Fine 20%	Coarse 10%	Coarse 20%	Mix 10%	Mix 20%
No. of Factors	2	4	15	15	2	5
R^2 %	85	90	88	32	84	75
RMSEP %	2.6	2.0	2.2	5.4	2.5	3.4
Max. Load. (cm^{-1})	2970-2860, 1280-1000	2970-2860, 1280-1000	2970-2860, 1280-1000	2970-2860, 1280-1000	2970-2860, 1280-1000	2970-2860, 1280-1000

3.2.3 All Soil Materials, Water Contents and Pollution Concentrations

To check the applicability of the model in conditions where the soil material, water content, and the pollution concentration are unknown, one regression was run on all of the samples combined together. Table 5 summarizes the PLSR outputs on all of the samples combined in different spectral forms and subsets.

Table 3. The PLSR output summary of the first derivative spectra of different samples

Sample	Fine 10%	Fine 20%	Coarse 10%	Coarse 20%	Mix 10%	Mix 20%
No. of Factors	6	6	5	8	7	6
R^2 %	90	70	79	52	79	75
RMSEP %	2.1	3.7	3	4.5	3.1	3.2
Max. Load. (cm^{-1})	2970-2860, 1280-1000	2970-2860, 1280-1000	2970-2860, 1280-1000	2970-2860, 1280-1000	2970-2860, 1280-1000	2970-2860, 1280-1000

Table 5. The PLSR output summary of all the samples combined

Input Spectra	Untrans.	Cont.Rm.	1st Deriv.
No. of Factors	7	6	5
R^2 %	65	57	60
RMSEP %	3.9	4.3	4.2

4. DISCUSSION

The lowest detectable concentration of motor oil in all of the three soil materials and in both moisture conditions was 1%. This means that soil moisture up to 20% and the grain size do not affect the detectability of motor oil in soil samples. This is particularly advantageous when the objective is to detect and delineate polluted areas rapidly. The prediction of the amount of pollution, however, is significantly dependant on the moisture content and the grain size. Although it is possible to explain 65% of the variance without knowing the grain size and water content, knowing these factors for more accurate predictions is essential.

Tables 6 and 7 show a summary of the R^2 and RMSEP of the PLSR, respectively. The samples with higher water content proved to produce less accurate predictions compared to the same samples with lower water content. This was mainly related to the strong interference of water by reducing overall soil albedo and attenuating the optical signals of both soil and oil (Hazel et al., 1997).

Table 6. R^2 of the PLS regression in all of the samples and analyses

	Fine 10%	Fine 20%	Coarse 10%	Coarse 20%	Mixed 10%	Mixed 20%	Comb.	Avg.
Untrans.	93	82	88	25	92	77	65	74.57
Cont. Rm.	85	90	88	32	84	75	57	73.00
1st Deriv.	90	70	79	52	79	75	60	72.14
Avg.	89.33	80.67	85.00	36.33	85.00	75.67	60.67	

Table 7. RMSEP of the PLS regression in all of the samples and analyses

	Fine 10%	Fine 20%	Coarse 10%	Coarse 20%	Mixed 10%	Mixed 20%	Comb.	Avg.
Untrans.	1.8	2.8	2.3	5.7	1.9	3.2	3.9	3.09
Cont. Rm.	2.6	2.0	2.2	5.4	2.5	3.4	4.3	3.20
1st Deriv.	2.1	3.7	3.0	4.5	3.1	3.2	4.2	3.40
Avg.	2.17	2.83	2.50	5.20	2.50	3.27	4.13	

The highest coefficient of determination (R^2=95.0%) and the smallest RMSEP (1.8%) are both obtained for the mixed soil sample with 10% water. The fine soil and the mixed soil with 10% water have the highest average variance explanation (R^2=87.8%) and the lowest average RMSEP (2.3%), and thus the best overall predictions. This is likely related to the reflecting surface of these soil materials. When the small sample cup was filled with the polluted soils for measurement, the surface of the fine grained soil could be smoothened, thus reducing the chances of inter-granular scattering, which might introduce noise into the spectral measurement. In the mixed grain soil samples, the fine grains could fill up the void spaces between the coarse particles, resulting in a smooth surface similar to the fine grained soil surface. However, the coarse grained materials could not be compressed or smoothened to fill the voids, and therefore, showed more irregular spectra.

Another explanation for this result is that the smaller the soil particles, the more the surface to volume ratio, and therefore, the more surface to which the oil molecules can adhere. Moreover, liquid behaviour differs based on the soil composition. While liquids tend to be absorbed to clay soils, they usually act as a pore space filler in coarser grained soils (Hazel et al., 1997). We observed that water and oil quickly drained to the bottom of the measuring container for coarse grained samples, and therefore less oil per surface could be measured by the spectrometer. This was more evident in the samples with oil concentrations of more than 8%. The fine grains, on the other hand, could retain the oil between the

particles and as their surface coating for enough time to place the sample in the FT-IR spectrometer, tuning the spectrometer to reach the maximum amplitude and measuring the spectrum. This process takes about three minutes.

The prediction results in this study (RMSEP=1.8%) show a better fit in the validation compared to similar studies, namely Hazel et al. (1997) RMSEP=3.7%, Schwartz et al. (2009) RMSEP=3.6%, and van der Meijde et al. (2012) RMSEP=1.9%.

Among the different analyses, on average, analyses on the untransformed spectra could explain more variance than the other forms, and had the least amount of error in prediction (Avg. R^2=74.6% and Avg. RMSEP=3.1%).

The most important spectral ranges in the MIR for quantification of hydrocarbons were roughly 3000-2800, 1480-1370, and 1280-1000 cm^{-1}. While the most prominent and deepest absorption features of hydrocarbons were observed in the 3000-2800 and 1480-1370 cm^{-1}, most of the analyses showed that the highest loading effect was related to the 1280-1000 cm^{-1} range. This range (1280-1000 cm^{-1}), although not observed to have important absorption features, was previously reported in studies of Stuart (2004), Reeves (2012) and van der Meijde et al. (2012).

5. CONCLUSION

5.1 Detection

It was concluded that the lowest detectable limit of the motor oil in soils with any of the grain size and water contents is 1 weight %, indicating that soil moisture up to 20% and the grain size do not affect the detectability of motor oil in soil samples. Moreover, analyses on the untransformed spectra could explain more variance than the other forms and had the least amount of error in prediction. This is particularly beneficial when the objective is to detect and delineate polluted areas rapidly. The processing is quick (no transformation is required) and the results can be used in large spatial scale.

5.2 Quantification

Unlike detection, quantifying oil pollution is significantly dependant on the moisture content and the grain size. Although the analysis on the combined soil materials and water contents showed that the method can have 60-65% accuracy in prediction of hydrocarbons when these factors are unknown or difficult to acquire, knowing these factors for more accurate predictions is essential.

The quantification limit based on MIR DRIFT spectroscopy and PLSR validation results (in the worst case: coarse material and 20% water) is about 5.7 weight %. This indicates that in low percentages of pollution (<5.7%) and in coarse grained materials with high water contents, the PLSR predicted values are not reliable.

In spite of the high absorbing nature of water, most predictions were able to explain a good percentage of variance (worst R^2=77%) and were in a good error range (worst RMSEP=3.2%), even with water contents as high as 20%.

The grain size proved to be an important factor in the prediction accuracy. Predictions in fine grained, as well as mixed grained soils, were shown to be significantly more accurate than the coarse grained soils (by an order of three in the samples with 20% water). The scattering effect of large particles, as well as the small surface to volume ratio and high permeability, is considered to be responsible for the decreasing of accuracy.

Based on the motor oil end-member spectra and the spectra of polluted samples, as well as the loading effects, MIR spectral ranges of 3000-2800, 1480-1370, and 1280-1000 cm^{-1} were shown to be the most useful ranges for the detection and prediction of hydrocarbons.

Since PLSR is a very robust method, and with current computer technology a very quick one, future studies may concentrate on improving the prediction results by including both MIR and Vis-NIR ranges in the regression. It is also recommended to perform a classification on hydrocarbon types and soil materials based on their detailed chemical analysis, and use each class to train the PLS model for its corresponding H-C and soil material.

6. REFERENCES

Bertrand I, Janik LJ, Holloway RE, Armstrong RD and McLaughlin MJ. 2002. The rapid assessment of concentrations and solid phase associations of macro- and micronutrients in alkaline soils by mid-infrared diffuse reflectance spectroscopy. Aust. J. Soil Res. 40:1339–1356.

Clark RN and Roush TL. 1984. Reflectance spectroscopy: quantitative analysis techniques for remote sensing applications. J. Geophys. Res. 89:6329–6340.

Cloutis EA. 1989. Spectral reflectance properties of hydrocarbons: remote-sensing implications. Science. [Internet] 245:165–168. Available from: http://www.ncbi.nlm.nih.gov/pubmed/17787874.

Dominguez-Rosado E and Pitchel J. 2003. "Chemical characterization of fresh, used and weathered motor oil via GC / MS , NMR and FTIR techniques". Proceedings of Indiana Academy of Science. Vol. 112. p. 109–116. Available from: http://www.indianaacademyofscience.org/Documents/Proceedings/V112/IAS_v112_n2_p109-116.aspx.

Environmental Protection Agency (EPA). 2011. Response to oil spills. Available from: http://www.epa.gov/osweroe1/content/learning/response.htm.

Fine P, Graber ER, Yaron B. 1997. Soil interactions with petroleum hydrocarbons: abiotic processes. Soil Technol. [Internet] 10:133–153. Available from: http://linkinghub.elsevier.com/retrieve/pii/S0933363096000888.

Forrester S, Janik LJ and Mclaughlin M. 2010. "An infrared spectroscopic test for total petroleum hydrocarbon (TPH) contamination in soils". Proceedings of the 19th World Congress of Soil Science, 1–6 August 2010, Brisbane, Australia. p. 13–16.

Graham KN. 1998. Evaluation of analytical methodologies for diesel fuel contaminants in soil (MSc Thesis). University of Manitoba.

Hazel G, Bucholtz F, Aggarwal ID, Nau G and Ewing KJ. 1997. Multivariate analysis of Mid-IR FT-IR spectra of hydrocarbon-contaminated wet soils. Appl. Spectrosc. [Internet] 51:984–989. Available from: http://openurl.ingenta.com/content/xref?genre=article&issn=0003-7028&volume=51&issue=7&spage=984.

Huang Z, Turner BJ, Dury SJ, Wallis IR and Foley WJ. 2004. Estimating foliage nitrogen concentration from HYMAP data using continuum removal analysis. Remote Sens. Environ. [Internet] 93:18–29. Available from: http://linkinghub.elsevier.com/retrieve/pii/S0034425704001920.

Janik LJ, Merry RH and Skjemstad JO. 1998. Can mid infrared diffuse reflectance analysis replace soil extractions? Aust. J. Exp. Agric. [Internet] 38:681–696. Available from: http://www.publish.csiro.au/?paper=EA97144.

Low MJD and Mark H. 1970. Derivative traces in infrared Fourier transform spectroscopy. Appl. Spectrosc. 24:129–130.

Mevik BH and Wehrens R. 2007. The pls package: principal component and partial least squares regression in R. J. Stat. Softw. 18:1–24.

Nanni MR and Demattê JAM. 2006. Spectral reflectance methodology in comparison to traditional soil analysis. Soil Sci. Soc. Am. J. [Internet] 70:393–407. Available from: https://www.soils.org/publications/sssaj/abstracts/70/2/393.

Nguyen T, Janik LJ and Raupach M. 1991. Diffuse reflectance infrared fourier transform (DRIFT) spectroscopy in soil studies. Aust. J. Soil Res. 29:49–67.

Reeves JB, McCarty GW and Reeves VB. 2001. Mid-infrared diffuse reflectance spectroscopy for the quantitative analysis of agricultural soils. J. Agric. Food Chem. [Internet] 49:766–72. Available from: http://www.ncbi.nlm.nih.gov/pubmed/11262026.

Reeves JB. 2012. Mid-infrared spectral interpretation of soils: Is it practical or accurate? Geoderma [Internet] 189-190:508–513. Available from: http://linkinghub.elsevier.com/retrieve/pii/S0016706112002431.

Schwartz G, Eshel G, Ben-Haim M and Ben-Dor E. 2009. "Reflectance spectroscopy as a rapid tool for qualitative mapping and classification of hydrocarbons soil contamination". Proceedings of the 6th EARSeL SIG IS workshop IMAGING SPECTROSCOPY: Innovative tool for scientific and commercial environmental applications, Tel Aviv, Israel, 16-18 March 2009. - Tel Aviv : EARSeL, 2009. Available from: http://www.earsel6th.tau.ac.il/~earsel6/CD/PDF/earsel-PROCEEDINGS/3080 Schwartz.pdf.

Smith BC. 1996. Fundamentals of Fourier Transform Infrared Spectroscopy. CRC Press, Inc.

Stenberg B and Viscarra Rossel RA. 2010. Diffuse reflectance spectroscopy for high-resolution soil sensing. In: Viscarra Rossel RA, McBratney AB and Minasny B (Eds.). Proximal Soil Sensing. Dordrecht: Springer Netherlands. p. 29–47. Available from: http://www.springerlink.com/index/10.1007/978-90-481-8859-8.

Stuart B. 2004. Infrared Spectroscopy: Fundamentals and Applications. John Wiley & Sons Ltd.

Total Petroleum Hydrocarbon Criteria Working Group (TPHCWG). 1998. Analysis of petroleum hydrocarbons in environmental media. Weisman W (Ed.). Amherst: Amherst Scientific Publishers.

Van der Meer F, van Dijk P, van der Werff H and Yang H. 2002. Remote sensing and petroleum seepage: a review and case study. Terra Nova. 14:1–17.

Van der Meijde M, Knox NM, Cundill SL, Noomen MF, van der Werff HMA, van der Meijde M and Hecker C. 2012. Detection of hydrocarbons in clay soils: a laboratory experiment using spectroscopy in the mid- and thermal infrared. Int. J. Appl. Earth Obs. Geoinf. 23:384-388.

Viscarra Rossel RA, Walvoort DJ, McBratney AB, Janik LJ and Skjemstad JO. 2006. Visible, near infrared, mid infrared or combined diffuse reflectance spectroscopy for simultaneous assessment of various soil properties. Geoderma [Internet] 131:59–75. Available from: http://linkinghub.elsevier.com/retrieve/pii/S0016706105000728.

Wold S, Sjöström M and Eriksson L. 2001. PLS-regression: a basic tool of chemometrics. Chemometr. Intell. Lab. Syst. 58:109–130.

INDEX